Surrogate - Assisted Optimisation -Based Verification & Validation

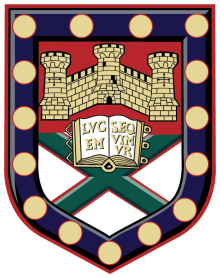

Submitted by **Atul Krishna Kamath** to the University of Exeter

as a thesis for the degree of

Doctor of Philosophy in Engineering

June 2014

I certify that all material in this thesis which is not my own work has been identified and that no material has previously been submitted and approved for the award of a degree by this or any other University.

Signature: _____

This thesis is dedicated to my loving parents for their love, endless support and encouragement.

Acknowledgements

I want to express my deep sense of gratitude to my adviser, Dr. Prathyush Menon, for his patient monitoring of my work, valuable guidance, unstinting support and constant motivation, all through the period of my work. I am thankful to Prof. Declan Bates for his invaluable help and guidance during various stages of my PhD. I felt privileged to work with Mark Watt, Michel Yu from Astrium UK and Martine Ganet-Schoeller and Maurice Guillaume from Astrium Space Transportation, France, Samir Benanni and Finn Ankersen from European Space Agency, Netherlands, on various projects during the course of my PhD. I would like to acknowledge with thanks the financial support received from European Space Agency and also the opportunity they provided to me to work on projects such as MAC study, SAFE-V and development of WCAT. I thank Prof. Christopher Edwards for his help and support during the final year of my course.

I am thankful to my lab colleagues, Anusha, Syi, Bharani, Varun, Lucky, Wessel and Chiara for creating a jovial working environment. My thanks goes to my friends Anup, Francesco, Toni, Charo, Mia, Zoe, Rajeswary, Sirisha and Sovish for making my stay pleasant and comfortable in Exeter. I would also like to thank my guru, Prof. Navdeep

Singh for providing guidance and inspiring me throughout my student life.

Finally, I would like to thank my parents and family members for their unconditional love and support.

Abstract

This thesis deals with the application of optimisation based Validation and Verification (V&V) analysis on aerospace vehicles in order to determine their worst case performance metrics. To this end, three aerospace models relating to satellite and launcher vehicles provided by European Space Agency (ESA) on various projects are utilised. As a means to quicken the process of optimisation based V&V analysis, surrogate models are developed using polynomial chaos method. Surrogate models provide a quick way to ascertain the worst case directions as computation time required for evaluating them is very small. A single evaluation of a surrogate model takes less than a second. Another contribution of this thesis is the evaluation of operational safety margin metric with the help of surrogate models. Operational safety margin is a metric defined in the uncertain parameter space and is related to the distance between the nominal parameter value and the first instance of performance criteria violation. This metric can help to gauge the robustness of the controller but requires the evaluation of the model in the constraint function and hence could be computationally intensive. As surrogate models are computationally very cheap, they are utilised to rapidly compute the operational safety margin metric. But this metric focuses only on finding a safe region around the nominal

parameter value and the possibility of other disjoint safe regions are not explored. In order to find other safe or failure regions in the parameter space, the method of Bernstein expansion method is utilised on surrogate polynomial models to help characterise the uncertain parameter space into safe and failure regions. Furthermore, Binomial failure analysis is used to assign failure probabilities to failure regions which might help the designer to determine if a re-design of the controller is required or not. The methodologies of optimisation based V&V, surrogate modelling, operational safety margin, Bernstein expansion method and risk assessment have been combined together to form the WCAT-II MATLAB toolbox.

Contents

Contents 1

List of Figures 5

List of Tables 8

List of Acronyms 10

1 Introduction 13

1.1 A review on Verification & Validation methods 16

1.1.1 Analytical based Verification & Validation methods 17

1.1.2 Simulation based Verification & Validation method 23

1.2 Research motivation 27

1.3 Contribution of thesis 30

1.4 Thesis organisation 33

2 Optimisation Based Verification & Validation Analysis 35

2.1 Introduction 35

2.1.1 A brief survey on optimisation based Verification and Validation (V&V) analysis 37

2.2 Analysis framework 39
2.2.1 Local optimisation 41
2.2.2 Genetic Algorithms 43
2.2.3 Differential Evolution 46
2.2.4 Hybrid evolutionary optimisation 48
2.3 BIOMASS: A flexible satellite model 50
2.3.1 Uncertain parameters 52
2.3.2 Specifications 52
2.3.3 Worst case analysis 53
2.4 Launch vehicle model 57
2.4.1 Roll coupling benchmark 58
2.4.2 Uncertainties 64
2.4.3 Specifications 64
2.4.4 Worst case analysis 64
2.4.5 Thrust Vector Control (TVC) benchmark model 69
2.4.6 Disturbances 74
2.4.7 Uncertainties 75
2.4.8 Specifications 77
2.4.9 Worst case analysis 78
2.4.10 Multi-objective Verification & Validation analysis 96
2.4.11 Non-Dominated Sorting Differential Evolution 96
2.4.12 Application to TVC benchmark problem 102

3 Polynomial Chaos Based Surrogate Models 105

3.1 Introduction 105

3.2 Polynomial chaos expansion . . . 110
3.2.1 Wiener Askey polynomial chaos . . . 111
3.2.2 Intrusive and Non-intrusive method . . . 113
3.3 Probabilistic collocation method . . . 115
3.3.1 A numerical example . . . 118
3.4 Surrogate modelling of TVC benchmark . . . 123
3.5 Worst case analysis . . . 127

4 Identification of safe/failure regions in the parameter space 136
4.1 Introduction . . . 136
4.2 Operational safety margin assessment . . . 137
4.2.1 Basic Concept . . . 137
4.2.2 Optimisation problem formulation . . . 139
4.2.3 Operational safety margin of TVC benchmark model . . . 143
4.2.4 Worst case analysis inside the safe region . . . 145
4.3 Bernstein expansion based approach . . . 148
4.3.1 Introduction . . . 148
4.3.2 Basic Concept . . . 149
4.3.3 An illustration of sub-division algorithm . . . 152
4.3.4 Application: TVC benchmark model . . . 155
4.4 Risk assessment . . . 160
4.4.1 Binomial failure analysis . . . 161
4.4.2 Application: TVC benchmark model . . . 162
4.4.3 Assigning risk to region around worst case . . . 164

5 Conclusions and future work **167**

5.1 Conclusions 167

5.2 Future work 171

Bibliography **176**

Appendix A: Recurrence relations for orthogonal polynomials **195**

List of Figures

2.1 Framework of the Worst Case Analysis Tool (WCAT) 40

2.2 Crossover process in GA 46

2.3 Optimisation technique comparison 55

2.4 Worst Case and Nominal plot comparison for $S(j\omega)$:HDE Algorithm 56

2.5 Worst Case and Nominal plot comparison for $T(j\omega)$: HDE Algorithm 56

2.6 3-axis launcher control loop 58

2.7 A complex perturbation introduced at the plant input u 61

2.8 Schematic representation for evaluation of Multi Input Multi Output (MIMO) Margins 62

2.9 Nichols plot of a SISO system showing Low Frequency (LF), High Frequency (HF) and phase margins 63

2.10 Degradation of MIMO margins 66

2.11 Block description of the flexible launcher vehicle 69

2.12 Single axis flexible launcher model([1]) 70

2.13 Wind profile 74

2.14 Uncertainties and dispersions 76

2.15 Rigid mode worst case perturbations at different wind instances for max $|Q_\alpha(t)|$ . . . 85
2.16 Aerodynamic AoA Q_α plots at different wind perturbation instances for max $|Q_\alpha(t)|$ . . . 86
2.17 Rigid uncertain parameters maximising $|\theta(t)|$ . . . 88
2.18 θ plots at different wind perturbation instances for max $|\theta(t)|$ . . . 89
2.19 Rigid uncertain parameters maximising $|\theta(t_f)|$ . . . 90
2.20 θ plots at different wind perturbation instances for max $|\theta(t_f)|$ . . . 91
2.21 Rigid uncertain parameters maximising $|\dot{\theta}(t_f)|$ . . . 92
2.22 $\dot{\theta}$ plots at different wind perturbation instances for max $|\dot{\theta}(t_f)|$ . . . 93
2.23 Rigid uncertain parameters maximising $|\beta(t)|$ . . . 94
2.24 β plots at different wind perturbation instances for max $|\beta(t)|$ . . . 95
2.25 Ilustration of Non-dominated sorting and Crowding distance . . . 98
2.26 Pareto Front associated with maximising the deviations in the aerodynamic load and the deflection angle . . . 103

3.1 Block description of a surrogate modelling . . . 114
3.2 Low-pass Sallen-Key Filter . . . 119
3.3 Comparison of accuracy of the surrogate model . . . 122
3.4 Polynomial modelling complexity. . . . 127
3.5 Comparison between launcher and polynomial models. . . . 128
3.6 Aerodynamic AoA Q_α plots at different wind perturbation instances for max $|Q_\alpha(t)|$ . . . 130
3.7 Rigid mode worst case perturbations at different wind instances for max $|Q_\alpha(t)|$ . . . 132

3.8 $\dot{\theta}$ plots at different wind perturbation instances for max $|\dot{\theta}(t_f)|$ . . . 133

3.9 β plots at different wind perturbation instances for max $|\beta(t)|$ . . . 133

3.10 Rigid uncertain parameters maximising $|\dot{\theta}(t_f)|$ 134

3.11 Rigid uncertain parameters maximising $|\beta(t)|$ 135

4.1 Dilations of Uncertainty Set. 141

4.2 Comparison of rigid mode worst case perturbations for max $|Q_\alpha(t)|$ 146

4.3 Stability regions: green region=stable red region = unstable 153

4.4 Sensitivity analysis: flexible uncertain parameters set to nominal values with rigid parameters varying 156

4.5 2-D slice of parameter space. 159

4.6 Risk assessment for a sample plan of (10,1000). 163

4.7 Risk assessment for a sample plan of (1,1000). 165

List of Tables

1.1 Analytical based Verification & Validation methods 18

1.2 Simulation based Verification & Validation methods 24

2.1 Functional performance requirements: BIOMASS 53

2.2 Worst case values of S & T 57

2.3 Variability of rigid mode uncertain parameters 64

2.4 MIMO stability specifications 65

2.5 Worst case results for roll coupling benchmark 68

2.6 TVC launcher notations 71

2.7 Variability of rigid and bending mode uncertain parameters 77

2.8 Functional performance requirements 78

2.9 Worst case results over the entire parameter range for wind perturbation at 30,35,40, 45, 50, 60 and 70 seconds 82

2.10 Worst case results over the entire parameter range for wind perturbation at 30,35,40, 45, 50, 60 and 70 seconds 83

2.11 A fast sort algorithm 99

3.1 Wiener-Askey polynomials with corresponding distribution 112

3.2 Generation of Collocation Points 117

3.3 Surrogate modelling 118
3.4 Legendre polynomial basis 120
3.5 Collocation points at which the original model is evaluated 121
3.6 Multivariate orthogonal polynomial basis 122
3.7 Coefficients of 1^{st} order surrogate model for each cost function . . . 124
3.8 Worst case results of 1^{st} order surrogate model for wind @ 50 sec . 126
3.9 Worst Case results for second order polynomial model 129

4.1 Critical similitude ratio ($\widetilde{\lambda}$) and operational safety margin (ρ) results for the launcher & polynomial surrogate model 145
4.2 Worst case results inside safe region 147
4.3 Sub-division algorithm based characterisation of uncertain parameter space 154
4.4 CR and PR for various wind instances corresponding to the deflection angle requirement 164
4.5 Bounds of failure region around worst case 165

List Of Acronyms

ADMIRE Aero-Data Model In a Research Environment

AOCS Attitude and Orbital Control System

DE Differential Evolution

DIRECT DIviding RECTangles

ESA European Space Agency

GA Genetic Algorithm

HDE Hybrid Differential Evolution

HF High Frequency

HGA Hybrid Genetic Algorithm

HIRM High Incidence Research Model

IMU Inertial Measurement Unit

IQC Integral Quadratic Constraints

KL Karhunen-Loeve

LF Low Frequency

LFR Linear Fractional Representation

LFT Linear Fractional Transformation

LTI Linear Time Invariant

MARS Multivariate Adaptive Regression Splines

MIMO Multi Input Multi Output

MODE Multi-Objective Differential Evolution

MOEA Multi-Objective Evolutionary Algorithm

MOGA Multi-Objective Genetic Algorithm

MOPS Multi-Objective Parameter Synthesis

NPGA Niched Pareto Genetic Algorithm

NSDE Non-dominated Sorting Differential Evolution

NSGA Non-dominated Sorting Genetic Algorithm

RACS Roll Attitude Control System

SAR Synthetic Aperture Radar

SISO Single Input Single Output

SSV Structured Singular Value

SOS Sum Of Squares

SQP Sequential Quadratic Programming

TVC Thrust Vector Control

TRP Technical Research Project

V&V Verification and Validation

WCAT Worst Case Analysis Toolbox

Chapter 1

Introduction

Verification & Validation of controllers for space applications is a process to certify the satisfactory performance of a given closed loop system during a specified mission. This is a crucial task, and a poor performance, or an onset of instability, can lead to the failure of the entire mission. It is common that many of the parameters in the system are not precisely known over the entire operating region of the system, but they are considered to lie within a bounded interval. Hence, it is very important, for ensuring the robust performance of a controller, that the worst-case stability and performance metrics of the given closed loop model is necessarily assessed for nominal as well as the expected level of variations of uncertain parameters, for e.g. the uncertainty in different aerodynamic coefficients, physical configuration parameters, flexible, bending and sloshing mode parameters. In aerospace applications, this is typically identified as flight clearance of the control laws, and carried out as the final step withinthe iterative design process. The scenario is not different in the case of space applications.

In the case of space missions, a typical Verification & Validation is carried out to evaluate the stability and performance of the closed loop control system models of spacecraft, re-entry vehicle, and satellite. The design process, at large, involves the modelling of the environment, aerodynamics, and various systems including the control system module which consists of the actuators and the sensors. Non-linearities, flexible modes and lumped delays are often present in these models. To account for the variations of the parameters, a nominal model is defined together with a series of tolerances which define the level of uncertainty of each parameter. The worst-case analysis problem is to carry out the robust stability and performance analysis of such complex, non-linear and high-fidelity simulation models of a space mission. It is assumed that the controller is available, and it would possibly have been designed using a simple dynamic model. The representation of the dynamic model may have been realised according to several assumptions so that a viable design technique may be employed. Verification & Validation is the last step in the design cycle of the controllers, therefore, it is important to make use of the best dynamic model that captures almost all the effect of nonlinearities, uncertainties, flexible modes, disturbances and various delays. As a consequence, the simulation model can become complex, non-linear, and of high-fidelity.

As an example, consider the guidance and control law of a re-entry vehicle which ensures robust tracking of a pre-defined mission trajectory. In order to guarantee the success of a mission, the worst-case deviations from the pre-defined trajectory due to the simultaneous variations in the multiple uncertain parameters need to be evaluated. Clearly, this task becomes cumbersome and computationally very challenging, where different combinations of large numbers of uncertain parameters

must be investigated such that an estimate about the worst-case stability and performance of the control laws can be made. To determine the deviation from the pre-defined trajectory, the closed loop re-entry vehicle system for a finite time period needs to be simulated. In accordance with this rationale, the framework applicable to any representation of the dynamical system, including the best one available is desired to be made use of. Moreover, computationally efficient tools need to be identified, developed and tested with different space applications.

A Verification & Validation process can provide confidence, by ensuring the control laws work as per the specifications without any safety critical malfunctions over the entire operating region. An overview of Verification & Validation methods and various challenges for Verification & Validation and certification for the adaptive control systems used in safety critical aircraft systems is given in [2]. According to [3] and the references therein, Verification & Validation can be defined as follows:

- Validation is the process of determining the degree to which a model is an accurate representation of the real world from the perspective of the intended uses of the model.

- Verification is the process of determining that a model implementation accurately represents the developer's conceptual description of the model and the solution to the model.

1.1 A review on Verification & Validation methods

During the design cycle [4], the performance of controller is assessed using a range of methods such as analytical techniques that could be employed on lower order models, simulations that are applicable to complex, high-fidelity models, hardware in loop analysis where actual subsystems replace some of the mathematical models and the flight tests. Analytical techniques such as gain/phase margins [5] and the nonlinear continuation/bifurcation analysis against single parameter variations [6] can be considered as the traditional analytical tools for worst-case analysis in the early phase of the design cycle. The multivariable methodologies such as μ-analysis and ν-gap metric analysis (chapters 17 and 18, of Ref. [7]) became more modern candidates for carrying out worst-case analysis based on robust control theory [8] that convert a given closed loop system to a Linear Fractional Transformation (LFT)-based model [9]. These techniques and their variants deal with multiple sources of uncertainty, however the complexity in determining the exact μ value is claimed to be an NP-hard problem [10]. Useful extensions of these approaches which can handle certain types of nonlinear dynamics have also recently been developed, such as Integral Quadratic Constraints (IQC) [11, 12] and Sum Of Squares (SOS) programming [13]. A common characteristic of the above modern methods is that specific requirements are made on the closed-loop simulation model under investigation, e.g. simplified versions of the full vehicle simulation model must be developed in order to generate LFT-based models for μ-analysis and IQCs and similarly polynomial representations for the SOS methodology. Few of these key techniques, classified as analytical methods that seem to be relevant

for Verification & Validation are tabulated in Table 1.1 and discussed in brief in sequel.

1.1.1 Analytical based Verification & Validation methods

Analytical based methods are discussed in this section and summarised in Table 1.1 which gives information on their applicability to different classes of systems and types of domains, indicator of engineers effort, indicator of computational complexity/overhead. The appearance of '✓' shows the applicability of the methods. The followings fields from the Table;'L', 'NL','DD', 'CD', 'EE', 'CC'; are Linear Models, Nonlinear Models, Discrete domain, Continuous domain, Engineer Effort and Computational Complexity respectively. The number of '−' shows reduced complexity/effort and the number of '+' shows increased complexity/effort. Absence of these symbols means no specific information. The term 'Engineer Effort' is a subjective estimation of the skills and time required by an engineer to write a code, test it on benchmark problems and then apply it to industrial problems. The methods SOS and IQC require more effort to learn and implement in industrial problems than for instance the gain and phase margin methods taught in undergraduate program. Hence in Table 1.1, increased 'Engineer Effort' is indicated for SOS and IQC methods.

1. Gain and phase margin / Nichols exclusion region analysis:

   For SISO case, gain margin indicates the possible level of increment in the gain of the plant before the gain of system at 180° phase lag frequency reaches unity, whereas the phase margin gives how many more degrees to 180 phase lag at which the system gain would cross unity. These are classical methods

Table 1.1: Analytical based Verification & Validation methods

Method	L	NL	DD	CD	EE	CC
Gain/Phase Margin	✓		✓			
μ - analysis	✓		✓		+	−
ν - gap analysis	✓		✓		+	−
IQC/Multiplier analysis	✓	✓	✓		++	+
SOS analysis	✓	✓	✓	✓	+++	++
Bifurcation and Continuation analysis		✓		✓	+	+
Interval analysis	✓	✓	✓	✓	−	−

[5] and still very much in use providing good insight of the system. However these are limited to linear time invariant systems and carried out one loop at a time. Extensions of the concept to evaluate exact MIMO stability margins can be found in [14]. In [15] methods are developed to determine the margins in near real time and employed to a modern fighter aircraft example. Recently, in [16] gain and phase margin are monitored 'online'.

2. Structured singular value (μ) analysis:

   The method is applicable to only those systems that are linear uncertain dynamical systems and realised in a Linear Fractional Representation (LFR) form (necessary modelling effort for designer). The computation of exact value of the Structured Singular Value (SSV) is an NP hard problem and hence the method evaluates the fulfilment of robust stability and performance criteria with upper and lower bounds for μ and the quality of the bounds depends on the size of the perturbation matrix in loop and whether the perturbation is complex, real or mixed. The solution of the upper bound is a convex problem that can be solved using Linear Matrix Inequalities (LMI) [17], whereas the calculation of lower bound is a non-convex problem and

often heuristic methods are required. In the case when there are complex elements in the perturbation block, polynomial time algorithms such as power iteration proposed in [18] is available to compute the lower bound. The computation of bounds for μ can also become very tedious, especially in the case of real μ. The worst-case perturbation is usually provided by the lower bound of μ. The computational complexity is a polynomial function of number of uncertainties in the model. See [19, 20, 21, 22] and Refs. there in for more details. The existence of powerful tools such as μ - analysis tools in MATLAB makes this approach more attractive. However traditional frequency gridding based methods might be less effective in case of the applications in which there are dominant flexible modes present. Since, such modes might be present in a narrow frequency region there exists a high chance for missing the mode and for over evaluating the robustness properties when gridding type approach is followed. Since the present application is flexible satellites, this point is very important. For more details on a specific suitable approach, see [23]. How the modern robustness metric such as SSV can be interpreted in terms of the classical gain/phase margin and the Nichols exclusion region robustness specifications is discussed in [24].

3. Gap metric (ν - gap) analysis:

   Like μ - analysis, this method also requires the uncertain linear model to be expressed in an LFR form. According to [25], a simple algorithm is used to compute the worst-case parameter combinations based on the gap metric that has roots on operator theory. A claim is made in [25] that the calculation of the worst-case using ν - gap metric is simpler than that of computing the

lower bound of μ. In [26] the robust performance of an integrated flight and propulsion control law had been analysed using the ν - gap metric and compared with μ analysis results. However, it might be stated that the methodology is yet to be popular among the practitioners, perhaps due to the inherent complexity of the concepts for an industrial practitioner.

4. Integral Quadratic Constraints (IQC) / Multiplier analysis:

   The IQC method is a unifying framework for system analysis that generalises the small gain theorem and passivity theorem [27] and many other results from robust control. This analysis allows a designer to handle different kinds of uncertainties, time invariant, time varying, delay and certain class of non-linear uncertainties simultaneously. Since the theory takes into account of time varying uncertainties and their variation rates, the method leads to less conservatism. The system under investigation is converted into a standard LFT form by pulling out the uncertainties which then can be described by IQCs. The multiplier/IQC framework is based on a special modelling where the analysed system is written as the Linear Time Invariant (LTI) interconnection of sub-systems of different nature: time-varying, a class of non linear, uncertain, time delay, etc. Each subsystem is characterised by a set of multipliers or IQCs. Static as well as dynamic multipliers have been proposed over the period; a mild criticism on this method by practitioners may be the lack of clear guidelines to choose a multiplier easily. However, powerful software such as IQC-β toolbox is available for the purpose. See [11, 28, 29] for details on IQC methods. From [30], it is apparent that the method is gaining popularity among the European Space community and their project.

5. Sum of Squares (SOS) analysis:

   SOS techniques study the stability or performance of a dynamical system represented only in a polynomial form. The method falls in a class of semi definite programming problems which involves solving (linear convex) optimisation problems in the cone of positive semidefinite matrices. SOS programming can be used to guarantee stability and performance of control systems including non linear systems, continuous/discrete hybrid systems, and time delay systems. In [31] for the first time, the SOS techniques had been extended to compute the $\mathcal{L}_2$ gain bound for affine nonlinear systems importantly by overcoming the computation of numerically difficult Hamilton Jacobi Inequality. Polynomial Lyapunov functions of possibly high degrees than a quadratic Lyapunov function are computed and tagged as certificates associated with the dynamical system. Hence, local stability and performance can be ensured in polynomial sublevel sets of the state space. Refs. [13, 32] apply the methodology for robustness analysis problems associated with aerospace applications.

6. Bifurcation and continuation method:

   The theory can be used to analyse the dynamical system represented as nonlinear differential equations. All possible steady and non-steady equilibrium solutions can be obtained as a function of its state and input variables by locally linearising the dynamical system about a continuum of equilibrium points. The solutions are obtained via suitable numerical continuation methods (especially powerful software AUTO implementing various such methods

is available for use [33]). This can provide useful insight into various nonlinear phenomena associated with the dynamical system [6]. Perhaps, one major drawback with this method is its limitation to vary single parameter at a time (there exists methods to vary two parameters at a time, and representation of the results becomes hard in cases of parameter dimension more than that.) and the smoothness assumption associated with the dynamical system. Moreover, the method does not guarantee worst-case of stability or performance will always be found. However, this can be used as a potential tool to identify the critical area in parametric region for further close analysis. This can offer a significant reduction of computational effort. Also, this analysis method in conjunction with optimisation method has significant potential; see for example a nonlinear method proposed in [34] for limit cycle analysis in an aerospace example.

7. Interval analysis (polynomial based method):

   In this analysis method the analysis criteria, or cost function, are defined as polynomial functions of uncertain parameters. In [7] (page 333-353), the method was used to assess a linear stability criteria of uncertain systems and found to be comparable with a classical grid analysis approach. However, the associated computational load is much lower. Lower computational load and simplicity of the approach makes this method attractive to engineers. The method can be used to investigate the entire operating region, or entire uncertain parameter space, treating it as a continuous domain. Provided, the assessment criteria can be expressed as an algebraic function, the method can be employed to any linear and nonlinear criteria. See [7, 35] for more details,

first reference with a flight control clearance problem and the last reference with a re-entry module clearance example.

1.1.2 Simulation based Verification & Validation method

The most common approaches used in industry are based on statistical techniques and/or evaluations over grids which are easily applicable. These methods can be applied to the full nonlinear, complex and high-fidelity simulation model of the vehicle with a minimum of effort on the part of the designer. In such approaches, mainly there are two possibilities: (a) the extreme points of the vehicles uncertain parameter space are considered and the analysis criteria are evaluated at these points; (b) the search space is randomly sampled and Monte-Carlo simulation is employed [7]. As the number of uncertain parameters considered (gridding of extreme points) increases, the computational effort associated with the Verification & Validation exponentially increases [7]. The case is not different with respect to the desired statistical confidence levels for the clearance results (Monte-Carlo simulation), [36, 37]. These constraints severely limit the reliability of the analysis in the case of complex models particularly those with the slow simulation speeds.

Moreover, there is no guarantee that the worst-case uncertainty combination has in fact been found, since it is possible that the worst-case combination of uncertain parameters does not lie on the extreme points, or in the sampled set used by Monte-Carlo approaches. To address this issue, the advanced optimisation algorithms that efficiently search the parameter space for the worst-case that violate the specific criterion can be considered [38]. Simulation based Verification & Validation methods are summarised in the Table 1.2 with similar notations to

that used in analytical based Verification & Validation. A brief discussion on each of the methods mentioned in the table is provided in this section.

Table 1.2: Simulation based Verification & Validation methods

Method	L	NL	DD	CD	EE	CC
Grid point analysis	✓					
Monte Carlo analysis (Nominal)		✓	✓		−−	−
Optimisation based analysis	✓	✓	✓	✓	−−	−−

1. Grid point method:

   In a grid point analysis method the dynamical system, mostly a realistic nonlinear model, is analysed at a number of grid points of the operating region, the effect of parameter variations are assessed by the stability and performance metrics of the locally linearised models about an equilibrium attained on these grid points as well as nonlinear simulations [39]. The reliability of results from this method depends extremely on the engineer's familiarisation with the model and the intuition of choosing the grid points. The main criticism with this method is that there is no guarantee that 'worst-case' has been obtained since the verification and validation process uses a discrete set of points. Better results can be obtained on a finer grid, however at the expense of a higher computational cost and without any guarantees that a worst-case will be found. Any analysis method which linearises the complex nonlinear model would usually bring forth conservatism in results due to the inherent linearisation errors.

2. Monte Carlo simulation analysis:

   Monte Carlo refers to a class of methods that perform repeated sampling

of the uncertain parameter space to obtain a desired numerical result. A Monte Carlo method can be used to perform V&V analysis by performing random sampling of the uncertain parameter space with an aim to obtain the worst case. These methods are widely used to assess the probability of exceeding a predefined limit of a performance metric arising from variation in uncertain input parameters. This form of robustness analysis is done by using statistical descriptions of parameter uncertainty. The uncertain parameter either has a known or an estimated probabilistic density function, e.g. Gaussian. Monte Carlo simulations are widely used in traditional validation processes, which are very common in the aerospace industry [40, 41]. However a major drawback, like any other statistical method, is that they are very time consuming. For a high level of probability and confidence level the associated computational time can be excessive. The Importance and Stratified sampling methods could be used to improve the convergence rate and probability of occurrence of a specified event in such simulations. New development of the Monte Carlo method such as methods based on polynomial chaos and surrogate models are attractive because they can reduce computational overhead significantly.

3. Optimisation based analysis:

   In optimisation methods, the validation problem is rewritten or reformulated as an equivalent distance maximisation/minimisation problem. The global solution to the optimisation problem is worst-case. The dependency of the considered performance criterion over the search space for this class of problem will in general be highly nonlinear and non-convex [42]. Hence, local

optimisation methods, depending on the given initial conditions, can get trapped in locally optimal solutions. Hence the global optimisation methods are necessary to avoid such situation and obtain solutions of good quality, i.e., global solution. Many different classes of optimisation algorithms are available in the literature which may be used for worst-case analysis of complex systems. Some of the most well known are: Gradient-based optimisation, e.g. Sequential Quadratic Programming (SQP), Simulated Annealing, Genetic Algorithm (GA), Differential Evolution (DE), DIviding RECTangles (DIRECT), Particle Filtering, , Mixed Integer Programming, Branch and Bound Methods, Interval Analysis and Multiobjective Algorithms. This concept can address any clearance criteria. Parametric models have to be available, which could be linear or non-linear. No matter how complex the model is, the problem is addressable. The computation time depends on the optimisation method and the type of problem. Leveraging the 'intelligence' embedded in global optimisation algorithms offers the potential to significantly reduce the number of simulations required to assess worst-case performance of complex systems, impacting directly on the time and cost requirements for the validation. In [43, 44], a few of the local, global and hybrid optimisation methods have been applied to a specific time domain flight clearance problem for a high performance aircraft, however the dimension of the uncertain space considered was of significantly low order.

1.2 Research motivation

From Table 1.1, it can be seen that most of the analytical methods are applicable to linear models, or a certain class of nonlinear models (often that satisfies the sector condition). Although, SOS methodology is applicable to linear and nonlinear models in discrete as well as continuous domain, the methodology requires a lot of effort on engineer's behalf to perform the analysis and has a high computational complexity. Interval analysis is applicable to linear and nonlinear models in discrete and continuous domain. Comparing with SOS, interval analysis has lesser computational complexity and lesser effort required by engineer. Unfortunately, the methodology is not very popular with the aerospace industries. In [45], SOS methodology has been used to assess the robust performance of a simplified closed loop rendezvous mission. As a consequence, it is evident that the complexity of the problem that can be dealt with the present SOS tools is of significantly low order. From [30], it is apparent that the IQC method is also gaining popularity among the European space community.

Verification & Validation is the last step of the design cycle, and hence it is important not to alter, or modify the given structure of the model for carrying out the analysis. The model is often treated as a 'black-box' representation with access limited to certain inputs and output variables. Obviously, the currently available analytical tools require further significant development to be absorbed in the industry, yet then the use of such tools, in the earlier stated manner for validating the general class of realistic industrial models, seems to be difficult.

On the other hand, the simulation based methods are more popular with the industry due to its applicability and the lesser effort required by the engineers

to perform the analysis. These methods aim to determine the deviations in the performance criterion for various uncertainty configurations. The maximum deviation of the performance criterion is of interest, and is treated as a gauge for assessing the robustness of the controller. In Grid point and Monte Carlo analysis, large number of simulations are required in order to accurately estimate the global maximum of a given performance metric. Even so, Monte Carlo analysis is popular among the aerospace industry because the statistical attributes like accuracy and confidence levels of the obtained result can be assigned. In order to ascertain the global maximum, researchers have employed the optimisation algorithms to evaluate the worst-case performance metrics using relatively less number of simulations as compared to the Monte Carlo techniques. Researchers in this area have used local, global and hybrid optimisation methods for performing the worst-case analysis.

European space industry is keen about developing this approach further, and develop it as a useful tool for carrying out Verification & Validation of different missions [1]. Though the concept had been applied earlier to certain lower order problems, it is necessary to assess the concept with a larger number of uncertainties, and with as many different time and frequency domain performance criterion of disparate missions as possible. The thesis aims to address this requirement by considering different time and frequency domain Verification & Validation problems in the presence of significantly large number of uncertain parameters.

Optimisation based V&V analysis for aerospace problems are often non-convex optimisation problem whose global solution is not always guaranteed. Stochastic

[1]Developed with support from WCAT-II, European Space Agency (ESA) supporting grant ESTEC Contract No 19783/06/NL/JD: 4000104541

optimisation procedure may have to be repeated a few times in order to guarantee that the worst-case has truly been found. In optimisation based Verification & Validation the performance criterion is evaluated by means of the finite time simulation or a frequency sweep. If the individual finite time simulation itself is computationally time consuming, the optimisation based analysis will naturally be even more so. Speeding up of the computational time of the simulation based Verification & Validation methods for such situation is another key issue that the thesis is aiming to address.

A potential solution for speeding up the computation time is the use of surrogate models, which are computationally inexpensive. In this thesis, accurate and computationally fast surrogate polynomial models are developed. The proposed surrogate models are polynomial expressions in terms of the respective uncertain parameters, and the evaluation of this polynomial expression would give the associated performance criterion under consideration. Each polynomial expression will be associated with a given performance metric, and its use with the optimisation can reduce the computational effort significantly.

In addition, this thesis also investigates to determine the safe operating region around the nominal parameter value in the uncertain parameter space. This safe operating region would satisfy all the performance criteria and the robustness could be associated by the size of the region to determine the safe operating region. Optimisation methods will have to be developed in order to determine the operational safety margin, and often the computational effort associated with such problem can be very high. Once again, the surrogate polynomial models could be used to speed up the conventional optimisation problem. As surrogates are polynomial expression in terms of uncertain parameters, it would determine the propagation

of uncertainty in the uncertain parameter space. Since safe regions indicate that all performance criteria are satisfied, failure regions corresponds to failure of one or more performance criterion. Additionally, a failure probability need to be assigned to the failure regions in order to assess the risk for re-design of controller.

1.3 Contribution of thesis

In this thesis, the methodology of the optimisation based worst-case analysis is extended to space applications including the Verification & Validation of Earth observation satellite and launch vehicle models. The efficiency of the conventional optimisation based worst-case analysis has been enhanced by exploiting the use of polynomial surrogate representation of the performance objective of simulation model, developed using the polynomial chaos theory and the probabilistic collocation methodology. Furthermore, the surrogate assisted optimisation based worst-case analysis is employed to identify the subset of the uncertain parameter space efficiently in which the multiple performance specification criteria are satisfied. The results of this thesis have been published, or are currently submitted and in the review process for publication [46, 47, 48, 49]. In addition, the technical development and application reported in this thesis are coded in the Matlab/Simulink environment, and these reusable, generic surrogate assisted Verification & Validation tools are available for download for different industries from European Space Agency[1]. The contribution is as follows:

- **Optimisation based Verification & Validation analysis to aerospace**

[1]Developed with support from WCAT-II, European Space Agency (ESA) supporting grant ESTEC Contract No 19783/06/NL/JD: 4000104541

models including Earth observation satellite and launch vehicle models

Optimisation based Verification & Validation is applied to a flexible satellite model and a flexible launch vehicle in its Thrust Vector Control (TVC) phase. The robustness of the controller is evaluated under uncertain parameter variations. For both the models, worst-case performance metrics are evaluated by employing different optimisation algorithms. The time and frequency domain performance metrics are translated into cost functions which are maximised by the optimisation algorithm to determine the worst case perturbation. With the flexible satellite model, for the first time, significantly large number of uncertain parameters are considered in the optimisation based Verification & Validation analysis. Frequency and temporal performance metrics are evaluated for the flexible launch vehicle and worst case uncertainty perturbation are determined. Specifically the roll coupling effects are studied by determining the MIMO gain and phase margins. Worst case performance metrics deviations of aerodynamic load, pitch angle and command deflections emanating due to uncertainties in rigid and flexible mode parameters are determined.

- **Development of surrogate models and its use in the simulation and optimisation based Verification & Validation**

  Surrogate models of the performance objectives of the flexible launch vehicle are developed using polynomial chaos technique. Specifically non-intrusive technique is adopted. The uncertainty space is sampled using probabilistic collocation technique to generate polynomial models in terms of the uncer-

tain parameters. Surrogate models are developed for each performance criterion considered. First and second order surrogate polynomials are developed for each performance criteria. The accuracy of the derived surrogate model is evaluated by comparing the results of both original and surrogate models. Subsequently the surrogate models are utilised in the simulation based Verification & Validation. For this, the performance cost requiring the evaluation of original model is replaced with the surrogate model and simulation based Verification & Validation is performed. The efficacy in speeding up the process is demonstrated.

- **Identify safe and failure regions in the uncertain parameter space and assigning risk to unsafe regions**

  The region around the nominal parameter value that satisfies all performance criteria is translated intro a metric called as the operational safety margin. The size of the region is indicative of robustness. Optimisation is employed on the original and surrogate model for evaluating the operational safety margin metric. Surrogate models are utilised to speed up the process of evaluating the operational safety margin metric. Surrogate models are also utilised in characterising the uncertain parameter space into safe and failure regions. Failure probability is assigned to the failure regions by employing binomial failure analysis. The failure probability would help assess the risk of re-designing a controller.

1.4 Thesis organisation

This thesis is organised as follows, in chapter 2 introduces optimisation based Verification & Validation analysis and provides a brief survey on the topic. Verification & Validation analysis method is then applied to an industrial model of flexible satellite for the BIOMASS mission consisting of large number of uncertainties. Analysis is performed for frequency domain characteristics on sensitivity and complementary sensitivity functions. Verification & Validation analysis is also applied to two launch vehicle models to study the impact of uncertainties and roll coupling on MIMO margins and temporal performance metrics.

Chapter 3 presents the polynomial chaos modelling to develop surrogate polynomial models. A non-intrusive method called probabilistic collocation method is utilised to generate surrogates. This methodology is used to develop surrogate models for the temporal performance criteria of the flexible launch vehicle. Surrogate models are developed using the rigid and flexible parameters of the launch vehicle and evaluation of the model gives the performance criterion under consideration. First and second order surrogate models are developed while discussion on complexity for generating higher order polynomials is provided. The accuracy of the surrogate models are determined by evaluation of both surrogate and original models for a set of uncertain parameter combinations. Finally, optimisation based Verification & Validation method is applied on these surrogate models and the results are compared with those obtained with the flexible launch vehicle for improvement in computational time and quality of the results.

In chapter 4 deals with identification of safe and failure regions in the uncertain parameter space. To this end the method of operational safety margin is utilised to

identify the largest safe region around the nominal parameter value. Operational safety margin defined in the uncertain parameter space is evaluated for the flexible launch vehicle. In order to speed up the process of evaluation of the metric, surrogate models of the flexible launch vehicle is also utilised. Next, Bernstein polynomial expansion method is employed on the surrogate models in order to characterise the uncertain parameter space into safe and failure regions. The method of binomial failure analysis is utilised to determine upper and lower bounds on failure probability of the failure regions identified by the Bernstein expansion method. This method is utilised to assess the risk for performing a re-design of the controller used in the flexible launch vehicle.

Finally Chapter 5 presents the conclusions of this study. A few future research directions are also explained in this chapter.

Chapter 2

Optimisation Based Verification & Validation Analysis

2.1 Introduction

In order to guarantee the safety of the mission, the worst case stability and performance metrics of the control laws must necessarily be assessed for nominal as well as the expected level of variations of uncertainty in the mission parameters, such as aero-thermodynamic parameters, physical configuration parameters such as mass, inertia, actuator and sensor uncertain parameters, and flexible mode parameters. For example, in the case of flexible satellites [50], the poorly damped flexible modes may get excited even in the presence of the attitude control of the spacecraft. Excitation of such flexible modes can lead to the degradation of the pointing performance of the spacecraft. The designed control law must be robust enough to suppress the vibrations during the attitude control of the spacecraft to ensure accurate pointing performance. In order to guarantee the safety of this

mission, it is apt to assess the worst case deviations of the pointing error in the presence of various uncertain parameters including those associated with flexible modes. One way to assess this is by perturbing the simulation model with several simultaneous variations of the multiple uncertain parameters, within their allowable bounds. However, this is computationally expensive and determining the worst-case efficiently is a challenging problem.

Given a bounded, multi dimensional uncertain parameter space, $\Delta \subset \mathcal{R}^m$, the aim is to determine the combination of the uncertain parameters associated with the maximum possible violation of a mission performance criterion, $\delta^* \in \Delta \subset \mathcal{R}^m$, which is identified as worst case perturbation. The corresponding optimisation problem specifically associated with a time domain performance criterion, is defined as:

$$\delta^* = \underset{\delta \in \Delta, t \in [t_0 \;\; t_f]}{\arg\max} \; J(\delta, \mathcal{C}, W, t) \tag{2.1}$$

where $\delta = \mathcal{C}ol(\delta_1, \ldots, \delta_m)$ represents the uncertain parameter vector and $\delta_{i,min} \leq \delta_i \leq \delta_{i,max}$, for all $i = 1, 2, \ldots, m$. The term t represents the simulation time of the model, $\mathcal{C}$ and W represent the controller and other configuration parameters of the simulation model. In optimisation based V&V analysis, the combination of uncertain parameters that yields a maximum value of the performance criterion $J(\cdot)$ is identified by using one or several optimisation techniques among the different local, global and hybrid optimisation methods.

In these studies, evaluation of the cost function requires the simulation of the model of the dynamics, and the model is treated as a 'black-box' with access limited to certain input and output parameters. This is often the case with many other

industrial models that are used for the purpose of verification and validation of the controllers. The model could be complex, nonlinear and can have large number of uncertain parameters. Here, the uncertain parameters and the measured states which are required to evaluate the performance criteria are considered as inputs and outputs of the 'black-box' model respectively.

2.1.1 A brief survey on optimisation based V&V analysis

In [7], the local gradient based SQP method and gradient free pattern search method have been used for assessing the perturbations that provided the worst case stability margin, which was a performance criterion for the flight clearance problem. The benchmark model was the High Incidence Research Model (HIRM) with 9 aerodynamic uncertainties along longitudinal axis and 15 aerodynamic uncertainties along lateral axis. Longitudinal and lateral cases were analysed separately. A comparison between the local optimisation and the classical gridding based methods were performed to show the superiority of the optimisation techniques. However, local optimisation methods do not guarantee that the worst case perturbations have been found, especially for the non-convex problems.

In order to address this issue, Menon et. al.,[43, 44, 51], utilised global and hybrid optimisation methods for the clearance of the nonlinear flight control laws. The global optimisation methods such as GA and DE were proposed for the flight clearance problems. In addition, novel hybrid algorithms that utilised local optimisation methods were proposed to improve the convergence results when compared with other existing techniques. These methods were applied and compared for the flight clearance problem of a highly augmented aircraft model called Aero-

Data Model In a Research Environment (ADMIRE). The analysis considered a nonlinear clearance criterion based on the angle of attack limit exceedence criterion defined in [7], with a limited number of uncertain parameters, (only 5), and concluded a superior performance for the hybrid DE, when compared with other optimisation techniques such as GA,DE and hybrid GA in terms of the faster convergence to a global/near global solution. Identical results were obtained in [52] on a similar analysis problem of 'medium' complexity, for eg., a flexible satellite with 26 uncertain parameters and in [46, 53] for a flexible launch vehicle with 28 uncertain parameters. In both studies, the uncertainties in configuration, aerodynamic and flexible mode parameters were accounted.

In [54], deterministic global optimisation method based on DIRECT and its hybridised version were applied to a re-usable launch vehicle problem. DIRECT algorithm partitions the normalised parameter space into small hypercubes or boxes and evaluates their centre points. The algorithm aims to find the optimal hypercube containing the global optimum. The worst case perturbations consisting of 8 time varying uncertain parameters were determined for time domain specifications on AoA and AOSS. A comparison with Hybrid Differential Evolution (HDE) and Monte Carlo method was also performed. Hybrid version of DIRECT algorithm performed better than other algorithms, and took less number of function evaluations to attain the global optimum. However, in [55], both conventional and hybrid versions of DIRECT failed on a VEGA launcher model with larger number of uncertain parameters. As the number of uncertain parameters increased, the number of functions evaluations increased, since the partitioned parameter space would have more number of hypercubes to explore. In this case, HDE provided better results than the DIRECT and the Monte Carlo method. A conclusion was

drawn that the DIRECT algorithm suffers from the increase in the dimension of the parameter space.

In [56], two different mutliobjective optimisation methods were employed to determine a worst case solution set, while considering multiple performance metrics simultaneously. First, a fast, elitist, evolutionary multiobjective optimisation algorithm known as Non-dominated Sorting Genetic Algorithm (NSGA)-II is employed. Second, hybrid multi objective optimisation algorithm which adaptively switches between three different strategies such as NSGA-II, differential evolution and the metropolis algorithm is employed.

The Worst Case Analysis Toolbox (WCAT) comprising of several local, global and hybrid optimisation algorithms, that was originally coded in [57][1] was recently significantly modified to WCAT-II and widely distributed in European aerospace industry as part of the study reported in this thesis. Another widely used tool by the aerospace industry is called the Multi-Objective Parameter Synthesis (MOPS), which is developed at the German aerospace centre DLR [58]. MOPS has been used for synthesising and tuning of robust controllers satisfying several design objectives, often some of them conflicting with each other. Recently in [59, 60], the tool has been used to carry out the worst case analysis.

2.2 Analysis framework

A block schematic representation of the key elements of the optimisation based V&V analysis framework is shown in Figure 2.1. The simulation models can be complex, nonlinear and with large number of uncertain parameters. Typically

[1]The work was carried out with the support from European Space Agency (ESA), under the Technical Research Project (TRP) - ESTEC Contract No 19784/06/NL/JD

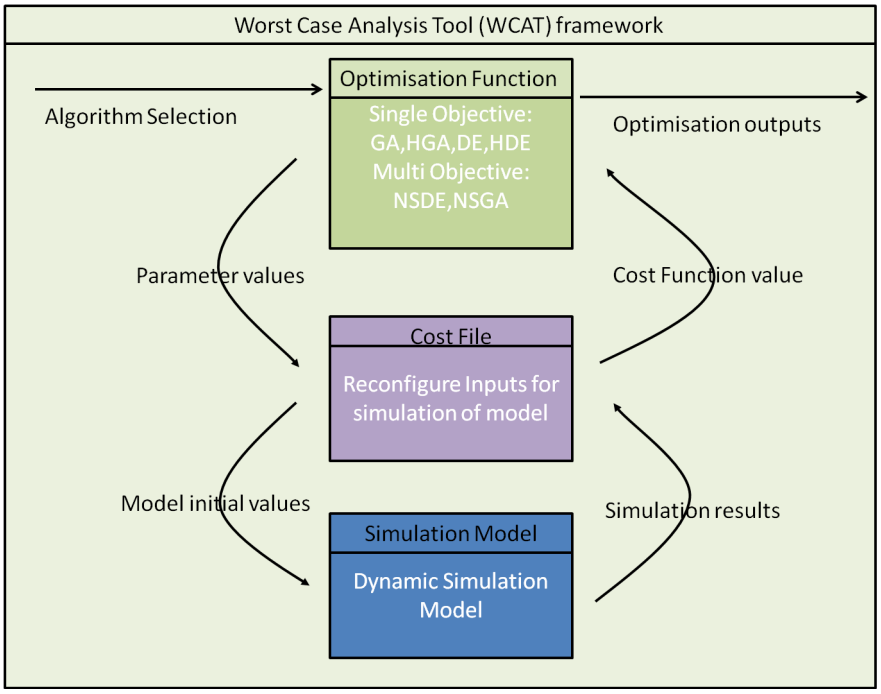

Figure 2.1: Framework of the Worst Case Analysis Tool (WCAT)

in this analysis framework, it is possible to modify the values of the uncertain parameters, and the model can be simulated with these perturbed uncertain parameters. The performance criterion, which is mathematically represented as cost function (J), either in time domain or in frequency domain, is evaluated using the time simulation or frequency sweep of the model. Often the performance criterion is represented as suitable norm (distance) maximisation problem defined on a bounded search space. During each iteration of the optimisation algorithm, WCAT generates a set of candidate uncertain parameters which are associated with their corresponding cost function values. The way a new candidate uncertain parameter is generated, depends on the type of optimisation algorithm selected in the WCAT. This could be any among the local, global (GA,DE) and hybrid (HGA,HDE) optimisation algorithm available. WCAT provides the solution, the

worst case uncertain parameter vector, when convergence to a solution is obtained with a desired accuracy level or computational budget (a finite number of simulations or iterations) is exceeded. The computational budget is usually fixed comparable to standard Monte Carlo simulations. The underlying principle of how the optimisation based V&V analysis framework is utilised to determine the solution can be summarised in the following five steps.

	Steps
i)	Initialise/ configure the simulation model, i.e, initialising the model with the default initial conditions, and the uncertain parameters with nominal values.
ii)	Assign the uncertain parameter variables with the perturbed values, if available.
iii)	Simulate the model for a finite time period.
iv)	Compute the cost function J based on the output data from simulation.
v)	Repeat Steps 2-4, till termination criteria of optimisation algorithm is satisfied.

The optimisation algorithms, that are coded in MATLAB within the WCAT are briefly discussed in sequel.

2.2.1 Local optimisation

In this thesis, the local optimisation technique employed is the gradient based Sequential Quadratic Programming method. The main idea behind the SQP method is to solve a constrained nonlinear optimisation problem using a sequence of quadratic programming subproblems. Consider a constrained nonlinear optimi-

sation problem described as, ([61])

$$\begin{aligned} \min_{\delta} \quad & J(\delta) \\ \text{Subject to} \quad & g_i(\delta) = 0, \quad i \in \mathcal{E} \\ & g_i(\delta) \leq 0, \quad i \in \mathcal{I} \end{aligned} \tag{2.2}$$

where, $\mathcal{E}$ represents the set of equality constraints and $\mathcal{I}$ represents the set of inequality constraints. During each iteration of the SQP, a quadratic subproblem is solved. The constraint function for this subproblem are formed by linearising the constriants of the the optimisation problem in (2.2). The cost function of the subproblem is an quadratic approximation to a Lagrangian function $\mathcal{L}(\delta, \lambda) = J(\delta) - \sum_{i=1}^{dim(\mathcal{E}+\mathcal{I})} \lambda_i^T g_i(\delta)$, where λ is the lagrangian multiplier. The quadratic subproblem modelled at iterate δ_k is given by, ([61])

$$\begin{aligned} \min_{d} \quad & J_k + \nabla J_k^T d + \frac{1}{2} d^T H_k d \\ \text{Subject to} \quad & \nabla g_i(\delta_k)^T d + g_i(\delta_k) = 0, \quad i \in \mathcal{E} \\ & \nabla g_i(\delta_k)^T d + g_i(\delta_k) \leq 0, \quad i \in \mathcal{I} \end{aligned} \tag{2.3}$$

where $d = \delta - \delta_k$, k represents the k^{th} quadratic subproblem, H_k is the Hessian of the Lagrangian. The Hessian is a positive definite matrix consisting of second order derivatives of the cost function and constraints. In the present study, the dynamic simulation model is treated as a 'black-box' and hence the second order derivatives are not available. In such cases, the Hessian is computed using a quasi-Newton

approximation given by:

$$\begin{aligned} H_k &= B_k^{-1} \\ B_{k+1} &= B_k - \frac{B_k S_k S_k^T B_k}{S_k^T B_k S_k} + \frac{Y_k Y_{k^T}}{Y_k^T S_k} \end{aligned}$$

where $S_K = \delta_{k+1} - \delta_k$ and $Y_k = \nabla_\delta \mathcal{L}(\delta_{k+1}, \lambda) - \nabla_\delta \mathcal{L}(\delta_k, \lambda)$. The quadratic subproblem in (2.3) is solved using a standard quadratic programming method called the active-set method. The solution to the quadratic subproblem δ_k is utilised to generate the next iterate by utilising the Line search method ([61])as follows,

$$\delta_{k+1} = \delta_k + \alpha d_k \tag{2.4}$$

where α, is the step-length parameter to generate a sufficient decrease in a merit function. Using the new iterate δ_{k+1} a quadratic subproblem is modelled in the next iteration. This algorithm runs several iterations until the termination criterion is met. In this thesis, SQP method is implemented by utilising the function `fmincon` provided in [62]. The function is implemented with the medium-scale optimisation scheme and the gradients are approximated using the finite difference method. In local optimisation methods, there is a chance that the solution could be trapped in a local optima, and depends on the initial starting point in the uncertain parameter space.

2.2.2 Genetic Algorithms

This is a popular global optimisation algorithm based on the evolutionary principles [63]. The underlying principle is to emulate the evolutionary process in the

nature. This process starts with generating a prerequisite number of randomised combinations of uncertain parameters. These combination of uncertain parameters are termed as the initial *population* and each combination is termed as an *individual* in the population. The cost function J in Eqn. 2.1 is termed as the fitness function. This fitness function is utilised to assign a performance index to each individuals in a population. The population is then used to reproduce new individuals by using genetic operators and a selection process for mating. There are various genetic operators available in literature, refer [64, 65] for general information on GAs and the different genetic operators associated with this approach. In this study, the WCAT software utilises internally the functionalities of the MATLAB GA toolbox. The GA algorithm is described briefly.

1. *Random Initialisation:* The GA algorithm begins by generating an initial population of random individuals in the uncertain parameter space that are constant over iteration.

2. *Evaluation of Fitness Function:* Each member of the current population is used to evaluate the fitness function. Minimum value of fitness function is desired.

3. *Reproduction of child population:* A new population is termed as a child whose entries are generated using individuals of the current population. The individuals in the current population are called parents. The child population is produced using genetic operators like crossover and mutation. The child population is then passed on to the next iteration of the algorithm. Each iteration is termed as generation and the entire process is repeated until maximum generations have exceeded. There are three ways in which a child population is generated,

(a) *Elite Count:* The number of individuals with the best fitness values in the current population that are guaranteed to survive to the next generation. These individuals are termed as elite children. In this study, the default value of Elite count is 2.

(b) *Crossover:* This process refers to those individuals in the child population that are created by combing the vectors of a pair of parents. Two members of the current population are randomly picked for mating crossover process. A randomly generated binary vector is used to select the genes from the parents. When the gene in the binary vector is 1 then the corresponding gene from the first parent is selected, and the gene from second parent is selected when it is 0,[62]. This process is illustrated in Figure 2.2. The fraction of individuals in the next generation, other than elite children, that are created by crossover are set to 0.8 in this study.

(c) *Mutation:* Some individuals of the child population are generated by applying random variations to a single individual in the current population. The algorithm generates random direction that are adaptive with respect to the last successful or unsuccessful generation [62].

GA's are very popular and it has a better chance of converging to a global optimum as compared to the local optimisation methods. This algorithm has been popular among optimisation based V&V methods since its application on flight clearance problems [51]. In recent years, several researchers have applied genetic methods to a wide variety of problems in the aircraft design optimisation, structural optimisation, and flight control problems in the aerospace science field. There are also many different applications in other fields of science, for example [66] have applied

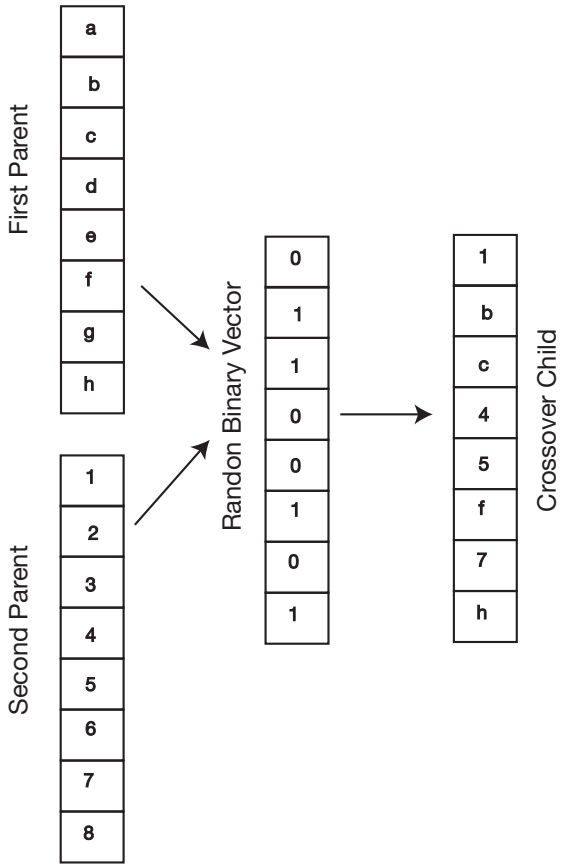

Figure 2.2: Crossover process in GA

evolutionary algorithms for prediction of protein structures. In [67], GA has been applied in the field of designing drugs. A review of GA as applied in the area of electromagnetics is provided in [68].

2.2.3 Differential Evolution

Differential Evolution (DE) method was first introduced by Storn and Price in [69] and is based on evolutionary principles. The results obtained by DE have been observed to be better than other evolutionary algorithms, both in terms of accuracy and computational overhead [51]. This method like GA starts with

random initial population. A new search point is generated by adding the weighted vector difference between two randomly selected individuals from the population with a third randomly chosen individual. The vector difference determines the search direction and a weighting factor decides the step size in that particular search direction. The DE methodology is briefly outlined as follows:

1. *Random initialisation:* The initial population consists of individuals that are chosen randomly over the parameter space. The size of the population is kept constant at N_p during all iterations of the DE algorithm. Each member of the population can be represented as $\mathbf{x_i} = [x_{1i}\ x_{2i}\ \ldots\ x_{di}]$, where $\mathbf{i} = 1, \ldots, N_p$ and d the total number of parameters.

2. *Evaluation of Fitness Function:* Cost function is evaluated for each member of the initial population. Minimum value of the cost function is desired.

3. *Mutation:* In this step, three uncertain parameter vectors are chosen randomly from the current population to generate new candidate members. The difference between the two vectors from the current population is scaled and added another randomly chosen third vector.

$$\bar{\mathbf{x}}_\mathbf{n}^{G+1} = \mathbf{x_k}^G + F_m D_{ij}, \qquad D_{ij} = \mathbf{x_i}^G - \mathbf{x_k}^G \tag{2.5}$$

   where F_m is the mutation factor that can be set between [0 1], G represents the iteration number.

4. *Crossover:* In this step, a new candidate individual $\mathbf{x_n}^{G+1}$ is reproduced from the mutant vector $\bar{\mathbf{x}}_\mathbf{n}^{G+1}$ and a parent individual $\mathbf{x_n}^G$. A random number is generated between [0 1] and compared with crossover factor $\rho_c \in [0\ 1]$. If

the random number is greater than the cross over factor then the parent is selected for the next iteration or else mutant vector is selected.

5. *Evaluation and Selection:* The cost function value for the new candidate $\mathbf{x_n}^{G+1}$ is evaluated. If the new candidate $\mathbf{x_n}^{G+1}$ has better cost function value than the parent $\mathbf{x_n}^{G}$, then $\mathbf{x_n}^{G+1}$ is selected to be the new member of the population for the next iteration. Otherwise $\mathbf{x_n}^{G}$ is selected and subsequently identified as $\mathbf{x_n}^{G+1}$.

6. *Termination criterion:* In the present study, a fixed termination criterion is utilised such that the total number of function evaluations does not exceed 1000.

For more details on the algorithm, refer [51, 69]. There are variants DE available based on the various operators that are employed. The one preferred in general and the one which is employed in the present studies is referred as DE/rand/1/bin. DE has been applied to problems in different fields of science, with promising results. For example in [70], the DE method has been applied in the field of electromagnetics. In [71], the DE method has been applied and compared with other local and global optimisation schemes in an aerodynamic shape optimisation problem for an aerofoil.

2.2.4 Hybrid evolutionary optimisation

With the use of local optimisation alone the chances of getting locked into a local optimum are high, particularly since there is little information available with which to choose a good initial starting point. If the initial guess is close to the true

worst case, however, local optimisation methods can converge to the global optimum extremely quickly. Global optimisation methods, on the other hand, have a high probability of converging to the global solution, if allowed to run for a long enough time with a sufficient initial population and reasonably correct probabilities. Their rate of convergence can be very slow and moreover, there is still no guarantee of convergence to the true global solution. In order to try to get the best from both schemes, several researchers have proposed combining the two approaches, [72, 73]. In such hybrid schemes there is the possibility of incorporating domain knowledge, which gives them an advantage over a pure blind search based on evolutionary principles such as GAs. Most of these hybrid schemes apply a technique of switching from the global scheme to the local scheme after the first optimisation algorithm finishes its search or optimisation. In [74], some guidelines are provided on designing more sophisticated hybrid GAs, along with experimental results and supporting mathematical analysis. In a similar way, the conventional DE methodology was augmented by combining it with a downhill simplex local optimisation scheme in [75]. At each iteration the local optimisation was applied to the best individual in a current random set. This hybrid scheme was applied to an aerofoil shape optimisation problem and was found to significantly improve the convergence properties of the method. There are many local optimisation schemes available and there are also different ways of hybridising the algorithms. However, the common aim of these schemes is to provide faster convergence to the true global solution. Refer [52] for further details on hybrid algorithms and its implementation in WCAT.

In sequel, the optimisation based V&V is carried out for three distinct scenarios which have not been considered in previous studies.

2.3 BIOMASS: A flexible satellite model

A flexible satellite benchmark model was provided by Astrium UK as part of the project "Modern Attitude Control for EO Satellites with Large Flexible Elements" an European Space Agency (ESA) Technical Research Project (TRP). This benchmark is based on a realistic satellite model that describes the dynamics of the model used in BIOMASS mission. Large number of uncertain parameters, emanating from rigid and flexible modes of the satellite are considered. For performing V&V analysis, the performance criteria considered is based on the frequency domain specifications

BIOMASS mission aims to collect scientific data relating to the global forest biomass distribution, annual changes thereof and their interaction with the carbon cycle, [76, 77]. It is a satellite radar mission operating at P-Band which is considered as a candidate for ESA 7^{th} Earth Explorer mission. Ariane space Vega launcher will be used to place the spacecraft into a sun-synchronous orbit while flying at an attitude of 600km. In order to achieve its objectives, Synthetic Aperture Radar (SAR) system with reflector antenna concept is positioned towards the dark side of the orbit [77]. The key point is that large size and flexibility of the antenna influences the design of Attitude and Orbital Control System (AOCS). Particularly, disturbance torques generated by the atmospheric drag and gravity gradient in low Earth orbit could also act on the large antenna [77]. Furthermore, the excitation of flexible modes along with the coupling of the flexible structures such as antenna and solar array degrade the mission performance considerably. Hence, there is a need to assess the robustness of the AOCS controller, and determine the worst case perturbations for which the AOCS exhibits poor performance,

or complete loss of control.

The BIOMASS simulator consists of a mechanical model ($\mathbf{G}_{mec}$), Reaction Wheel (RW) model ($\mathbf{G}_{RW}$), a delay ($\mathbf{G}_{delay}$) and a controller (AOCS) in feedback. The mechanical model ($\mathbf{G}_{mec}$) consists of a rigid platform on which the SAR payload along with the solar array is mounted. Propellant slosh effects are taken into account and the baseline propulsion system consists of a conventional monopropellant system with two propellant tanks (58 litre volume), operated in blow-down configuration [77]. The reaction wheel model $\mathbf{G}_{RW}$ corresponds to the dynamics of the Reaction Wheel (RW) system, and a standard 1^{st} order lag filter of the form,

$$G_{RW} := \frac{T_{act}(s)}{T_{dem}(s)} = \frac{1}{(1+\tau s)} \tag{2.6}$$

where $T_{dem}(s)$ is the demanded torque signal sent to the RW subsystem from the controller, $T_{act}(s)$ is the actual actuated torque (applied to the plant), and τ is the delay in seconds, captures the required dynamics. $\mathbf{G}_{delay}$ corresponds to the delay in-the-loop modelled as a 4th order Pade Approximation [77]. Controller block corresponding to the AOCS system is an H_∞ controller developed as in[77]. The H_∞ controller is designed to reject the disturbance torques generated by the atmospheric drag, solar radiation pressure, magnetic torque and gravity-gradient; and provide robust stability and performance with respect to the specifications in Table 2.1, in the presence of the uncertainties which are listed in sequel.

2.3.1 Uncertain parameters

The robustness of the controller has to be assessed in the presence of the uncertain parameters emanating from the four elements of the satellite such as central rigid platform, antenna, solar array and slosh dynamics of the satellite model. In total, 132 uncertain parameters are considered, which are, masses of all the four elements (4 in total), moments of inertia of all the four elements (6 per element, 24 in total), modal participations of those elements with flexible modes, i.e., antenna, solar array and slosh (3 per element, 12 in total), cantilever frequency of all flexible modes (15 for antenna, 12 for solar array and 6 for slosh, 33 in total), cantilever damping of all flexible modes (15 for antenna, 12 for solar array and 6 for slosh, 33 in total), x, y and z axis components of Center of Mass (CoM) vector for all the elements (3 per element, 12), translation and rotation of the interface of all the appendages with the central rigid platform (3 per element,12 in total) and time constants for $\mathbf{G}_{delay}$ and $\mathbf{G}_{RW}$, (2 in total). The uncertainties are all normalised to vary between ± 1 and scaling is addressed internally in the simulation model.

2.3.2 Specifications

The H_∞ controller is designed in order to achieve two main specifications listed in Table 2.1. The satisfaction of these specifications indicates a good robust performance of the design. Robust performance is achieved when the system satisfies the performance specifications for all the perturbed plants about the nominal model up to the worst-case model uncertainty [78].

Table 2.1: Functional performance requirements: BIOMASS

Specification Description	Requirement
$\mathbf{s}_1$: Maximum singular value of the sensitivity function $S(j\omega)$	$< 6dB$
$\mathbf{s}_2$: Maximum singular value of complementary sensitivity function $T(j\omega)$	$< 6dB$

2.3.3 Worst case analysis

In previous studies reported in [43, 44, 51, 79], specifications on the time domain performance have been considered. Contrary to this, frequency domain specifications similar to that considered in [52], but with significantly large number of uncertain parameters, have been considered. In order to investigate whether there exist an uncertain parameter combination within its bounds that can cause a violation of an requirement, the specifications are considered as cost functions. The problem is formulated as a maximisation problem as follows.

$$\begin{aligned} J_S &= \max_{\omega} \bar{\sigma}(S(j\omega)) \\ J_T &= \max_{\omega} \bar{\sigma}(T(j\omega)) \end{aligned} \tag{2.7}$$

The worst case perturbation is determined using different optimisation algorithms such as SQP, GA, DE, HGA and HDE. The results are compared in terms of accuracy and complexity. To have a fare comparison, a fixed computational budget, i.e. the maximum number of function evaluations allowed for each optimisation techniques is set to 1000. Different configuration parameters for the optimisation algorithms have been chosen according to the suggestions in the published works [44, 52, 54]. For DE, population size is set to 25, the crossover factor, which is used to generate new members of the population which are utilised for next gen-

eration, is set to 0.8. The mutation factor which is used to generate a mutant vector during each generation of DE is set to 0.8. For GA, population size is set to 10. Migration fraction, i.e. the fraction of those individuals scoring the best value that will migrate, is set to 0.2. Crossover fraction, i.e. the fraction of genes swapped between individuals is set to 0.8. For hybrid GA, local optimisation is performed at the end of GA, where as for DE, local optimisation is performed when there is no improvement in cost function values for two successive iterations. The maximum iterations performed by the local optimisation for both hybrid GA and DE is set to 30.

Worst case analysis results from various optimisation algorithms along with Monte Carlo results are tabulated in Table 2.2. Table 2.2 gives the maximum singular values of sensitivity and complementary sensitivity functions and the total number of simulations performed by each algorithm to generate worst case result. With the fixed computational budget termination criterion, it can be seen from the Table 2.2 that HDE algorithm is capable of violating sensitivity function ($\max_{\omega}\bar{\sigma}(S(j\omega)) = 6.1145$ dB). A Monte Carlo simulation of 1000 campaigns is performed for comparison. Even though Monte Carlo results for sensitivity function ($\max_{\omega}\bar{\sigma}(S(j\omega)) = 4.9402$ dB) does not violate the performance criteria, it provides better results as compared to SQP, GA and Hybrid Genetic Algorithm (HGA). Performance of SQP depends on the initial condition which was chosen randomly. An intelligent choice of initial condition based on designer expertise can improve the performance of SQP algorithm. An increase in population/generation size of GA/HGA could provide better results but this has not been investigated further since the objective of the consortium was to identify optimisation algorithms which could potentially give very good solutions with a fixed computational budget, fixed

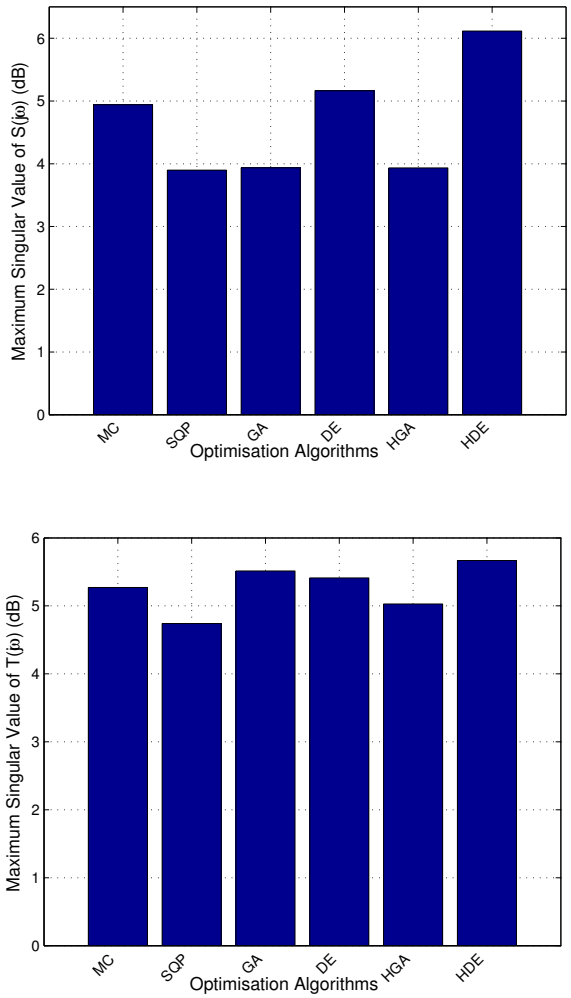

Figure 2.3: Optimisation technique comparison

at 1000. For co-sensitivity function T, no performance violation is recorded for any optimisation techniques. Even so, HDE provides better result when compared to other optimisation techniques.

Figure 2.3, shows the worst case trend based on the performance criteria on S and T functions for algorithms. It is observed that HDE and DE perform better than other techniques when the optimisation parameters are set to the default values and maximum function evaluations are restricted to 1000 simulations. Identical

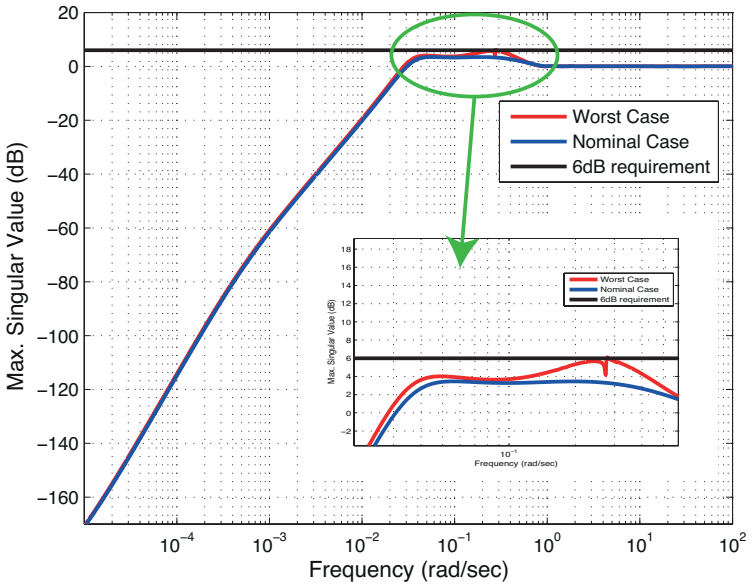

Figure 2.4: Worst Case and Nominal plot comparison for $S(j\omega)$:HDE Algorithm

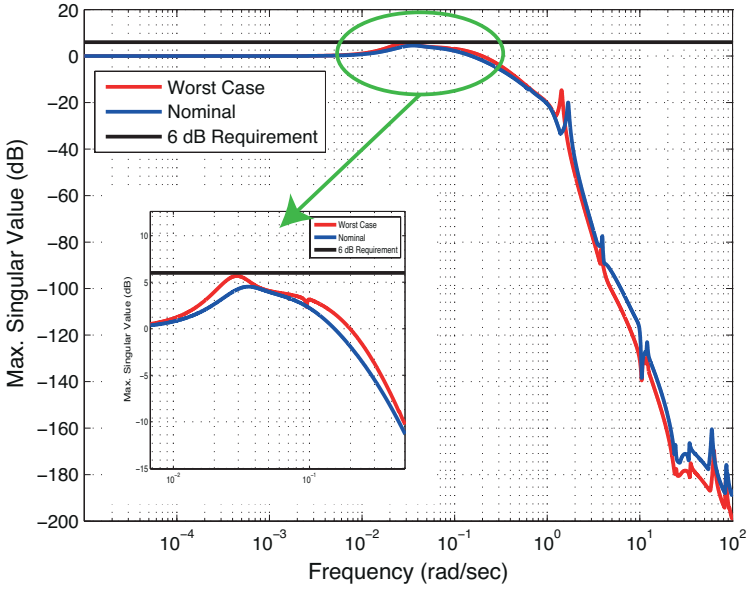

Figure 2.5: Worst Case and Nominal plot comparison for $T(j\omega)$: HDE Algorithm

Table 2.2: Worst case values of S & T

	Criteria	MC	SQP	GA	DE	HGA	HDE
$\max_{\omega}\bar{\sigma}(S(j\omega))$	< 6	4.9402	3.8982	3.9367	5.1637	3.9334	6.1145
$\max_{\omega}\bar{\sigma}(T(j\omega))$	< 6	5.2716	4.7397	5.5134	5.4110	5.0277	5.6677

performance of HDE and DE, when compared to other optimisation algorithms, have been reported previously in [43, 44, 52, 55] for lower order problems. The worst case and nominal plots for sensitivity and co-sensitivity functions as generated by HDE algorithm is shown in Figure 2.4-2.5. Here the concept of using HDE and DE has been validated and demonstrated to be effective even in the case of flexible systems with large number of uncertainties. Furthermore, the solutions are obtained with a reasonable computational effort, and infact significantly better than many other existing simulation based techniques including Monte Carlo and several other optimisation techniques. In addition, the robustness of optimisation parameter setting is also demonstrated.

2.4 Launch vehicle model

To study the impact of uncertainties, roll coupling and external wind perturbation on frequency and time domain specifications of a launch vehicle in its TVC phase, Astrium Space Transportation Ltd., France provided flexible launch vehicle models as a part of the project SAFE-V an ESA TRP[1]. In this study, two different models of the launch mission are considered. Each model focus on separate aspects of the launch mission. Each model and the specific analysis carried out with that model are explained in sequel.

[1] "*Robust Flight Control System Design Verification and Validation Framework*" Contract No. 4000102288 with Astrium Space Transportation, ESA project

2.4.1 Roll coupling benchmark

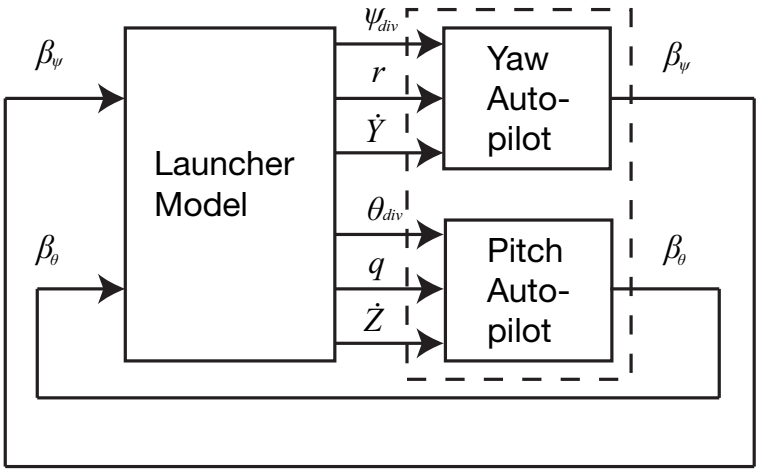

Figure 2.6: 3-axis launcher control loop

During the atmospheric flight phase of the launcher, the perturbations on the solid rocket motor, aerodynamics and the Centre of Gravity (CoG) offset parameters may induce an undesired roll torque. Main Roll Attitude Control System (RACS) can be used to control the roll rate to zero all the time. However, utilising RACS all the time would lead to the propellant consumption, and as a consequence will affect the overall performance of the mission. Hence, often the solution is to allow a limited roll rate to be built up, and activate the RACS only when the roll rate exceeds an acceptable pre-defined threshold. The yaw and pitch axis are coupled in the presence of roll rate. When the roll rate of the vehicle exceeds the acceptable limits, the coupling effect could lead to excessive rotations in the pitch, roll and yaw axes. The benchmark, in this section deals with the impact of roll coupling on the launcher control during the ascent phase of TVC launcher and in the presence of several uncertainties. The aim is to analyse the stability of the 3 axis launcher model without roll attitude control during the ascent phase,

so that the extreme behaviour emanating due to the roll coupling effect can be studied.

Figure 2.6, presents the general structure of the 3 axis launcher control loop of the benchmark. There are yaw and pitch auto-pilots, the controller does not include any gyroscopic compensation. The state space representation of the launcher model under consideration is given below.

$$\dot{x} = Ax + Bu \tag{2.8}$$

where $x = \begin{bmatrix} \psi_{div} & q & \dot{Z} & \theta_{div} & r & \dot{Y} \end{bmatrix}^T$, $u = \begin{bmatrix} \beta_{R\psi} & \beta_{R\theta} \end{bmatrix}^T$. The plant and input distribution matrices are respectively:

$$\begin{aligned} A &= \begin{bmatrix} 0 & 1 & 0 & p & 0 & 0 \\ A_{6\psi} & 0 & A_{6\psi}/V & 0 & p(I_{yy} - I_{xx})/I_{zz} & 0 \\ -a_\psi - \gamma & 0 & -a_\psi/V & 0 & 0 & p \\ -p & 0 & 0 & 0 & 1 & 0 \\ 0 & -p(I_{zz} - I_{xx})/I_{yy} & 0 & A_{6\theta} & 0 & A_{6\theta}/V \\ 0 & 0 & -p & -a_\theta - \gamma & 0 & -a_\theta/V \end{bmatrix} \\ B &= \begin{bmatrix} 0 & K_{1\psi} & -\gamma_T & 0 & 0 & 0 \\ 0 & 0 & 0 & 0 & K_{1\theta} & -\gamma_T \end{bmatrix}^T \end{aligned} \tag{2.9}$$

where ψ_{div} is the launcher yaw angle deviation w.r.t the commanded yaw angle (in radians), θ_{div} is the launcher pitch angle deviation w.r.t the commanded pitch angle (in radians), p, q, r are the angular rate (rad/s) in the roll, pitch and yaw axis respectively ,Y and Z are the transverse accelerations (m/s^2) along y and z axis. The input signals $\beta_{R\psi}$ and $\beta_{R\theta}$ are the realised actuator deflections (in radians)

along yaw and pitch axis. V is the absolute velocity (m/s) of the launcher, and I_{xx}, I_{yy} and I_{zz} are the principal moments of inertia in x, y, z axis respectively.

$$A_{6\psi} = \frac{QS_{ref}C_{N\alpha\psi}L_f}{I_{yy}}, \quad A_{6\theta} = \frac{QS_{ref}C_{N\alpha\theta}L_f}{I_{zz}}, \quad K_{1\psi} = \frac{P_C l_{tu}}{I_{yy}}, \quad K_{1\theta} = \frac{P_C l_{tu}}{I_{zz}},$$
$$a_\psi = \frac{1}{2}\rho V^2 S_{ref}\frac{C_{N\alpha\psi}}{mass}, \quad a_\theta = \frac{1}{2}\rho V^2 S_{ref}\frac{C_{N\alpha\theta}}{mass}, \quad \gamma = \frac{thrust-drag}{mass}, \quad \gamma_T = \frac{thrust}{mass}$$

where, Q, S_{ref}, $C_{N\alpha\psi/\theta}$, L_F, P_C, l_{tu} and V_r are dynamic pressure, reference area, normal aerodynamic force coefficients derivative w.r.t angle of attack expressed in body frame, distance between CoG and Centre of Pressure (on longitudinal axis), commanded thrust level, position of nozzle rotation point w.r.t launcher CoG, absolute velocity and relative velocity respectively.

In this analysis, the impact of the roll coupling on the MIMO stability margins is studied. An H_∞ controller is designed and provided in the yaw and pitch axis alone, and the roll is not controlled. The controller is a gain scheduled controller where the scheduling variable is time. Previously, the MIMO stability margins have been evaluated for multi loop flight control systems in [14], and for the VEGA launcher model in [80]. In [14], exact MIMO stability margins are evaluated by inserting the negative value of the inverse of the open loop transfer function at the input channels of the model. This would destabilise the closed loop system, and the locus of negative value of inverse of the open loop transfer function is utilised to evaluate the MIMO stability margins. Whereas, in [80], MIMO stability margins are evaluated by perturbing all the input channels at the same time. The value of the perturbation which just destabilises the closed loop system gives the MIMO stability margins. European aerospace industry have been using a tool that was developed in MATLAB to evaluate the MIMO margins based on [14]. However,

the use of this tool in the optimisation based V&V framework took considerable time, in the order of minutes to evaluate single function evaluation. Later, a tool based on [80] was developed to conduct the analysis in this study and explained in sequel.

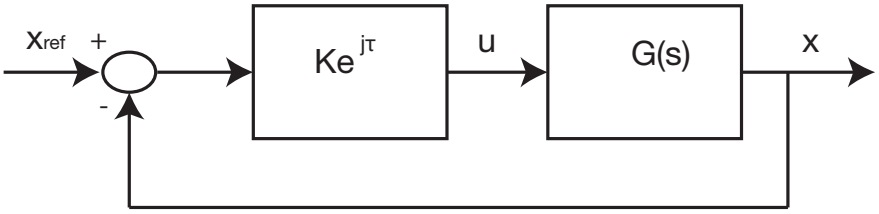

Figure 2.7: A complex perturbation introduced at the plant input u

The underlying concept for evaluating the MIMO stability margins is an extension of the Single Input Single Output (SISO) stability margins. In the case of a SISO system, a complex perturbation $Ke^{j\tau}$is introduced at the input of the plant, as shown in Figure 2.7. Let $K^*e^{j\tau^*}$ be the value of the complex perturbation associated with the first occurrence of destabilisation of the closed loop SISO system. Then the amplitude K^* and phase τ^* of this complex perturbation is used to evaluate the gain and phase margin respectively as.

$$\begin{aligned} \text{Gain Margin } Gm &= -20\log_{10}(K^*) \\ \text{Phase Margin } Pm &= \frac{\tau^* 180}{\pi} \end{aligned}$$

In [80], the idea is extended to MIMO system. For a MIMO system, a square diagonal complex perturbation matrix $Diag[K_i e^{j\tau_i}]$ is introduced at the MIMO plant inputs, were the i^{th} diagonal element corresponds to the complex perturba-

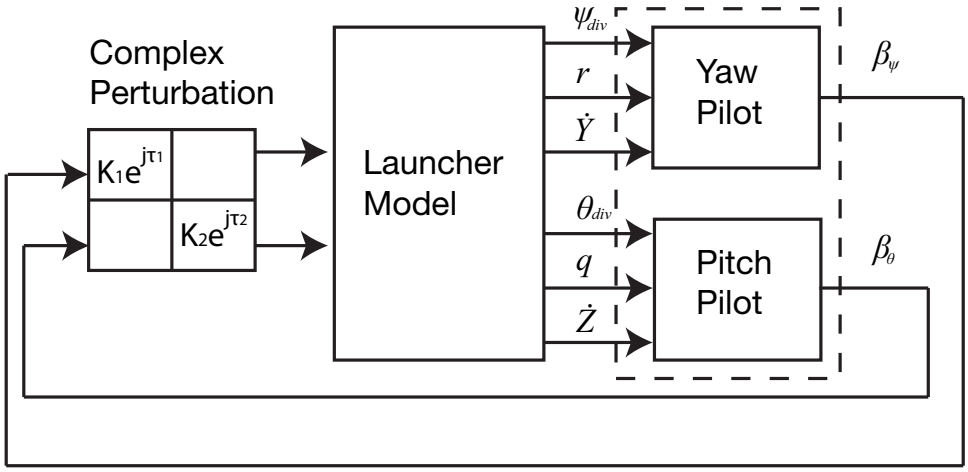

Figure 2.8: Schematic representation for evaluation of MIMO Margins

tion applied to the i^{th} input of the plant. The schematic representation is shown in Figure 2.8. Though the approach is conservative, the values of K_i and τ_i are varied separately to evaluate the MIMO gain and phase margins respectively.

LF and HF gain margins are evaluated in this study. Figure 2.9 shows the evaluation of LF,HF and phase margins for a SISO system. LF margin is defined as the magnitude of the open loop transfer function at the crossing of the vertical axis at $-180°$ above 0dB. HF margin is defined as the magnitude of the open loop transfer function at the crossing of the vertical axis at $-180°$ below 0dB. Phase margin is the value of the phase of the transfer function at the crossing of 0dB axis.

For a MIMO system, the LF gain margin is computed when the amplitude K_i has values less than 1 ($K_i < 1$), since this corresponds to the magnitude of the open loop transfer function at the crossing of the of the vertical axis at $-180°$ above 0dB in Figure 2.9. Similarly, for HF gain margin the amplitude K_i has values greater than 1, $K_i > 1$. Let $K_1^* e^{-j\tau_1^*}$ and $K_2^* e^{-j\tau_2^*}$ be the value of complex

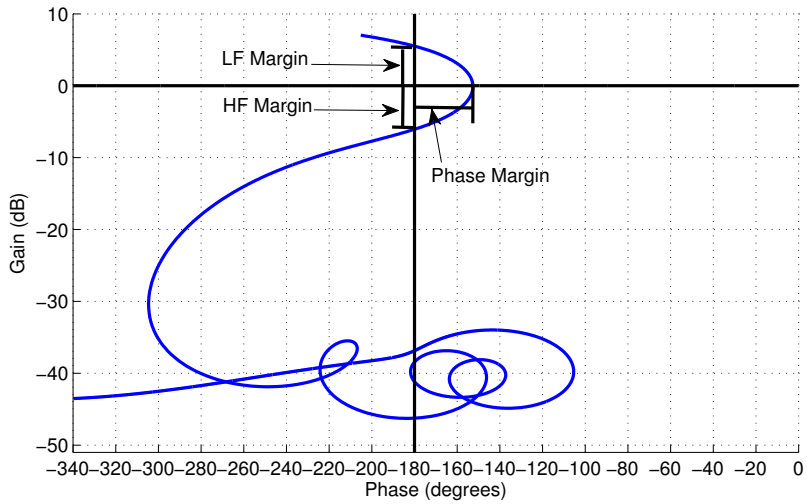

Figure 2.9: Nichols plot of a SISO system showing LF, HF and phase margins

perturbations introduced in both input channels simultaneously. These values are associated with the first occurrence of the destabilisation of the closed loop MIMO system. Then the gain and phase margins can be determined for each input using

$$\begin{aligned}
\text{Gain margin in yaw axis } Gm_\psi &= -20\log_{10}(K_1^*) \\
\text{Gain margin in pitch axis } Gm_\theta &= -20\log_{10}(K_2^*) \\
\text{Phase margin in yaw axis } Pm_\psi &= \frac{\tau_1^* 180}{\pi} \\
\text{Phase margin in pitch axis } Pm_\theta &= \frac{\tau_2^* 180}{\pi}
\end{aligned}$$

Then the MIMO gain and phase margins can be evaluated as,

$$\begin{aligned}
Gm &= \min(Gm_\psi, Gm_\theta) \\
Pm &= \min(Pm_\psi, Pm_\theta)
\end{aligned}$$

In this study, the complex perturbations are varied simultaneously and equally in all input channels i.e. $K_1 = K_2$ and $\tau_1 = \tau_2$. In the current model the pitch and yaw channels are coupled, through the angular rate in the roll axis.

2.4.2 Uncertainties

In this benchmark, the uncertainties emanating from the rigid mode alone are considered. These uncertainties are listed in Table 2.3 and vary uniformly between $[-1,\ 1]$.

Table 2.3: Variability of rigid mode uncertain parameters

Name	Description	Nominal Value	Variation
MI_{xx}	Inertia	0	$[-1,\ 1]$
MI_{yy}	Inertia	0	$[-1,\ 1]$
MI_{zz}	Inertia	0	$[-1,\ 1]$
MP	Thrust	0	$[-1,\ 1]$
$MC_{z\theta}$	Normal Aerodynamic coefficient along pitch axis	0	$[-1,\ 1]$
$MC_{z\psi}$	Normal Aerodynamic coefficient along yaw axis	0	$[-1,\ 1]$
$MX_{f\theta}$	Centre of pressure along pitch axis	0	$[-1,\ 1]$
$MX_{f\psi}$	Centre of pressure along pitch axis	0	$[-1,\ 1]$
MQ	Dynamic pressure	0	$[-1,\ 1]$
MX_g	Centre of gravity	0	$[-1,\ 1]$
MM	Mass	0	$[-1,\ 1]$
MC_x	Axial Aerodynamic coefficient	0	$[-1,\ 1]$

2.4.3 Specifications

In order to validate the controller in the presence of uncertainties and increasing roll rate, the performance specifications are defined for V&V analysis in Table 2.4.

2.4.4 Worst case analysis

The specifications given in Table 2.4 are used to formulate the following minimisation problem as follows:

Table 2.4: MIMO stability specifications

Specification Description	Stability Margins
s_1: Minimum value of LF open loop gain margin	$= 0$ dB
s_2: Minimum value of HF open loop gain margin	< 2 dB
s_3: Minimum value of phase margin	$< 20°$

$$\begin{aligned} \min \quad & J_i \\ \text{Subject to} \quad & \delta_{i,min} \leq \delta \leq \delta_{i,max} \end{aligned} \tag{2.10}$$

where J_i becomes

$$\begin{aligned} J_1 &= \min Gm_{LF} \\ J_2 &= \min Gm_{HF} \\ J_3 &= \min Pm \end{aligned} \tag{2.11}$$

where Gm_{LF} and Gm_{HF} corresponds to the LF and HF gain margins respectively. The worst case perturbation vector corresponding to the uncertainties described in Table 2.3 has been identified for each of the cost functions defined in (2.11). Note that the complex perturbation $K_i e^{-j\tau_i}$ are not treated as uncertainties, and the values of K_i and τ_i are varied separately inside each cost function until the first occurrence of instability. A promising candidate optimisation methodology as claimed in references [44, 52, 53], hybrid differential evolution (HDE) with default optimisation setting is considered here with a fixed termination criteria of 1000 simulations, population size of 30, mutation scale factor of 0.8 and crossover factor of 0.8. The local optimisation method used in the hybridisation strategy of HDE is SQP. The maximum number of local iterations is set to 30. These optimisation tuning parameters provided promising results, similar to the other studies reported in [44, 52, 54].

As discussed in [80], the minimum and maximum value of the roll rate occurs at 20 and 58 seconds respectively of the launcher flight time. Hence these time instances are chosen for performing the worst case analysis. At these time instance the effect of increasing roll rate on MIMO stability margins are studied. Five different roll rates, 10, 20, 30, 40 and 50 deg/sec are considered for the analysis. The worst case stability margins are evaluated and are reported in the Table 2.5.

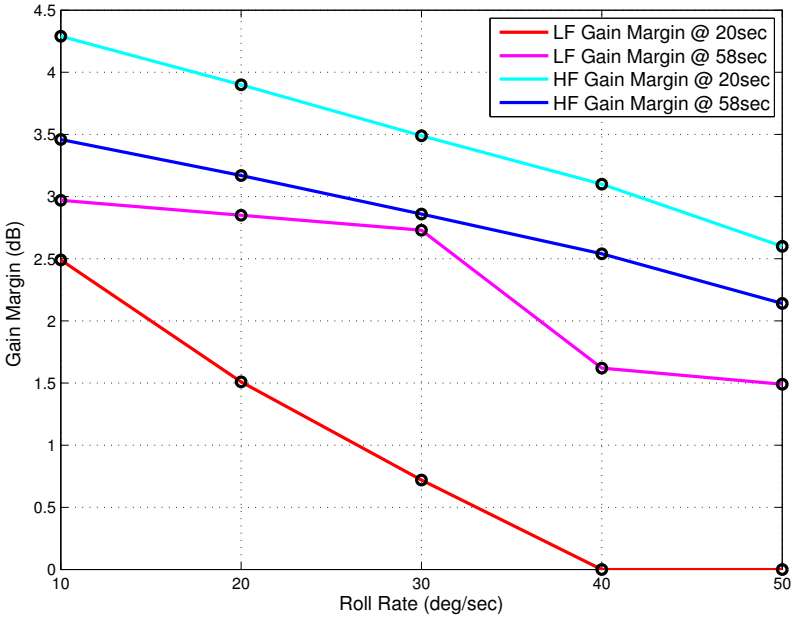

Figure 2.10: Degradation of MIMO margins

When increasing the roll rate for a fixed nominal configuration, it can be seen from Figure 2.10 that the stability margins degrade. As the roll rate increases, the oscillations are induced along yaw and pitch axis, and these oscillations eventually lead to instability of the MIMO system. Unstable cases are found at the time instant of 20 seconds, for the roll rates 40 and 50 deg/s. In particularly, the

performance specification on the open loop LF gain margin and the phase margin are violated, whereas the specifications on the open loop HF gain margin are within acceptable limits. It is observed that the LF margin and phase margin worst case values are larger at 58 seconds, where as the trend is reversed for HF margin and occur at 20 seconds. A high roll rate during initial part of the flight phase reduces the LF and phase margin considerably, whereas a high roll rate during the latter part of the flight reduces HF gain margin. From the results, we can draw a conclusion that a high roll rate occurring at the during the initial part of the flight time can degrade the LF and phase margins to the point of instability, wheres the roll rates occurring at the later part of the flight time are not that severe. It is also observed that the worst case parameter combinations corresponding to performance criteria violations of LF and phase margins at 20 seconds are not at their bounds.

Table 2.5: Worst case results for roll coupling benchmark

Cost Function	Time (sec)	Roll Rates (deg/sec)				
		10	20	30	40	50
		Worst case values				
LF Margin $= 0dB$	20	2.49	1.51	0.72	0	0
	58	2.97	2.85	2.73	1.62	1.49
HF Margin $< 2dB$	20	4.29	3.9	3.49	3.1	2.6
	58	3.46	3.17	2.86	2.54	2.14
Phase Margin $< 20deg$	20	24.06	21.77	18.91	5.72	0.01
	58	18.33	16.61	14.89	13.17	10.88

2.4.5 Thrust Vector Control (TVC) benchmark model

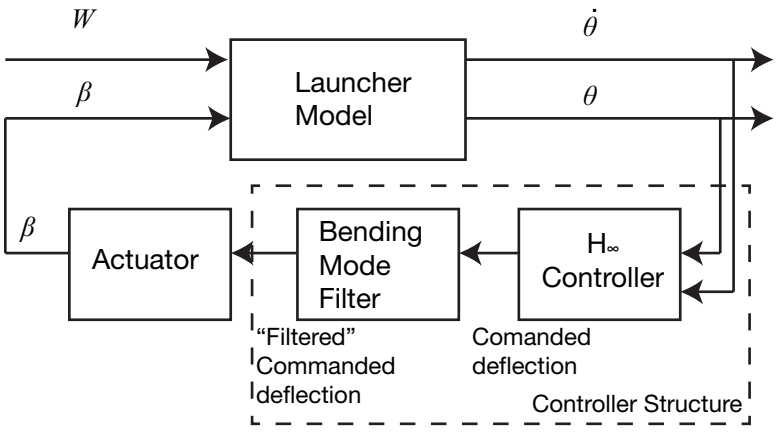

Figure 2.11: Block description of the flexible launcher vehicle

This benchmark model consists of a single axis, parameter varying model [81], derived by linearisation of complete non-linear dynamic equations of motion of the flexible launcher about different equilibrium flight conditions, is considered as the benchmark for this study. A H_∞ controller is provided for the pitch control of the launcher during the atmospheric flight phase from take-off to tail-off [81]. Rigid and bending mode dynamics together with an actuator, bending mode filter and a H_∞ controller are modelled, and implemented in MATLAB simulink . The rigid body dynamics during the atmospheric flight phase is described by the following three state representation:

$$\begin{bmatrix} \ddot{\theta} \\ \dot{\theta} \\ \ddot{Z} \end{bmatrix} = \begin{bmatrix} 0 & A_6(t) & A_6(t)/V(t) \\ 1 & 0 & 0 \\ 0 & A_1(t) & -A_6(t)\alpha_3(t) \end{bmatrix} \begin{bmatrix} \dot{\theta} \\ \theta \\ \dot{Z} \end{bmatrix} + \begin{bmatrix} K_1(t) & -A_6(t)/V(t) \\ 0 & 0 \\ K_2(t) & A_6(t)\alpha_3(t) \end{bmatrix} \begin{bmatrix} \beta \\ W \end{bmatrix} \tag{2.12}$$

where, $\mathcal{C}ol(\dot{\theta}, \theta, \dot{Z})$ are states of the rigid mode dynamics of the launcher and

corresponds to pitch rate (deg/sec), pitch angle (deg) and drift velocity (m/sec) in the body frame respectively. β_R and W represents the realised control input deflections around the nominal value to follow the reference trajectory and the wind perturbation respectively.

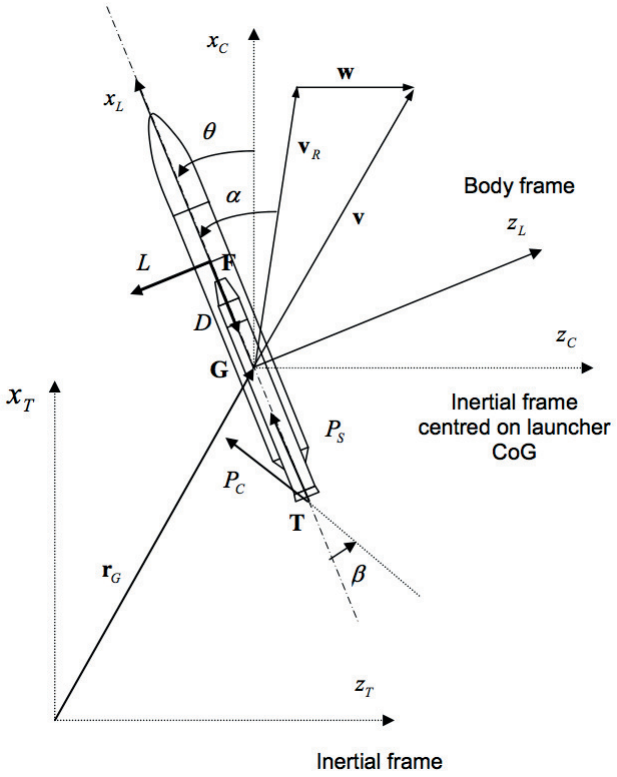

Figure 2.12: Single axis flexible launcher model([1])

In (2.12) aerodynamic efficiency A_6, thrusters efficiency K_1 and K_2 and α_3 are time varying parameters along the trajectory and are defined as follows [81]:

$$\begin{aligned} A_1 &= -\frac{P_C + P_S}{m} + \frac{QS_{ref}}{m}(C_A - C_{N\alpha}) \\ A_6 &= \frac{QS_{ref}C_{N\alpha}L_F}{I} \\ K_1 &= \frac{P_C l_{tu}}{I}, \quad K_2 = -\frac{P_C}{m}, \quad \alpha_3 = \frac{I}{mV}L_F \end{aligned}$$

Table 2.6: TVC launcher notations

Notations	
θ	Launcher pitch angle
α	Angle of attack
β	Deflection angle
ξ_i	i^{th} bending mode damping
ω_i	i^{th} bending mode pulsation
C_A	Axial aerodynamic force coefficient
$C_{N\alpha}$	Normal aerodynamic force coefficient
D	Drag in body axis
F	Aerodynamic focus or Centre of Pressure
G	Launcher Centre of Gravity
h_{tu_i}	i^{th} bending mode deformation at nozzle rotation point
h_{ptu_i}	i^{th} bending mode slide of deformation at nozzle rotation point
I	Total inertia
I_T	Nozzle pitch inertia
L	Lift in body axis
L_F	Distance between CoG and Centre of Pressure
L_{tu}	Position of nozzle CoG respective to nozzle rotation point
l_{tu}	Position of nozzle rotation point w.r.t. centre of gravity
M_{tu}	Nozzle mass
m	Launcher total mass
P_C	Commanded thurst
P_S	thrust level along longitudinal axis
Q	Dynamic pressure
S_{ref}	Reference area
T	Nozzle
V	Absolute velocity
V_R	Relative velocity
W	Wind perturbations

A second order model with a small damping value represents the flexible bending mode dynamics associated with the flexible launcher and is modelled as an additive perturbation on the rigid body model. The flexible mode dynamics are represented as follows [81]

$$\ddot{q}_i + 2\xi_i\omega_i\dot{q}_i + \omega_i^2 q_i = -P_C h_{tu_i}\beta_C + (I_T h_{ptu_i} - M_{tu}L_{tu}(h_{tu_i} - L_{tu}h_{ptu_i}))\ddot{\beta}_C \quad (2.13)$$

where β_C represents the commanded deflections around the nominal value to follow the reference trajectory. A total of five bending modes are considered in this benchmark. Actuator model for the pitch control is characterised by a second order system having commanded deflection as a single input, and the realised deflection and its two derivatives as the three outputs.

$$\ddot{\beta}_R + 2\xi_\beta\omega_\beta\dot{\beta}_R + \omega_\beta^2\beta_R = \omega_\beta^2\beta_C \quad (2.14)$$

where, ξ_β and ω_β represents damping of the actuator model and actuator model pulsation. The final effective deflection angle β corresponds to sum of the realised control input deflection and the misalignment deflection, and is given as:

$$\beta = \beta_R + \beta_{FZ} \quad (2.15)$$

Pitch angle is derived from the attitude measurement by Inertial Measurement Unit (IMU) and the pitch rate from the angular rate measurement by the gyrometer. Noises are added to these measurements. Angular noise and angular rate noises are treated as gaussian with 0.02° and 0.15°/s standard deviation respectively.

$$\begin{aligned} \theta_m &= \theta - \sum_i hp_{IMUi}q_i + noises \\ \dot{\theta}_m &= \dot{\theta} - \sum_i hp_{GYi}\dot{q}_i + noises \end{aligned} \quad (2.16)$$

The linear time varying model of the flexible launcher, which combines the rigid

dynamics given in (2.12) and the flexible mode dynamics given in (2.13) models together with actuator (2.14)-(2.15) and measurement models (2.16), is described as:

$$\dot{x}(t) = A(t)x(t) + B(t)u(t) \tag{2.17}$$

$$y(t) = C(t)x(t) \tag{2.18}$$

where $x(t) = \mathcal{C}ol(\dot{\theta}, \theta, \dot{Z}, \dot{\beta}_R, \beta_R, \dot{q}_i, q_i)$ represents the states, $u(t) = \mathcal{C}ol(\beta_C, W, \beta_{FZ})$ represents the control inputs, $y = \mathcal{C}ol(\theta_m, \dot{\theta}_m)$ represents the pitch angle and pitch rate measurements respectively. The matrices A,B and C are given as follows

$$A = \begin{bmatrix} 0 & A_6(t) & A_6(t)/V(t) & 0 & K_1(t) & 0 & 0 \\ 1 & 0 & 0 & 0 & 0 & 0 & 0 \\ 0 & A_1(t) & -A_6(t)\alpha_3(t) & 0 & K_2(t) & 0 & 0 \\ 0 & 0 & 0 & -2\xi_\beta\omega_\beta & -\omega_\beta^2 & 0 & 0 \\ 0 & 0 & 0 & 1 & 0 & 0 & 0 \\ 0 & 0 & 0 & -2\xi_\beta\omega_\beta M_{b_i} & -\omega_\beta^2 M_{b_i} - P_C h_{tu_i} & -2\xi_i\omega_i & -\omega_i^2 \\ 0 & 0 & 0 & 0 & 0 & 1 & 0 \end{bmatrix}$$

$$B = \begin{bmatrix} 0 & 0 & 0 & \omega_\beta^2 & 0 & \omega_\beta^2 M_{b_i} & 0 \\ -A_6(t)/V(t) & 0 & A_6(t)\alpha_3(t) & 0 & 0 & 0 & 0 \\ K_1(t) & 0 & K_2(t) & 0 & 0 & 0 & 0 \end{bmatrix}^T$$

$$C = \begin{bmatrix} 0 & 1 & 0 & 0 & 0 & 0 & -hp_{IMUi} \\ 1 & 0 & 0 & 0 & 0 & -hp_{GYi} & 0 \end{bmatrix}$$

where $M_{b_i} = I_T h_{ptu_i} - M_{tu} L_{tu}(h_{tu_i} - L_{tu} h_{ptu_i})$.

The controller used with this benchmark model, consists of a H_∞ rigid mode

controller and a bending mode filter, which is kept in series with the controller, for robust attenuation of the bending modes. The measurements of angular position and angular rate are the inputs of the controller and the filtered commanded deflection is the output. Controller and bending mode filter is defined for several time instants of the flight and linearly interpolated between these instants. Further details on the model can be found in [81, 82].

2.4.6 Disturbances

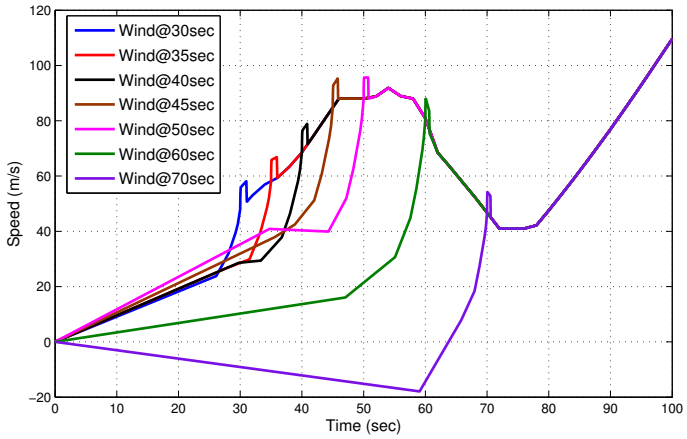

Figure 2.13: Wind profile

External disturbance corresponds to the wind gradient and the wind gust. As the equations of the launcher model are derived at the centre of gravity, the wind disturbance is assumed to be applied at the point itself. Applying wind disturbance at centre of gravity is a common practice in industry and used herein because accounting for wind disturbance away from centre of gravity makes little difference, [81]. In this study, the wind perturbation is modelled by a synthetic wind from a wind envelope, wind shear (wind speed change divided by the altitude

interval) and wind gust according to NASA specification in [83]. Wind envelop and wind shear both come from wind measurements collected at the area of interest for a long period and wind gust is an arbitrary characterisation of the small scale motion. The NASA database given in [83] is followed. The synthetic wind is determined by an altitude which corresponds to the maximum wind gradient. It is also the altitude at which the wind takes the value of the envelope. The altitude is computed using the trajectory data and the time instant of the flight. We have considered a deterministic wind profile occurring at seven flight instances, 30, 35, 40, 45, 50, 60 and 70 seconds (refer Figure 2.13).

2.4.7 Uncertainties

Twenty eight uncertain parameters are considered in this study, which constitutes of eight rigid mode uncertain parameters and five bending mode uncertain parameters with four different bending modes. The list of uncertain parameters is given in Table 2.7. Following type of bounds were defined by ASTRIUM and CNES for launcher application as presented in [84]. The uncertainty domain considered in this study consists of two aspects: (i) a possible nominal domain which is not well known prior to the flight but can be known and reduced after the qualifications of the flights (reducible uncertainty) and (ii) a dispersion domain in which the parameter value can change from one mission to another. In the framework of worst case analysis, uncertain parameters with uniform distribution are utilised by optimisation methods. These bounds should be able to incorporate both uncertainties and dispersions associated with the parameters.

For each uncertain parameter, δ, two sources of variability are considered

such as: i) uncertainties which are uniformly distributed ($\mathcal{U}(-\delta_u, +\delta_u)$) with support set $\delta \in [-\delta_u, +\delta_u] \subset \Delta$ and ii) dispersions which have a normal distribution ($\mathcal{N}(\mu, \delta^2_{disp})$). The possible domain is considered as a bias on the un-

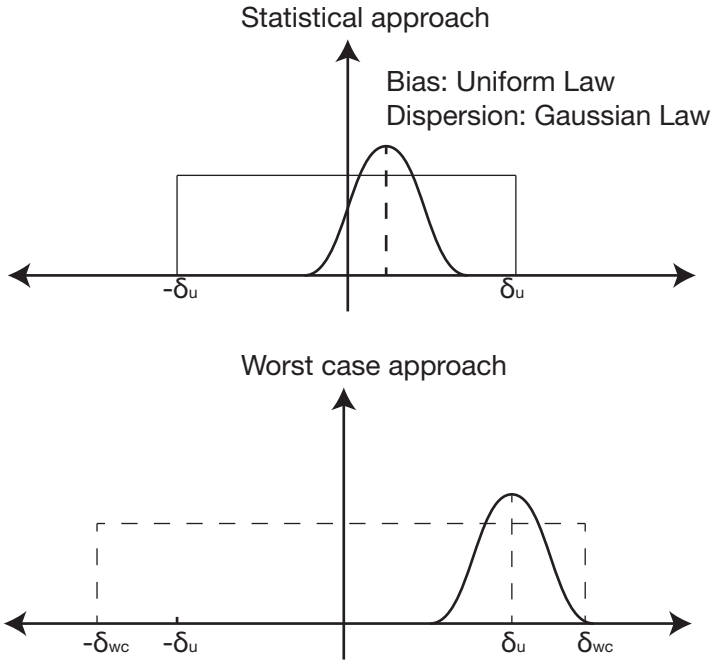

Figure 2.14: Uncertainties and dispersions

certain parameter value, and modelled by taking the worst case in the domain w.r.t the requested objective, selecting randomly with a uniform law since every value $\delta \in [-\delta_u, +\delta_u] \subset \Delta$ is equiprobable. Hence, the dispersion domain can also be treated as worst case. The two sources of variability for rigid uncertain parameters are combined to form worst case bounds and is shown in Figure 2.14. The worst case bounds for the rigid parameter uncertainties are defined by $\delta_{wc} = \pm(\delta_u + N\delta_{disp})$. Here, $N = 2.8$ corresponds to the number of dispersion variance (δ_{disp}) of the quantity of interest. The term $2.8\delta_{disp}$ provides 99.7% probability and 95% confidence levels for the objectives on aerodynamic load (Q_α) and

attitude (θ). A general law to be used with the optimisation algorithms is to sample uniformly in $[-\delta_{wc}, +\delta_{wc}]$, which is certainly outside the $[-\delta_u, +\delta_u]$. Obviously, uncertain parameters close to the worst case bounds $\pm\delta_{wc}$ will have less probability of occurrence and should be rejected. In order to reject such uncertain parameter combinations, probabilistic constraints are defined when optimisation methods are employed for V&V analysis. Such constraints are defined and explained in section 2.4.9.

Table 2.7: Variability of rigid and bending mode uncertain parameters

	Name	Description	Uncertainty	Dispersion
Rigid	MI	Inertia	10%	3%
	MP	Thrust	3%	1%
	MCz	Aerodynamic coefficient	20%	10%
	MXf	Centre of pressure	1.79m	$0.2m$
	MQ	Dynamic pressure	20%	4%
	MXg	Centre of gravity	0.3m	$0.05m$
	MM	Mass	5%	––
	$\Delta\beta$	Deflection Misalignment	1°	––
Bending mode	$Mpuls\_1$	Pulsation of 1^{st} bending mode	20%	––
	$Mpuls\_2$	Pulsation of 2^{nd} bending mode	20%	––
	$Mpuls\_3$	Pulsation of 3^{rd} bending mode	20%	––
	$Mpuls\_4$	Pulsation of 4^{th} bending mode	20%	––
	$Mhtu\_1$	Deformation at nozzle of 1^{st} bending mode	30%	––
	$Mhtu\_2$	Deformation at nozzle of 2^{nd} bending mode	30%	––
	$Mhtu\_3$	Deformation at nozzle of 3^{rd} bending mode	30%	––
	$Mhtu\_4$	Deformation at nozzle of 4^{th} bending mode	30%	––
	$Mhptu\_1$	Slide deformation at nozzle of 1^{st} bending mode	30%	––
	$Mhptu\_2$	Slide deformation at nozzle of 2^{nd} bending mode	30%	––
	$Mhptu\_3$	Slide deformation at nozzle of 3^{rd} bending mode	30%	––
	$Mhptu\_4$	Slide deformation at nozzle of 4^{th} bending mode	30%	––
	$MhpIMU\_1$	Slide deformation at IMU of 1^{st} bending mode	30%	––
	$MhpIMU\_2$	Slide deformation at IMU of 2^{nd} bending mode	30%	––
	$MhpIMU\_3$	Slide deformation at IMU of 3^{rd} bending mode	30%	––
	$MhpIMU\_4$	Slide deformation at IMU of 4^{th} bending mode	30%	––
	$MhpGY\_1$	Slide deformation at Gyro of 1^{st} bending mode	30%	––
	$MhpGY\_2$	Slide deformation at Gyro of 2^{nd} bending mode	30%	––
	$MhpGY\_3$	Slide deformation at Gyro of 3^{rd} bending mode	30%	––
	$MhpGY\_4$	Slide deformation at Gyro of 4^{th} bending mode	30%	––

2.4.8 Specifications

The controller structure ($\mathcal{C}_{\mathcal{H}_\infty}$), consisting of H_∞ controller and bending mode filter, must satisfy various functional performance requirements during the atmo-

spheric phase control. The main functional requirements are the compensation for external wind and wind gust perturbations and compensation for the internal perturbations which includes the thrust misalignment, the static error of the servo-actuators and thrust asymmetry. The compensation scheme must maintain minimum aerodynamic loads (Q_α, which is angle of attack times the dynamic pressure($kPadeg$)), for structural sizing reasons. The main temporal performance specifications that are to be validated in the presence of multiple uncertain parameter perturbations and dispersions, are listed in the Table 2.8.

Table 2.8: Functional performance requirements

Specification Description	Requirement	Cost function
$\mathbf{s}_1$: Maximum absolute value of aerodynamic angle of attack ($Q_\alpha(t)$) compatible with general load specification simulated over finite time period	$< 500kPadeg$	$\max_{t\in[t_0\ t_f]} \lvert Q_\alpha(t)\rvert$
$\mathbf{s}_2$: Maximum absolute value of attitude over finite time period	$\leq 2^\circ$	$\max_{t\in[t_0\ t_f]} \lvert\theta(t)\rvert$
$\mathbf{s}_3$: Maximum absolute final value of attitude ($\theta(t_f)$)	$\leq 2^\circ$	$\max \lvert\theta(t_f)\rvert$
$\mathbf{s}_4$: Maximum absolute final value of attitude rate ($\dot{\theta}(t_f)$)	$\leq 0.8^\circ/s$	$\max \lvert\dot{\theta}(t_f)\rvert$
$\mathbf{s}_5$: Maximum absolute value of deflection angle ($\beta(t)$) simulated over a finite time period	$< 6^\circ$	$\max_{t\in[t_0\ t_f]} \lvert\beta(t)\rvert$
$\mathbf{s}_6$: Cumulated deflection over a finite time period	$< 200^\circ$	$\max \sum_{t_0}^{t_f} \lvert\beta_C\rvert$

2.4.9 Worst case analysis

As discussed in Section 2.4.7, dispersions are associated with the rigid parameters, there is a possibility that these rigid parameters may be sampled outside the

uncertainty domain. If the rigid parameters are sampled outside the uncertainty domain then we may find cases of instability, or even worst cases which are worse than the ones found inside the uncertainty domain. As the probability of the rigid parameters occurring in this region is very low, we introduce a constrained optimisation which evaluates the combined probability of rigid parameters and checks if its within 99.7%. The combined probability of 99.7% corresponds to 95% confidence levels on aerodynamic load and attitude objectives. The rigid parameters are rejected whenever the requested 99.7% probability is not met. Combined probability is computed as follows[1]:

$$P_c(\delta_{rigid}) = \prod_{i=1}^{dim(\delta)} P(\delta^i) \tag{2.19}$$

and $\delta = \mathcal{C}ol(\delta^1, \ldots, \delta^k)$, for TVC benchmark model, $dim(\delta_{rigid}) = k = 8$. This is best explained with an example with two uncertain parameters, say δ^1 and δ^2, drawn uniformly over the worst case search domain $[-\delta_{wc}, \delta_{wc}]$ as shown in Figure 2.14 and discussed in subsection 2.4.7. If δ^i is chosen within the interval $[-\delta^i_u, \delta^i_u]$, where δ^i_u represents the bound of the uniform distribution, then the associated probability is $P(\delta^i) = 1$. Thus the parameter δ^i is inside the original uncertainty domain and no excursions due to dispersions. Whereas, if δ_i is inside $[\delta^i_u, \delta^i + 2.8\delta^i_{disp}]$ (similar analysis could be done for$[-\delta^i_u, -(\delta^i + 2.8\delta^i_{disp})]$) then the associated probability is computed with Gaussian law and bilateral distribution. To explain further, consider three cases:

- If $\delta^1 = \delta^1_u$ and $\delta^2 = \delta^2_u$, then $P_c(\delta) = P(\delta^1)P(\delta^2) = 1$ since both $P(\delta^i)$ are

[1]This probability constraint was defined by Astrium Space Transportation Ltd. during the SAFE-V project.

equal to one. Such an uncertain parameter can be considered for analysis.

- Assume $\delta^1 = \delta^1_u$ and $\delta^2 = \delta^2_u + 2.8\delta^2_{disp}$. In this case, the cumulative probability of the uncertain parameter combination becomes $P_c(\delta) = P(\delta^1)P(\delta^2) = 1(1 - 0.997) = 3 \times 10^{-3}$. This combination of uncertain parameters cannot be rejected as its cumulative probability is equal to the required 99.7% probability.

- Let $\delta^1 = \delta^1_u + 2.8\delta^1_{disp}$ and $\delta^2 = \delta^2_u + 2.8\delta^2_{disp}$. The cumulative probability associated with this specific uncertain parameter vector becomes $P_c(\delta) = P(\delta^1)P(\delta^2) = (1-0.997)^2 = 9\times10^{-6}$. Since the cumulative probability of this uncertain parameter combination is less than 99.7% i.e. $1-0.997 = 3\times10^{-3}$, this element must be rejected.

In general, whenever $P_c(\delta)$ of an uncertain parameter combination of rigid parameters is found to be less than 3×10^{-3}, then corresponding uncertain parameters are to be rejected. The worst case analysis performed in a constrained search space. The constrained worst case analysis problem for this study is a constrained global optimisation problem and formally defined as a follows:

$$\delta^*_i := \max_{\delta \in \Delta} J_i(\delta, \mathcal{C}_{\mathcal{H}_\infty}, W) \tag{2.20}$$

$$\texttt{sub to } P_c(\delta) \geq \epsilon \tag{2.21}$$

$$\delta_{i,min} \leq \delta \leq \delta_{i,max}$$

for all $i = 1, \ldots, dim(J)$, where $P_c(\delta)$ represents the cumulative probability of the uncertain parameter vector (emanating due to the presence of dispersions), and ϵ fixed at 3×10^{-3}. $J_i(\delta, \mathcal{C}_{\mathcal{H}_\infty}, W)$ represents the i^{th} functional performance

requirement formulated as a norm based cost function as listed in the last column of Table 2.8. The cumulative probability associated with the occurrence of uncertain parameter vector is addressed explicitly.

The objective is to determine the worst case uncertain parameter combinations associated with different functional performance criteria defined as cost functions listed in the Table 2.8. The entire parameter space $[-\delta_{wc}, \delta_{wc}]$ is considered for this analysis. The worst case analysis is carried out for different wind perturbations occurring during the TVC phase at 30, 35, 40, 45, 50, 60 and 70 seconds. Hybrid Differential Evolution algorithm, with the same optimisation tuning parameters as used in the flexible launch vehicle model in section 2.4.1, is used to determine the worst-case perturbations.

The numerical results for six different cost functions at seven different wind perturbations are given in Table 2.9 - 2.10. In Table 2.9, consider the cost function representing the performance on aerodynamic load $|Q_\alpha(t)|$ and wind occurring at 45seconds. Among the 1000 candidate uncertain parameter vectors in the search space, the maximum cost function value associated with the worst case is 561.91 and has a mean of 436.11 with a standard deviation of 79.57. Mean and standard deviation statistics gives us an idea of variability of cost function values in the search space. A high value of standard deviation indicates that the cost function values are spread out over a large range in search space whereas a low value indicates that the cost function values lie too close to the mean. This shows the exploration property of the optimisation algorithm which is its ability to access uncertain parameter vectors spread out in the search space. In order to find the global solution, the optimisation algorithm should be able to explore the search space as thoroughly as possible. In this case, Standard deviation is high and it

indicates that the algorithm was able to access uncertain parameter vectors spread out over the search space.

Table 2.9: Worst case results over the entire parameter range for wind perturbation at 30,35,40, 45, 50, 60 and 70 seconds

			Worst case values						
			30sec	35sec	40sec	45sec	50sec	60sec	70sec
$\max_{t\in[t_0 t_f]} \lvert Q_\alpha(t)\rvert$	HDE	max	432.23	460.61	509.65	561.91	543.23	411.07	189.43
		mean	336.68	369.56	406.95	436.11	430.48	324.13	142.48
		std	62.53	66.12	75.46	79.57	77.49	56.87	27.8
		failures	0	0	37	383	370	0	0
	MC	max	424.74	449.14	493.08	549.26	532.14	438.35	184.46
		mean	319.58	340.42	376.16	411.67	402.38	305.68	131.23
		std	41.6	46.62	50.13	53.76	54.26	49.20	23.3
		failures	0	0	0	60	40	0	0
$\max_{t\in[t_0 t_f]} \lvert\theta(t)\rvert$	HDE	max	5.85	Unstable	Unstable	Unstable	6.91	5.43	3.76
		mean	3.51				3.41	2.95	2.15
		std	0.87				1.12	1.13	0.721
		failures	0				0	0	0
	MC	max	4.65	7.03	8.8	8.2	5.54	5.4	3.8
		mean	3.14	3.24	3.35	3.34	2.73	2.28	1.73
		std	0.59	0.7	0.76	0.95	0.63	0.82	0.53
		failures	0	0	0	0	0	0	0
$\max \lvert\theta(t_{tf})\rvert$	HDE	max	0.15	0.16	Unstable	Unstable	0.139	0.164	0.244
		mean	0.038	0.035			0.04	0.038	0.053
		std	0.027	0.029			0.03	0.028	0.037
		failures	0	0			0	0	0
	MC	max	0.22	0.18	0.19	0.184	0.177	0.15	0.27
		mean	0.04	0.04	0.04	0.04	0.047	0.04	0.05
		std	0.03	0.03	0.03	0.03	0.03	0.02	0.04
		failures	0	0	0	0	0	0	0

The table entry 'failures' indicates the number of occasions the performance criterion has violated. Among the candidate points, 383 cases out of 1000 violated the performance requirement on $|Q_\alpha(t)| \leq 500$kPa during the execution of HDE optimisation algorithm. It was noticed that the rigid uncertain parameters was the main cause for the worst case performance in all the cases and the flexible modes were well suppressed by the bending mode filters.

Table 2.10: Worst case results over the entire parameter range for wind perturbation at 30,35,40, 45, 50, 60 and 70 seconds

			Worst case values						
			30sec	35sec	40sec	45sec	50sec	60sec	70sec
$\max \lvert\dot{\theta}(t_{tf})\rvert$	HDE	max	0.595	0.498	Unstable	Unstable	0.493	0.445	0.493
		mean	0.117	0.138			0.112	0.110	0.118
		std	0.09	0.101			0.088	0.088	0.094
		failures	0	0			0	0	0
	MC	max	0.556	0.54	0.53	0.58	0.536	0.54	0.45
		mean	0.13	0.13	0.13	0.13	0.122	0.12	0.12
		std	0.1	0.09	0.1	0.1	0.09	0.09	0.09
		failures	0	0	0	0	0	0	0
$\max_{t\in[t_0\,t_f]} \lvert\beta(t)\rvert$	HDE	max	6.5	6.5	6.5	6.5	6.5	4.54	2.09
		mean	4.29	4.72	4.27	4.86	4.43	2.79	1.18
		std	1.32	1.38	1.44	1.35	1.38	0.82	0.4
		failures	187	516	582	517	366	0	0
	MC	max	6.47	6.5	6.5	6.5	6.5	5.08	2.22
		mean	3.79	4.26	4.36	4.4	3.88	2.41	0.98
		std	0.95	1.05	1.08	1.12	1.01	0.75	0.32
		failures	13	67	93	111	29	0	0
Cumulated Deflection	HDE	max	136.44	153.7	Unstable	Unstable	141.64	136.32	133.42
		mean	125.87	127.28			125.43	124.27	123.69
		std	14.05	13.55			13.60	12.63	12.4
		failures	0	0			0	0	0
	MC	max	136.52	142.51	151.14	142.18	135.63	138.17	134.03
		mean	126.81	127.3	127	127	126.36	125.82	124.84
		std	3.07	3.5	3.5	3.43	3.07	3.04	2.9
		failures	0	0	0	0	0	0	0

The normalised rigid mode worst case directions corresponding to seven different wind perturbations are shown in Figure 2.15 and the comparison of nominal and worst case transient responses are given in Figure 2.16. The corresponding worst case directions shown in Figure 2.15 are explained by three main physical reasons. At first, since the dynamic pressure has a direct impact on the aerodynamic loads, the worst case perturbation providing maximum Q_α corresponds to maximum dynamic pressure (MQ). Secondly, the angle of attack (α, AoA) will be maximum for minimum aerodynamic efficiency ($A_{6_{min}}$) which is opposite to maximum attitude ($\alpha = \theta + W/V$). This can be easily shown by writing the transfer

function from the wind perturbation to AoA (open loop $\alpha/W = s^2/(V(s^2 - A_6))$ $\rightarrow$ 1/V ($A_6 \rightarrow 0$), 1/V for closed loop with PD). Thus worst case corresponds to the uncertain parameter combination with minimum value for aerodynamic coefficient (Cz) and centre of pressure Xf, and maximum value for centre of gravity Xg. Finally, maximum thrust misalignment (FZ_{max}) and maximum propulsive efficiency ($K_{1_{max}}$) will lead to a maximum contribution of static part of the angle of attack ($\alpha_{static} = K_1/A_6 FZ$). Worst case directions are oriented towards the parameters which are simultaneously the most influent ones (dynamic pressure MQ, aerodynamic coefficient MCz, center of pressure MXf, centre of gravity MXg) and the more dispersed ones (deflection misalignment).

Unstable cases are found for attitude, attitude rate and cumulative deflection angle performance criteria, when the wind perturbation corresponds to 35, 40, and 45 seconds (refer Figures 2.18, 2.20). For these cases, sustained actuator saturation is observed (refer Figure 2.24) and the instability occurs just after the wind perturbation starts to act on the system. Two factors explain the worst case parameters value. First, the effect of wind (W) on attitude is maximal for maximal aerodynamic efficiency A_6 (maximal Q, Cz and Xf); this can be easily shown by writing the open loop or closed loop transfer function from the wind perturbation to the attitude (open loop $\theta/W = A_6/(V(s^2 - A_6)) \rightarrow 1/V$ as $A_6 \rightarrow \infty$), Then the possibility for the controller to counter the wind is minimal for minimal propulsive efficiency K_1 (minimal thrust MP and highest centre of gravity Xg).

For the wind perturbations corresponding to 60 and 70 seconds, no performance criteria violation is recorded, refer Table 2.9 - 2.10. It is observed that the launch vehicle model is able to withstand wind perturbations after 50 seconds whereas for the perturbations occurring between 35 to 50 seconds leads to instability of the

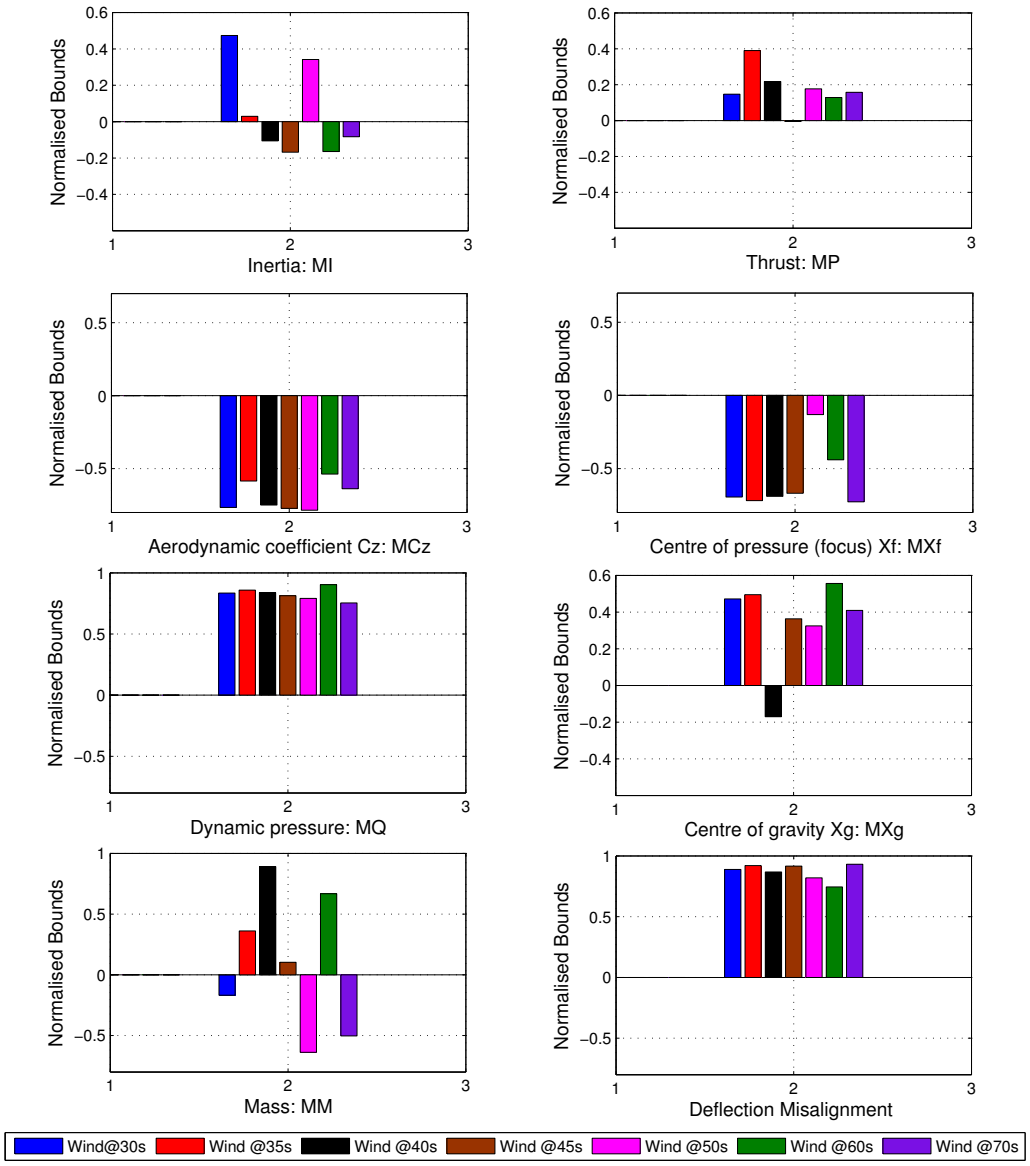

Figure 2.15: Rigid mode worst case perturbations at different wind instances for $\max |Q_\alpha(t)|$

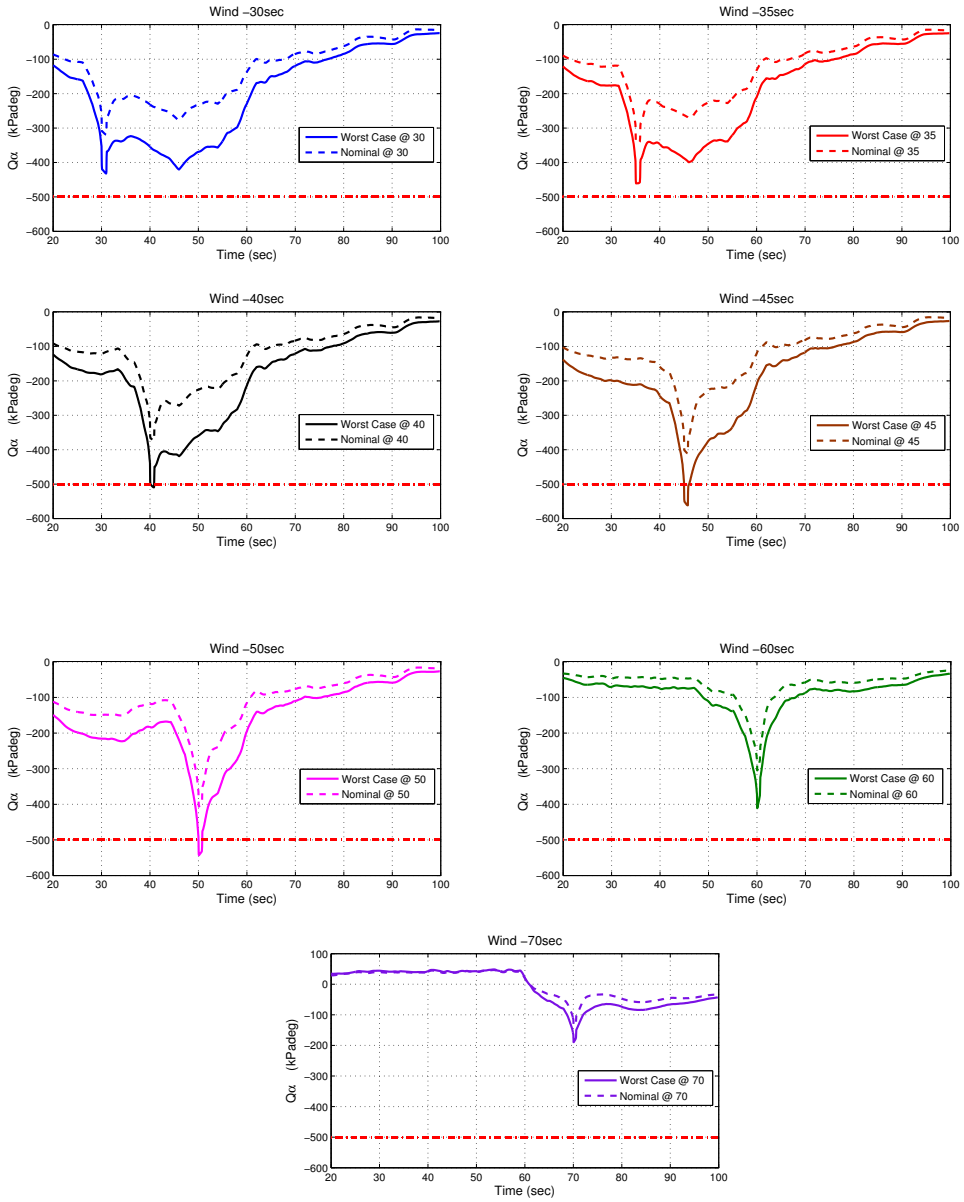

Figure 2.16: Aerodynamic AoA Q_α plots at different wind perturbation instances for $\max|Q_\alpha(t)|$

launch vehicle.

Monte Carlo analysis is also performed and the results are also tabulated for comparison in Table 2.9 and Table 2.10. These results are provided to compare it with those found by optimisation based analysis. A 1000 Monte Carlo campaigns are performed for each cost function. It is observed that optimisation based method is able to find more performance criteria violations and even better worst cases than those found by Monte Carlo method, which can be attributed to the intelligence embedded in the search process of optimisation scheme. Monte Carlo is unable to capture any unstable cases corresponding to the performance criteria of attitude, attitude rate and cumulated deflection. Also, apart from objectives based on aerodynamic load and attitude, no failures i.e performance criteria violations were recorded for other objectives.

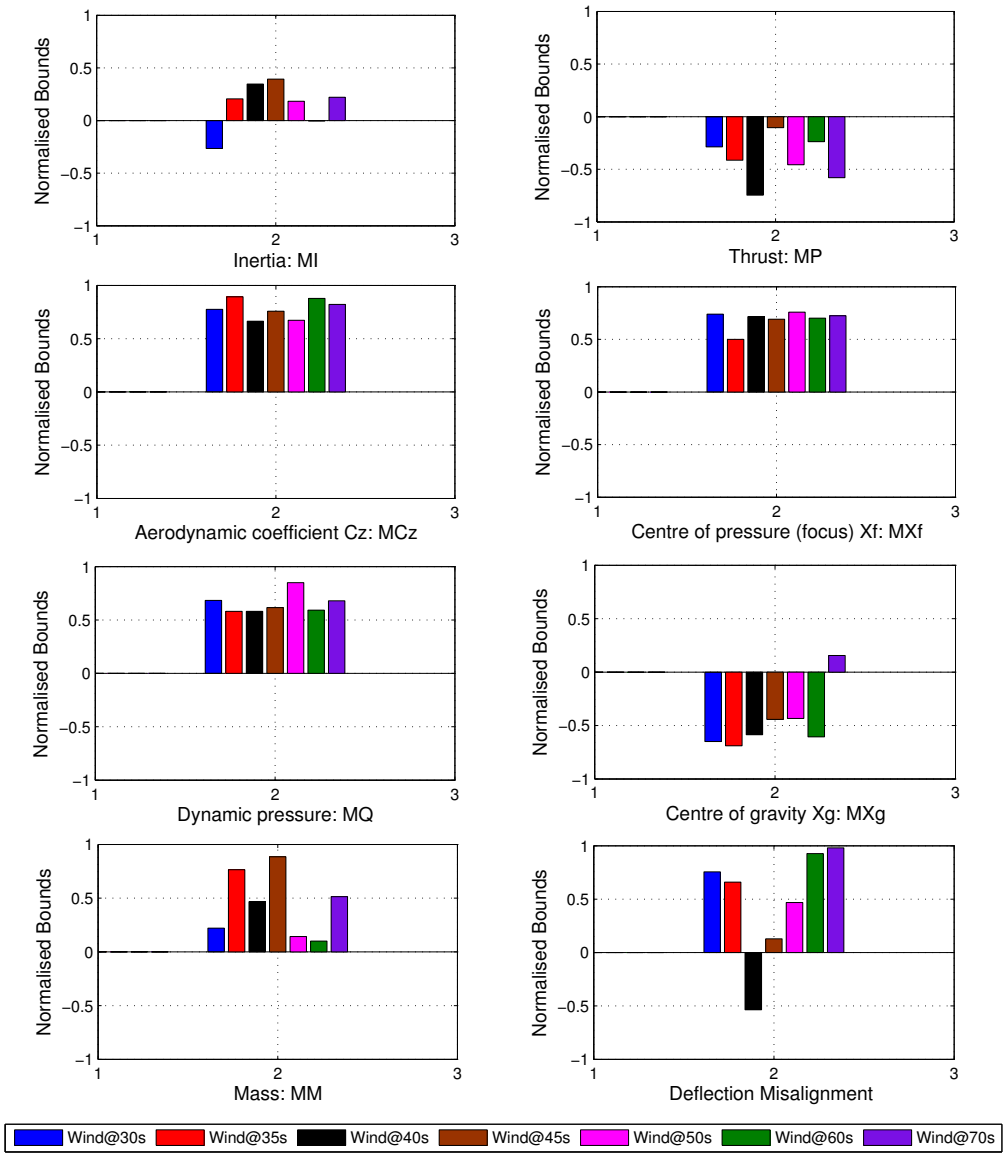

Figure 2.17: Rigid uncertain parameters maximising $|\theta(t)|$

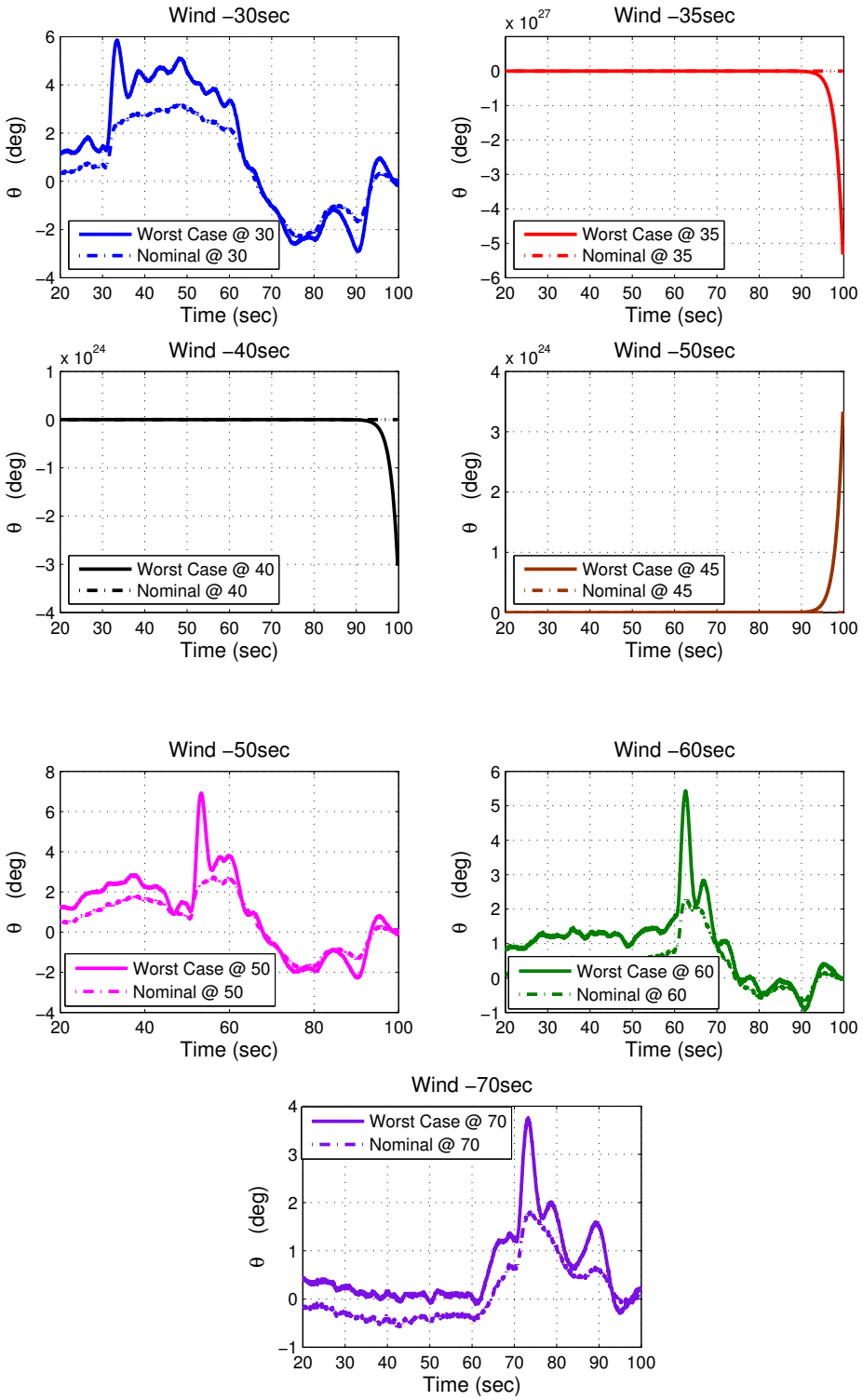

Figure 2.18: θ plots at different wind perturbation instances for $\max|\theta(t)|$

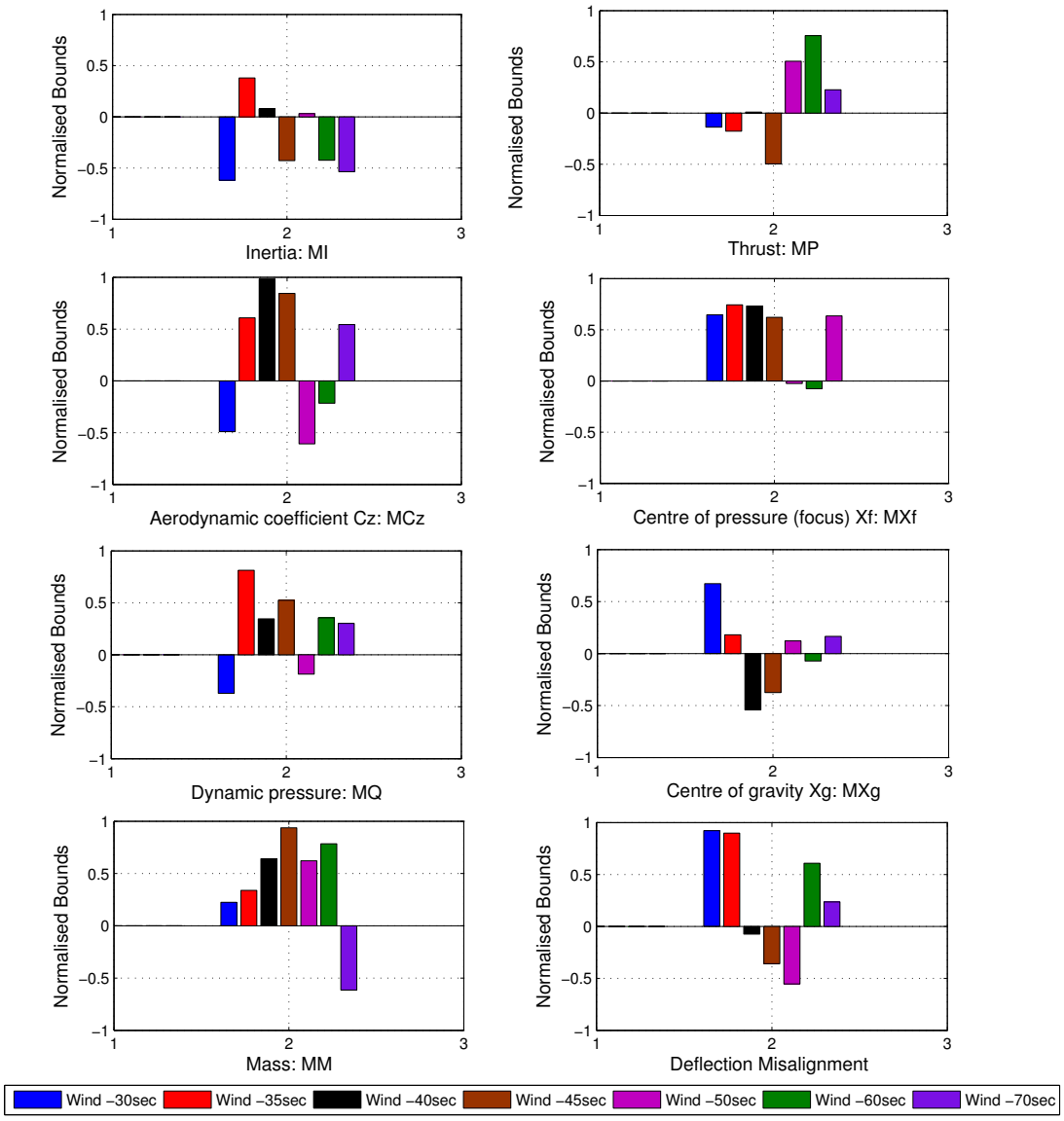

Figure 2.19: Rigid uncertain parameters maximising $|\theta(t_f)|$

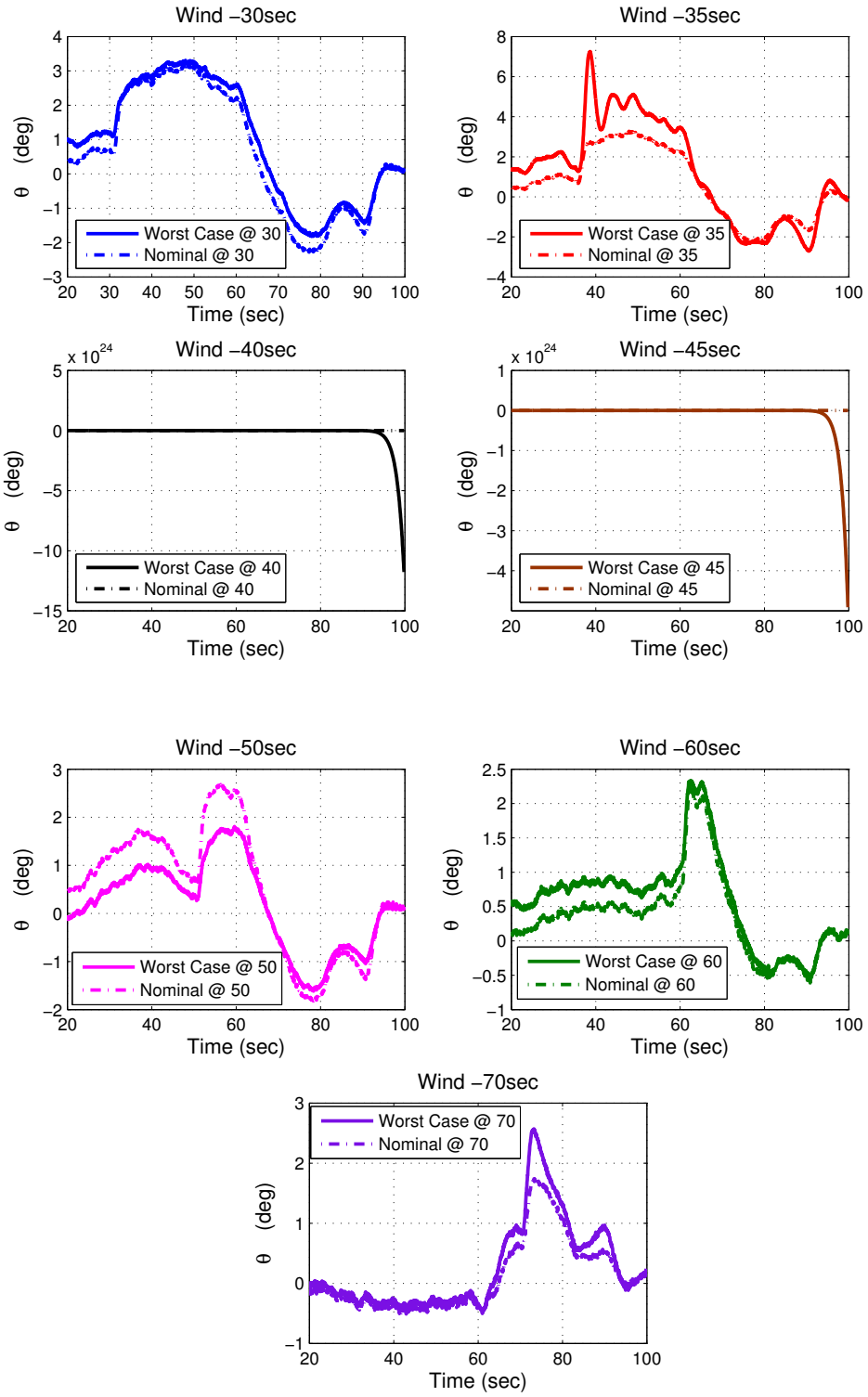

Figure 2.20: θ plots at different wind perturbation instances for $\max|\theta(t_f)|$

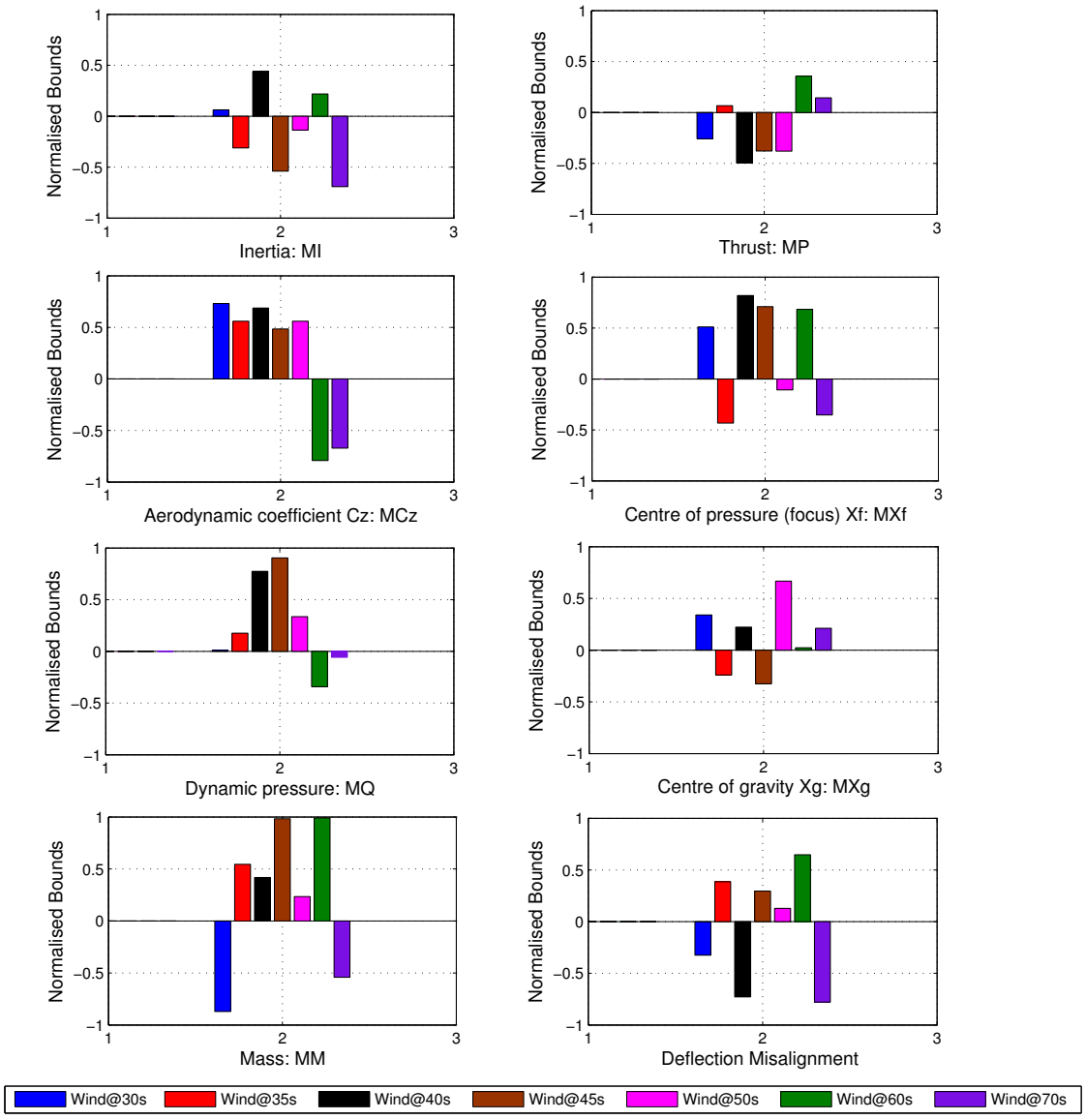

Figure 2.21: Rigid uncertain parameters maximising $|\dot{\theta}(t_f)|$

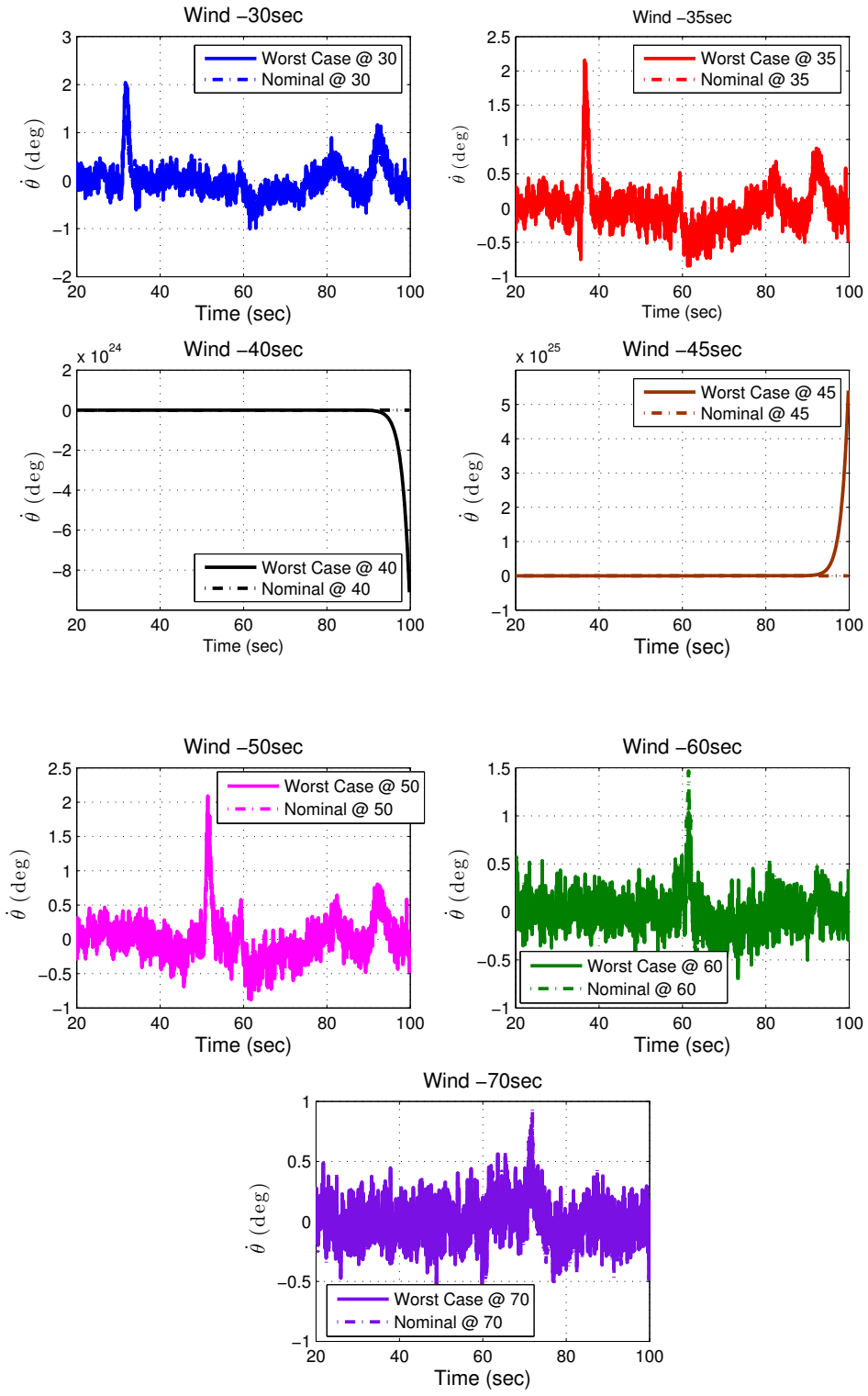

Figure 2.22: $\dot{\theta}$ plots at different wind perturbation instances for $\max|\dot{\theta}(t_f)|$

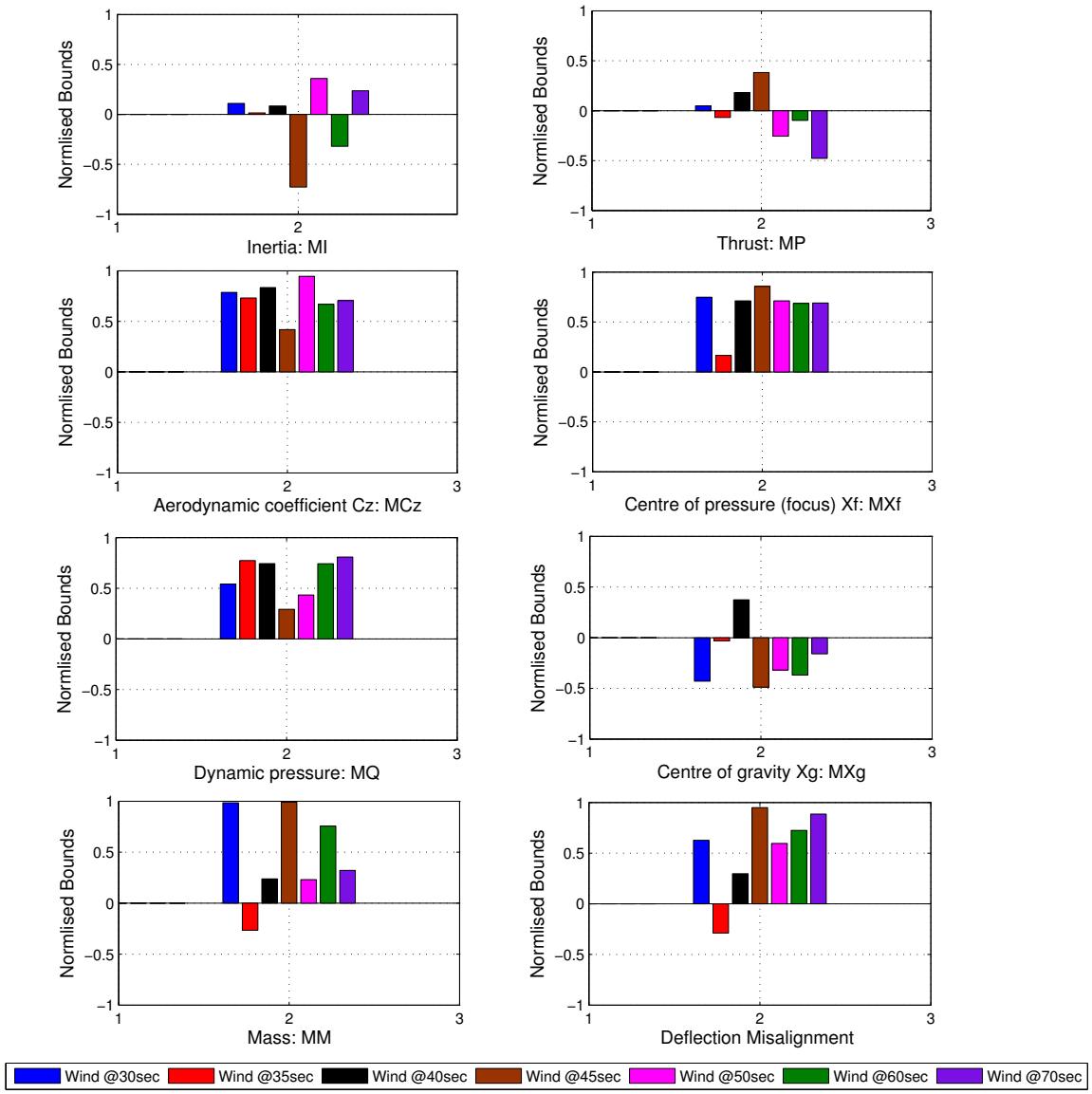

Figure 2.23: Rigid uncertain parameters maximising $|\beta(t)|$

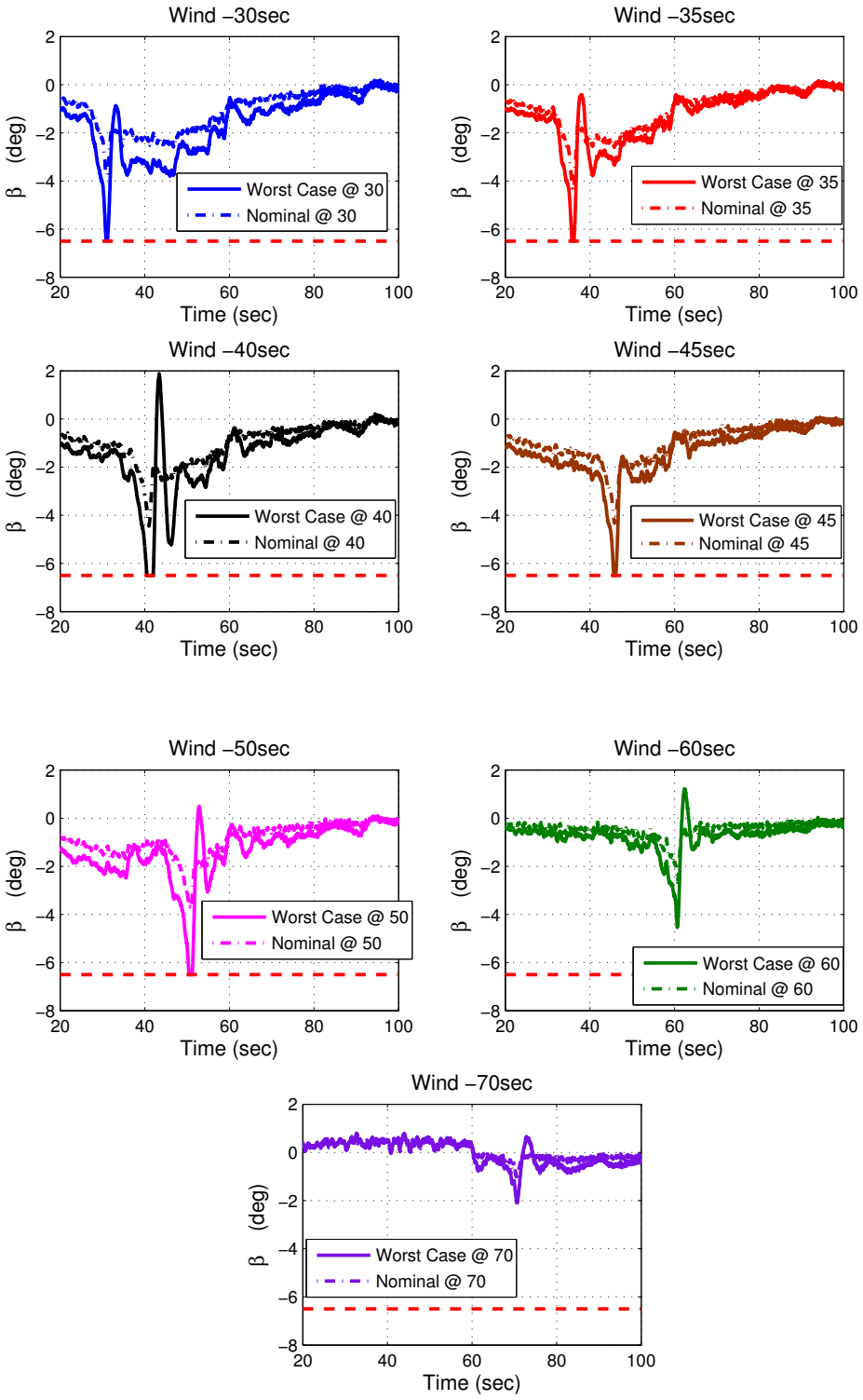

Figure 2.24: β plots at different wind perturbation instances for $\max|\beta(t)|$

2.4.10 Multi-objective Verification & Validation analysis

Uptill now, in this chapter the goal was to perform V&V analysis to identify the worst case solution w.r.t a single performance criterion. However in this section, worst case solutions are generated using two performance criteria simultaneously and contradicting to each other. When there is more than one objective to be maximised, there exists solutions for which performance on one objective cannot be improved without sacrificing performance on at least one other. Such solutions are said to be Pareto optimal and the set of all Pareto optimal solutions is said to form the Pareto front. Multi-objective algorithms based on evolutionary principles are popular approaches to generate Pareto optimal solutions,[85]. In [85] a survey is given on a number of evolutionary multi-objective optimisation techniques including Schaffers Vector Evaluated Genetic Algorithm (VEGA) [86], Fonseca and Flemings Multi-Objective Genetic Algorithm (MOGA) [87], Srinivas and Debs Non-domination Sorted Genetic Algorithm (NSGA) [88], Horn and Naffpliotis Niched Pareto Genetic Algorithm (NPGA) [89] etc. The general procedure of Multi-Objective Evolutionary Algorithm (MOEA) follows the same way as in EAs for single objective optimisation.

2.4.11 Non-Dominated Sorting Differential Evolution

Multi-objective algorithm based on Differential Evolution principles was first proposed by Xue in [90]. Xue's proposed Multi-Objective Differential Evolution (MODE) method combined the principles of Differential Evolution and non-dominated sorting algorithm developed by Deb ,[91]. Non-dominated Sorting Differential Evolution (NSDE) is similar to MODE and generates new members of the population

by following DE principles, but it differs from MODE as it utilises non-dominated sorting algorithm for selecting individuals for the next generation.

The NSDE algorithm starts by initialising a random population $P_i(j)$, where $i = 1, \ldots, N$, N is the number of individuals in a population and $j = 1, \ldots, M$, M is the number of generations.For each member of the initial population, the objective functions are evaluated. For every generation j, DE operators such as greediness factor and scaling factor are used to produce a new population $P^{new}(j)$ which is combined with the parent population $[P^{new}(j) \cup P(j)]$. Then N best individuals (same as the population size) based on their objective function values are selected for next generation and the process is repeated till a termination criterion is fulfilled. Steps involved in NSDE algorithm is described here in brief:

1. *Population Initialisation:* The population is initialised based on the range of the uncertain parameters under consideration and constraints if any. Initial population consists of randomly generated uncertain parameters.

2. *Non-Dominated sort:* Objective functions are evaluated for all the individuals in the population. The term dominated is used for indicating if any individuals with better objective function values exist w.r.t a certain individual, if not then it indicates that the considered individual is non-dominated. Based on the objective function values, for each member of the population, determine how many individuals are dominated/non-dominated by it. If an individual is not dominated by any other individual in the population then it is considered as a non-dominated individual and assigned rank 1. All individuals with rank 1 are grouped to form a 'front' so all individuals with rank 1 will be assigned to front 1 and so on. Figure

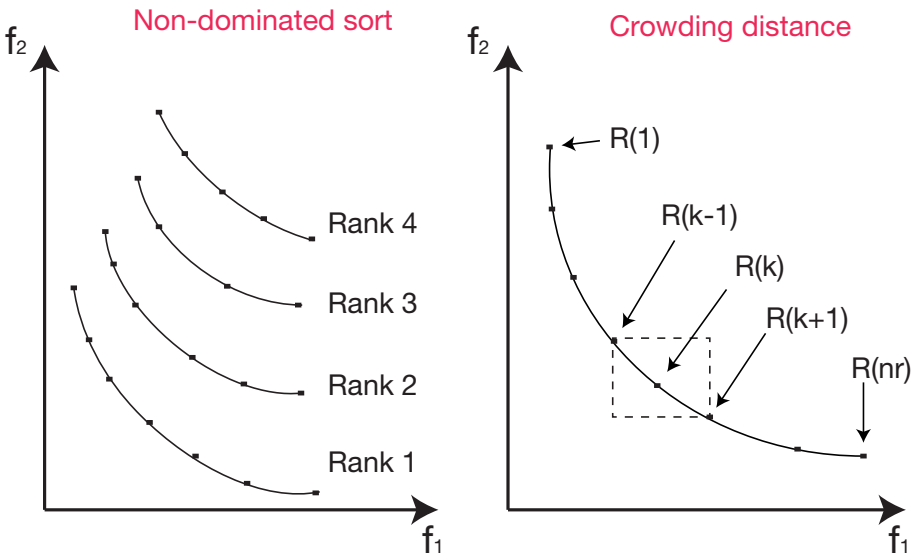

Figure 2.25: Ilustration of Non-dominated sorting and Crowding distance

2.25 shows individuals grouped into different fronts based on their rank values. The initialised population is sorted based on non-domination into each front. The first front being completely non-dominated set in the current population and the second front being dominated by individuals in the first front only and so on. The fast sort algorithm described in [92] is utilised here to sort the initial population based on their fronts. This algorithm is provided here in Table 2.11

3. *Crowding Distance:* In non-domination sorting, the population is sorted according to the ascending order of the objective function value. Then the minimum and maximum values for each objective function are assigned an infinite distance value. For all other intermediate solutions, the crowding distances are assigned equal to the normalised absolute difference in the objective function values of the two adjacent solutions in the sorted set. The overall crowding distance is calculated as the sum of individual distance values corresponding to each objective function value,

Table 2.11: A fast sort algorithm

1. **For** each individual $P_i(j) \in P(j)$ do the following
   (a) Initialise the set S_p which would contain all the individuals that is being dominated by $P_i(j)$. $S_p \leftarrow \{\emptyset\}$.
   (b) Initialise the number of individuals that dominate $P_i(j)$, as $n_p = 0$.
   (c) **For** each individual $P_k(j) \in P(j)$
      i. **If** $P_i(j)$ dominates $P_k(j)$ **then**
         A. Add $P_k(j)$ to the set S_p i.e. $S_p = S_p \cup P_k(j)$
      ii. **Else if** $P_k(j)$ dominates $P_i(j)$ **then**
         A. Increment the domination counter for $P_i(j)$ i.e. $n_p = n_p + 1$
      iii. **End if**
   (d) **End For**
   (e) if $n_p = 0$, i.e. no individuals dominate $P_i(j)$ then $P_i(j)$ belongs to the first front. Set rank of the individual $P_i(j)$ to one, $P_{irank} = 1$. Update the first front set by adding element $P_i(j)$ to that set i.e. $F_1 = F_1 \cup P_i(j)$.
2. **End For**
3. Initialise the front counter to one. $r = 1$.
4. **While** r^{th} front is nonempty i.e. $F_1 \neq 0$.
   (a) $\mathcal{Q} = \{\emptyset\}$. This set for storing the individuals for $(r+1)^{th}$ front.
   (b) **For** each individual $P_i(j)$ in front F_r
      i. **For** each individual $P_k(i)$ in S_p, n_q is total individuals in set S_p.
         A. $n_q = n_q - 1$, decrement the domination count for individual $P_k(j)$.
         B. If $n_q = 0$ then none of the individuals in the subsequent fronts would dominate $P_k(j)$. Hence set $P_{irank} = r + 1$. Update the set $\mathcal{Q}$ with individual $P_k(j)$, $\mathcal{Q} \cup P_k(j)$.
      ii. **End For**
   (c) **End For**
   (d) Increment the front counter by one.
   (e) Now the set $\mathcal{Q}$ is the next front and hence $F_r = \mathcal{Q}$.
5. **End While**.

which are normalised prior to calculation. The general idea is to assign the Euclidian distance between each individual in a front and it is assigned front wise.

4. *Offspring population:* In order to generate the offspring population, two vectors, the differential vector and perturbation vectors are defined for each individual in the population. In the DE for single-objective problems, the differential vector is defined as the vector between the best individual and the individual under consideration for reproduction. This best individual is usually the individual with the highest objective function value in the population. However, in multi-objective optimisation, assigning the best individual among the population could be difficult as there might be solutions which are maximum along one objective and minimum along other. To define the differential vector, the non-domination based sorting method is used to identify the best individual. For each individual, P_i, in the population, a non-dominated set D_i is identified. A solution, P_{best}, is chosen randomly from the set D_i. The differential vector is defined between P_i and P_{best}. If the individual is already a non-dominated individual, then $P_{best} = P_i$ and the differential vector will have zero value. Hence, the best solution, P_{best}, will dynamically change depending on the individual's position in the criteria space. This is the major difference from the single-objective DE, where the best solution is fixed for the reproduction for all solutions in the population. The perturbation vectors are defined by randomly chosen distinct pairs of individuals from the parent population. The number of the perturbation vectors is determined by a pre-defined parameter K and is set to a value of 2 for this analysis. Once the differential vector and the perturbation vectors are defined, the reproduction operation is defined in a similar way as in the single-objective DE.

$$P_i^{new} = \begin{cases} P_i + F \cdot \sum_{k=1}^{K} (P_{i_a}^k - P_{i_b}^k) & P_i \text{ is non-dominated} \\ \gamma \cdot P_{best} + (1-\gamma) \cdot P_i + F \cdot \sum_{k=1}^{K} (P_{i_a}^k - P_{i_b}^k) & P_i \text{ is dominated} \end{cases} \tag{2.22}$$

where P_{best} is the best individual in the Pareto sense chosen from the parent population, $\gamma \in [0\ 1]$ represents the greediness of the operator, and K is the number of perturbation vectors, F is the factor that scales the perturbation, $P_{i_a}^k$ and $P_{i_b}^k$ are randomly selected mutually distinct individuals in the parent population, and P_i^{new} is the offspring.

5. *Recombination and selection:* The offspring population is combined with the current population and selection operation is performed to select N individuals for the next generation. Since all the previous and current best individuals are added in the population, elitism is ensured. Population is now sorted based on non-domination. The new population for the next generation is filled by each front subsequently until the population size N is exceeded. If by adding all the individuals in front, the population exceeds N then individuals in front are selected based on their crowding distance in the descending order until the population size is N. The process is repeated to generate the subsequent generations. A fixed termination criteria of maximum allowed generations is used to terminate the algorithm.

2.4.12 Application to TVC benchmark problem

The TVC benchmark problem described in Chapter 2 Section 2.4.5 is defined as a multi-objective optimisation problem in Equation (5.1). The optimisation problem is formulated to identify Pareto front for maximum deviations of aerodynamic load and deflection angle performance objectives.

$$\begin{aligned} \delta_i^* \quad := \quad & \max_{\delta \in \Delta} J_i(\delta, \mathcal{C}_{\mathcal{H}_\infty}, W) \\ & \texttt{sub to} \;\; P_c(\delta) \geq \epsilon \qquad \texttt{for} \; i = 1, 2. \end{aligned} \tag{2.23}$$

where

$$\begin{aligned} J_1 \quad = \quad & \max_{t \in [t_0 t_f]} |Q_\alpha(t)| \\ J_2 \quad = \quad & \max_{t \in [t_0 t_f]} |\beta(t)| \end{aligned} \tag{2.24}$$

Two objectives considered are related to the performance criteria on maximum deviations of aerodynamic load (s_1) and deflection angle (s_4). The wind perturbation occurring at 50 seconds is considered for this analysis. NSDE and NSGA-II algorithm are utilised to perform multi-objective optimisation. The following optimiser configuration parameters are used: population size is set to 25, maximum generations is set to 100 for both NSDE and NSGA. For NSDE algorithm, scaling factor F is set to 0.8, γ greediness operator is set to 0.8 is generated and is shown in Figure 2.26. Worst case solutions have been found were the performance criterion is violated for one objective while not violating the other criterion. From the Figure 2.26, it can be seen that when maximum deviation in deflection angle is 6.5°, violating the performance criterion of 6°, does not violate the maximum deviation in aerodynamic load which has a value of $483.6kPadeg$. Similarly, when

maximum deviations in aerodynamic load has a value of 536.9, which violates the performance criterion of $500kPadeg$, no violation is found for the performance criterion on the deflection angle which has a value of 3.96°. While performing the single objective worst case analysis (refer Section 2.4.9), the worst case value of maximum deviations of aerodynamic load is accompanied by actuator saturation. Deflection angle is saturated at 6.5°. In addition to conventional worst case solution, Multi-objective analysis has identified other potential solutions, which violate the criterion on the aerodynamic load while the deflection angle is not saturated and in fact with low values.

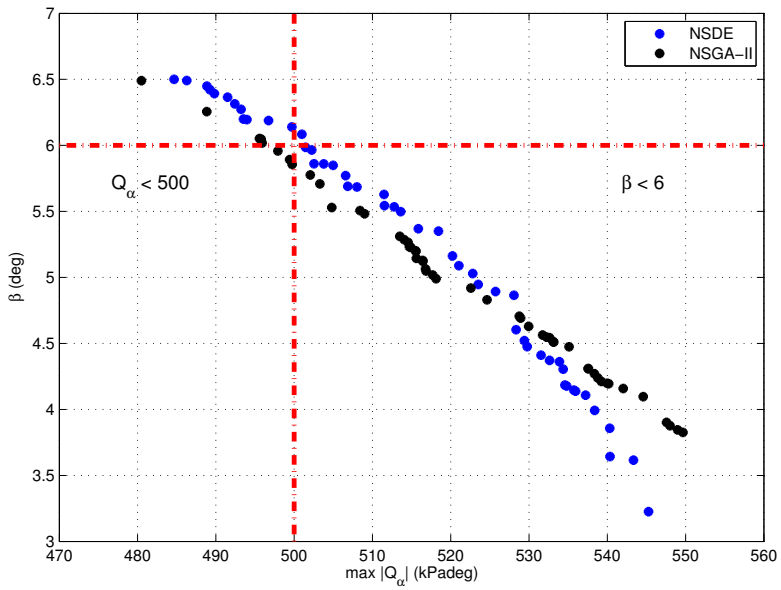

Figure 2.26: Pareto Front associated with maximising the deviations in the aerodynamic load and the deflection angle

Both NSGA-II and NSDE have comparable performance in identifying the Pareto solution set, while the latter converges faster. It is observed that NSDE solutions are no better than NSGA-II. Even so, NSDE algorithm requires more

testing on other industrial models in order to highlight any benefits or lack thereof over NSGA-II.

Chapter 3

Polynomial Chaos Based Surrogate Models

3.1 Introduction

Traditionally, the aerospace industry relies extensively on Monte Carlo and optimisation based methods to perform the V&V ([52, 53, 76, 79]). The Monte Carlo method requires several sampling points in order to provide a strong statistical confidence that the worst case has been found [7, 37]. In this thesis, the evaluation of the sampling points entails running the simulations of a mathematical model, which could be linear or non-linear. The models are considered as black-box models. The inputs are assumed to be the uncertainties in the model. The outputs are the performance objectives. For example, in [93], Wang performs V&V on an autonomous rendezvous problem using the Monte Carlo and the optimisation based methods. The nonlinear mathematical model for the autonomous rendezvous problem is computationally expensive, and each function evaluation

requires 30minutes of simulation time. Hence, a detailed Monte Carlo analysis or a complete optimisation-based analysis is prohibitive with this model. In Monte Carlo analysis, it is obvious that the more simulation are performed, the higher the probability of finding the worst case would be. With the computationally expensive black box models, similar to the one considered in [93], one has to limit the analysis with a fixed computational budget and a low number of simulations.

The probability of finding the worst case would be low if a small number of simulations were to be performed. The total number of simulations (N_{MC}) required to estimate the probability of finding a worst case with an accuracy of ϵ and a confidence of $1-\kappa$ is given by [37]:

$$N_{MC} \geq \frac{1}{2\epsilon^2} \ln \frac{2}{\kappa} \tag{3.1}$$

The inequality provides the statistical guarantee of determining the worst case with a minimum number of simulations. For example, in order to be 99% (i.e. $\kappa = 1 - 0.99$) sure that the probability of finding a worst case is within 0.01(i.e. $\epsilon = 0.01$) of the true value, the total number of simulations (N_{MC}) needed is at least $26,492$. Varga in [7] and Wang in [52], also discuss the computational complexity associated with the statistical guarantees of high confidence value. Similarly, in the case of the optimisation based analysis, the convergence to the global optimum is often requires large number of function evaluations. In the case of non-convex optimisation problems, the convergence to the global solution requires even more function evaluations, and in some cases the convergence might not even be guaranteed. According to [7, 51] typical worst-case analysis problems fall in this class of optimisation problem. Also, as argued in [93], with computationally

expensive simulation models, even the optimisation based methods could become prohibitive.

In the field of multidisciplinary design optimisation, the surrogate models have been developed for the high fidelity finite element simulation models using different methods such as the polynomial regression [94], multivariate adaptive regression splines [95], response surface methods [96] and Kriging [97]. The surrogate models are approximate representations of the original models, and far less time consuming to evaluate compared to the original models. Surrogate models are also often identified as response surface models. The aim is to have the surrogate models as accurate as possible to the original model and thereby speed up the design optimisation process without compromising on the quality of the solution, [94, 98]. In an identical manner, the surrogate models can be utilised in the optimisation based worst case analysis and the convergence to the worst case solution can be enhanced significantly. Suppose an accurate surrogate model can be determined to represent a computationally expensive original model in an efficient way. Then, this computationally inexpensive, equivalent model could be used for the large number of Monte Carlo simulations. The worst case determined from these large number of Monte Carlo simulations will have a high degree of statistical confidence, however the time required to do this activity would be significantly shorter when compared to that with equivalent number of simulations of original model. This chapter discusses the derivation of surrogate models using the concepts of polynomial chaos theory and its application to the TVC benchmark problem.

In the literature, there are several ways to develop surrogate models. Khuri and Mukhopadhyay give a comprehensive review on the response surface methodology in [96]. There they explain the classical response surface method and its develop-

ment from 1951-2010. Kleijnen, [97], provides a review on Kriging method and also presents a method to develop surrogate models by applying Kriging to data sets generated by Latin hypercube sampling. Cheng and Titterington, [99], presents a review on artificial neural networks from the statistical perspective, wherein, their use in developing the surrogate models is explained. In [95], Friedman developed a statistical technique called Multivariate Adaptive Regression Splines (MARS) to model complex nonlinear functions. Chung and Alonso, [98], provide a comparison between response surface method and the Kriging method when applied to a supersonic business jet design problem. It was observed that the response surface method did not provide a good approximation to the models with multiple local minima, whereas the Kriging method was found to be less accurate in estimating the global extrema. Jin et al., [94], compare various methods like polynomial regression, Kriging, MARS and radial basis functions under multiple modelling criteria for the vehicle design problem. Among the methods that were applied for vehicle design, the most efficient method was found to be polynomial regression.

In conventional Monte Carlo V&V analysis, the model is evaluated about many input parameters sampled from a distribution, and the corresponding output function values are determined. Thus, the inputs may be considered as the random excitations to the black-box model leading to different performance outputs. The random excitations often belong to a specific probability distribution, for e.g., uniform or Gaussian. The performance metrics will be different to each of these random fluctuations. Hence, It is possible to interpret the relation between the performance metric and the uncertain parameters as a random process. Formally, a random process is defined as, ([100])

$$F(t,\delta) = \int g(t) d\mu(\delta) \tag{3.2}$$

where, $g(t)$ is a deterministic process, t is time and $d\mu(\delta)$ is an orthogonal set of functions in terms of uncertain parameter δ. $F(t,\delta)$ represents a random process whose covariance function $R(t_1,t_2)$ satisfies the following relation

$$\int R(t_1,t_2)\phi_i(t_1)dt_1 = \lambda_{eig_i}\phi_i(t_2) \tag{3.3}$$

where t_1 and t_2 are temporal coordinates, λ_{eig_i} and $\phi_i(\cdot)$ represents i^{th} eigenvalue and i^{th} eigenfunction respectively.

In 1946, [101], a method called as the Karhunen-Loeve (KL) expansion method was proposed to develop surrogate models by making use of the covariance function. Typically, in the KL expansion method, the random process $F(\cdot)$ is represented as the sum of infinite terms of the eigenfunctions ($\phi_i(\cdot)$) and the eigenvalues (λ_{eig_i}) appearing in the covariance function ($R(\cdot)$) [102]. The KL expansion of the random process $F(\cdot)$ can be represented as

$$F(t,\delta) = \tilde{F} + \sum_{i=1}^{\infty} \sqrt{\lambda_{eig_i}}\phi_i(t)\xi_i(\delta) \tag{3.4}$$

where $\tilde{F}$ denotes the mean of the random process and the terms $\xi_i(\cdot)$ form the set of uncorrelated random variables. See [102] for more details on additional theoretical aspects of the KL expansion. The KL expansion method, though attractive and efficient, assumes the *a priori* knowledge of the covariance function ($R(\cdot)$) for the performance metrics. This can be considered as the main draw back of the KL expansion method. In a typical V&V analysis, there is no *a priori* information

about the covariance function. This is the major impediment to adopt the KL expansion technique directly in the type of V&V analysis carried out in the thesis.

Another efficient method for developing surrogate models in the case of complex industrial models is based on the principles of polynomial chaos expansion. In this thesis, the surrogate models are developed using polynomial chaos technique, the fundamentals of which are discussed in sequel. Subsequently, the surrogate models for the performance metrics of the TVC benchmark problem have been constructed using the polynomial chaos expansion method and the efficacy of the methodology is demonstrated.

3.2 Polynomial chaos expansion

Norbert Wiener introduced the concept of polynomial chaos in 1938 ([103]), in which stochastic processes with Gaussian random variables was modelled in terms of the Hermite polynomials. Later in 1944, Cameron and Martin ([104]) showed that any random process $F(\cdot)$ with a finite variance can be expressed as a weighted infinite sum of Hermite polynomials in a Gaussian random variable $\delta \in \mathbb{R}$, with zero mean and unit variance as

$$F(\delta) = \sum_{q=0}^{\infty} a_q \Phi_q(\delta) \tag{3.5}$$

where the terms a_q are the co-efficients of the univariate polynomial and the terms $\Phi_q(\cdot)$ are the basis of the Hermite polynomials. For example, the first three basis

of univariate Hermite polynomial are.

$$\begin{aligned}\Phi_1(\delta) &= 1\\ \Phi_2(\delta) &= \delta\\ \Phi_3(\delta) &= \delta^2 - 1\end{aligned}$$

3.2.1 Wiener Askey polynomial chaos

Subsequently, similar representations were derived for stochastic process with non-Gaussian random variables in [105]. For this purpose, properties of other orthogonal polynomials from the family of Askey scheme such as Legendre, Laguerre and Jacobi polynomials are exploited. In [105], it was shown that for the continuous random variables with uniform, gamma and beta distributions, Legendre, Laguerre and Jacobi orthogonal polynomial basis can be used to develop the corresponding asymptotically convergent polynomial representation.

The basic concept of polynomial chaos modelling is to approximate the response of the model using a polynomial function of the uncertain parameters. The polynomial function is constructed using an orthogonal polynomial basis ($\Phi_q(\delta)$). Here, the underlying idea is as follows: represent the random variables, i.e., various uncertain parameters to be perturbed, as orthogonal functions and determine the coefficients in Eqn. 3.5 to develop the polynomial model. A truncated version of Eqn. 3.5 is given as follows [105]:

$$F(\delta) = \sum_{q=0}^{M} a_q \Phi_q(\delta) \tag{3.6}$$

where $M = q_c - 1$, where $q_c = \frac{(q_v+q_o)!}{(q_v!q_o!)}$ is the total number of coefficients, and

q_v is the number of independent sources of uncertainty and q_o is the maximum order of the polynomial. Here, the coefficient, a_q, for $q = 0, \ldots, M$ have to be determined. The terms $\Phi_q(\cdot)$, for $q = 0, \ldots, M$ are a set of polynomials that belong to a family of polynomials which are orthogonal and satisfy complete basis in the square integrable space.

$$\int_{\mathcal{D}_\delta} \Phi_i(\delta)\Phi_j(\delta)\mathrm{w}(\delta)d\delta = \begin{cases} 0 & \text{if } i \neq j \\ h_i^2 & \text{if } i = j \end{cases} \tag{3.7}$$

where h_i^2 is a constant term corresponding to $\int_{\mathcal{D}_\delta} \Phi_i^2(\delta)\mathrm{w}(\delta)d\delta$. $\mathcal{D}_\delta$ is the domain of the random variable δ. The term $\mathrm{w}(\delta)$ is the weighting function and has same form as the probability density function of the random variable δ. In the case of multiple random variables, the weighting function corresponds to a joint probability density function of the independent random variables.

Table 3.1 gives different distributions of random variables and the associated orthogonal polynomial functionals from the Wiener-Askey scheme together with the support set. For example, for a continuous uniform distributed random variable, a Legendre polynomial basis with corresponding support set $[-1, 1]$ can be utilised for constructing representation as in Eqn 3.6.

Table 3.1: Wiener-Askey polynomials with corresponding distribution

	Random variable δ	Wiener-Askey Scheme	Support Set
Continuous	Gaussian	Hermite	$(-\infty, \infty)$
	Gamma	Laguerre	$[0, \infty)$
	Uniform	Legendre	$[-1, 1]$
	Beta	Jacobi	$[a, b]$

The weight functions $(w(\delta))$ and the recurrence relations that generate the

basis of orthogonal polynomials in Table 3.1 are given in Appendix A.

3.2.2 Intrusive and Non-intrusive method

In general, there are two distinct methodologies for constructing the polynomial chaos representations, and can be classified as intrusive and non-intrusive methods. This distinction is based on the availability of the explicit mathematical equation that describes the dynamics of the model. Intrusive method relies on the availability of analytical equations of the system and utilises the method of Galerkin projection to develop polynomial representations.

Let us consider a stochastic differential equation, [105]:

$$\mathcal{L}(x,t,\delta) = f(x,t,\delta)$$

where the operator $\mathcal{L}$ generally involves differentiation in space/time and can be nonlinear, x represents the states of the system, t represents time and δ the random parameter that could be introduced via initial conditions, material properties etc. Say, $F(x,t,\delta)$ denotes the solution to the above stochastic differential equation, then the solution can be expanded as a Wiener-Askey polynomial chaos as follows:

$$F(x,t,\delta) = \sum_{q=0}^{M} a_q(x,t)\Phi_q(\delta)$$

The coefficients $(a_q(x,t))$ can be evaluated using the Galerkin projection method:

$$a_q(x,t) = \frac{< \mathcal{L}(x,t,\delta), \Phi_q(\delta) >}{< \Phi_q(\delta), \Phi_q(\delta) >} \tag{3.8}$$

where, $< \cdot, \cdot >$ denotes the inner product. For example, let f and g be two real

functions defined over a closed interval $[a,\ b]$. Then the inner product is defined as $< f, g >= \int_a^b fgdx$.

Evaluation of (3.8) requires solving multiple integrals which depends on the dimension of δ, which are the random variables often representing uncertainties. Hence, polynomial approximation of models with larger number of uncertainties, using Galerkin projection method results in excessive computational overhead due to the numerical integration that requires evaluation of the original model at various combination of uncertainty configuration.

Non-intrusive methods does not require explicit availability of the analytic expressions of the dynamics of the model. The model can be treated as a 'black box' with access limited to certain pre-defined inputs and outputs of the model, which may be complex, non-linear and of high fidelity. This is represented in Figure 3.1. The idea is to obtain a surrogate polynomial representation for the performance specification in terms of the uncertain parameters that robustly mimic the actual model over a wide region.

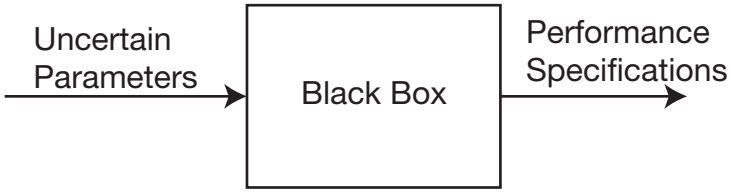

Figure 3.1: Block description of a surrogate modelling

Probabilistic collocation is a non-intrusive method, which is based on intelligent sampling of the uncertain parameter space such that the original model is evaluated at a predefined set of points. Probabilistic collocation is utilised here to generate surrogate models that take uncertain parameters as its input and performance criterion as its output. Details on probabilistic collocation method can be

found in Section 3.3. Both intrusive and non-intrusive polynomial chaos methods have been previously applied to different areas such as solid mechanics [106, 107], stochastic finite elements [100] and stochastic fluid dynamics [108, 109]. In [110], the power series expansion as well as polynomial chaos expansion have been used to quantify the effects of uncertainty on the sates and outputs of nonlinear systems, and illustrate it on a batch crystallisation process. In [111], Polynomial Chaos is used to analyse stability and control of a dynamical system whose gains are treated as uncertainties. Singh, [112], used the generalised polynomial chaos (gPC) method to design robust input shapers for precise control of mass-spring systems. In aerospace applications, Fisher, [113], provided a framework based on gPC to analyse a linear flight control design for an F-16 aircraft model.

The concepts of the polynomial chaos modelling is applied to the TVC benchmark with 29 uncertainties.

3.3 Probabilistic collocation method

In probabilistic collocation method, the original model has to be evaluated at a specific set of points sampled in the uncertain parameter space. The idea here is to generate a set of sampling points such that the behaviour of the original model can be captured. These sampling points are termed as collocation points. In the literature collocation points have been generated using various methods, For example, Hosder in [114], utilises the sampling methods like random sampling, latin hypercube sampling and Hammersley sampling for generating collocation points. Loeven in [115] uses the Gauss quadrature method to generate the collocation points where the recurrence coefficients (α_i, β_i) are generated using the Darboux's

formulae [115, 116]. According to [115], the orthogonal polynomials satisfies the three term recurrence relationship

$$\begin{aligned} \Phi_{i+1}(\delta) &= (\delta - \alpha_i)\Phi_i(\delta) - \beta_i \Phi_{i-1} \qquad i = 1, 2, \ldots, q. \\ & \Phi_0(\delta) = 0, \Phi_1(\delta) = 1 \end{aligned} \tag{3.9}$$

where, recurrence coefficients are evaluated as follows:

$$\begin{aligned} \alpha_i &= \frac{< \delta\Phi_i, \Phi_i >}{< \Phi_i, \Phi_i >} \qquad i = 1, 2, \ldots, q. \\ \beta_i &= \frac{< \Phi_i, \Phi_i >}{< \Phi_{i-1}, \Phi_{i-1} >} \qquad i = 2, 3, \ldots, q. \end{aligned}$$

where $< \cdot, \cdot >$ is the inner product. These recurrence coefficients are then utilised to generate a matrix. The eigenvalues of the matrix T in (3.10) are the roots of the polynomial in the orthogonal basis [115]. These eigenvalues becomes the collocation points at which the original model has to be evaluated to achieve the polynomial representation.

$$T = \begin{bmatrix} \alpha_1 & \sqrt{\beta_2} & & & & \\ \sqrt{\beta_2} & \alpha_2 & \sqrt{\beta_3} & & 0 & \\ & \sqrt{\beta_3} & \alpha_3 & \sqrt{\beta_4} & & \\ & & \ddots & \ddots & \ddots & \\ & 0 & & \sqrt{\beta_{q-1}} & \alpha_{q-1} & \sqrt{\beta_q} \\ & & & & \sqrt{\beta_q} & \alpha_q \end{bmatrix} \tag{3.10}$$

A simpler method to generate collocation points is provided by Webster in [117]. Wherein the roots of the next higher order polynomial in the orthogonal polyno-

mial basis is considered as collocation points. This method is utilised in this thesis for generating collocation points. Table 3.2, enumerates the steps for generation of collocation points.

Table 3.2: Generation of Collocation Points

Steps for generating collocation points	
i)	Set the desired order (q_o) of the polynomial ($F(\cdot)$), i.e. surrogate model.
ii)	Pick the next higher order polynomial ($q_o + 1$) in the orthogonal polynomial basis ($\Phi_q(\delta)$).
iii)	Evaluate the roots of the polynomial.
iv)	Set the roots as collocation points.

All the roots of the orthogonal polynomials ($\Phi_q(\delta)$) lie equally distributed in the interior of their support set, [118]. For example, all the roots of the Legendre polynomials will all lie inside $[-1,\ 1]$. Moreover, these roots are equally distributed over the interval $[-1,\ 1]$. Since the roots are equally distributed inside the support set, they can be used as the collocation points. If the collocation points are not equally spread out in the uncertain parameter space then the resulting model will be less accurate.

In this thesis, the original model is evaluated at the roots of the next higher order polynomial in the orthogonal polynomial basis. In fact, (refer Eqn. 3.6) the output of the original model at these collocation points is equated to the product of coefficients and orthogonal polynomial basis ($\Phi_q(\delta)$) in order to generate a system of equations with coefficients as unknowns. The total number of collocation points have to be at least equal to the number of coefficients of the polynomial chaos expansion. If the number of collocation points are equal to the coefficients then their system of linear equations can be solved simultaneously. The main steps involved in deriving surrogate model using the non-intrusive method based on

probabilistic collocation strategy is provided in Table 3.3.

Table 3.3: Surrogate modelling

	Steps for surrogate modelling
i)	Initialise the number of basis for the orthogonal polynomial (q), the order of the surrogate model (q_o) and the number of uncertain parameters (q_v).
ii)	Calculate the number of coefficients for the polynomial surrogate model $q_c = \frac{(q_v+q_o)!}{(q_v!q_o!)}$.
iii)	Generate the basis of the orthogonal polynomial ($\Phi_q(\delta)$) based on the distribution of the random variable δ (Table 3.1).
iv)	Determine the collocation points by solving the roots of the polynomial from the orthogonal polynomial basis($\Phi_q(\delta)$) whose order is $q_o + 1$.
v)	Evaluate the response of the original model at each of the collocation points and obtain a set of linear equations by using equation (3.6).
vi)	Solve the simultaneous equations to determine the coefficients (a_q).

3.3.1 A numerical example

In order to illustrate the development of a surrogate model, consider the example that calculates the magnitude of frequency response of a low-pass Sallen-Key filter,[119]. Although the surrogate polynomial model of this filter may seem as or even more complex than the filter itself, the surrogate models developed for the launcher model are not as complex as the original launcher models. The Sallen-Key filter example is used here to illustrate the steps for development of a surrogate polynomial model. The Sallen-Key filter is shown in Figure 3.2 and its transfer function is given as:

$$H(s) = \frac{1}{1 + C_2(R_1 + R_2)s + C_1C_2R_1R_2s^2} \tag{3.11}$$

where R_1, R_2, C_1, C_2 are the resistance and capacitance respectively. In this ex-

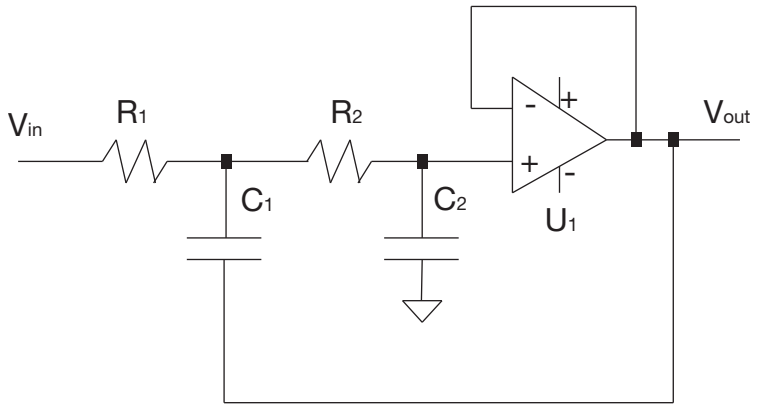

Figure 3.2: Low-pass Sallen-Key Filter

ample, the resistance R_1 and capacitor C_1 are assumed to be uncertain where as resistance R_2 and capacitor C_2 are fixed at 100Ω and $22.5\mu F$ respectively. The uncertain parameters are assumed to have uniform distribution with $R_1 \in [90\Omega, 110\Omega]$ and $C_1 \in [15\mu F, 30\mu F]$. The uncertainty in R_1 and C_1 could be represented as

$$\begin{aligned} R_1 &= 100 + 10\delta_1 \\ C_1 &= 22.5 + 7.5\delta_2 \end{aligned} \tag{3.12}$$

where δ_1 and δ_2 are uncertainties in the resistance R_1 and capacitor C_1 respectively, which vary uniformly, $\delta_i \in [-1, 1]$. The magnitude of the frequency response of the filter transfer function (Eqn. 3.11) is:

$$|H(j\omega)| = \sqrt{\left(\frac{1 - C_1C_2R_1R_2\omega^2}{f(\omega)}\right)^2 + \left(\frac{-C_2R_1\omega - C_2R_2\omega}{f(\omega)}\right)^2} \tag{3.13}$$

where

$$f(\omega) = 1 + (-2C_1C_2R_1R_2 + C_2^2R_1^2 + 2C_2^2R_1R_2 + C_2^2R_2^2)\omega^2 + C_1^2C_2^2R_1^2R_2^2\omega^4 \quad (3.14)$$

Here the output is the magnitude of the frequency response, ($|H(j\omega)|$), computed at a specific frequency, $\omega = 376.99rad/s$. If δ_1 and δ_2 can then be considered as inputs of $|H(j\omega)|$, then the idea of surrogate modelling is to obtain an equivalent polynomial representation of $|H(j\omega)|$ in terms of the uncertain parameters δ_1 and δ_2.

In this case, the total number of uncertainties (q_v) equals 2; let the order (q_o) of the surrogate model to be constructed be 3. Then, following the procedure listed in Table 3.3, the number of coefficients (q_c) of the surrogate polynomial which are to be determined becomes 10. Since, δ_1 and δ_2 are uniformly distributed, from the Table 3.1, it is obvious that Legendre polynomial basis have to be used. Subsequently, the univariate orthogonal polynomial basis (Φ') are generated for each uncertain parameters and are provided in Table 3.4.

Table 3.4: Legendre polynomial basis

Basis	Uncertain parameter δ_1	Uncertain parameter δ_2
Φ'_0	1	1
Φ'_1	δ_1	δ_2
Φ'_2	$1.5\delta_1^2 - 0.5$	$1.5\delta_2^2 - 0.5$
Φ'_3	$2.5\delta_1^3 - 1.5\delta_1$	$2.5\delta_2^3 - 1.5\delta_2$
Φ'_4	$4.375\delta_1^4 - 3.75\delta_1^2 + 0.375$	$4.375\delta_2^4 - 3.75\delta_2^2 + 0.375$

The subscript i of Φ'_i indicates the order of the polynomial. The next step is to generate collocation points. So that the coefficients can be determined. For that, the solution to the next higher order polynomial, (q_o+1 = 4), in the Legendre polynomial basis is used. This corresponds to solving Φ'_4 for δ_1 and δ_2 in the Table 3.4.

Solving the two polynomial equalities $4.375\delta_1^4 - 3.75\delta_1^2 + 0.375 = 0$ and $4.375\delta_2^4 - 3.75\delta_2^2 + 0.375 = 0$ yields the solution set $\delta_1 = \delta_2 = \{-0.34, -0.86, 0.34, 0.86\}$. This solution set is combined to form a unique set of sampling points for δ_1 and δ_2, which are termed as collocation points and given in Table 3.5.

Table 3.5: Collocation points at which the original model is evaluated

Collocation Points	
Uncertain parameter δ_1	Uncertain parameter δ_2
-0.34	-0.34
-0.34	-0.86
-0.34	0.34
-0.34	0.86
-0.86	-0.34
-0.86	-0.86
-0.86	0.34
-0.86	0.86
0.34	-0.86
0.34	0.86

Since there are two uncertain parameters, a multivariate orthogonal polynomial basis (Φ_q) is required, which is formed by combining the first two Legendre polynomial basis from the Table 3.4, such that each of them satisfies the orthogonality property and the bound on the required order of the polynomial. Furthermore, the number of the multivariate orthogonal polynomial basis should be equal to the number of coefficients i.e. $q_c = 10$. The obtained multivariate orthogonal polynomial basis are given in Table 3.6.

The magnitude of the frequency response of the filter $|H(j\omega)|$ in Eqn. 3.13 is evaluated at each of the collocation points listed in Table 3.5. Our aim is to determine the coefficients a_q of $F := |H(j\omega)| = \sum_{q=0}^{10} a_q \Phi_q(\delta)$. The set of $|H(j\omega)|$ values obtained by evaluating at each collocation points, then provide ten linear equations that has to be solved simultaneously to obtain the coefficients a_q. The

Table 3.6: Multivariate orthogonal polynomial basis

Multivariate Orthogonal Polynomial Basis (Φ_q)	
Φ_0	1
Φ_1	δ_1
Φ_2	δ_2
Φ_3	$1.5\delta_1^2 - 0.5$
Φ_4	$1.5\delta_2^2 - 0.5$
Φ_5	$2.5\delta_1^3 - 1.5\delta_1$
Φ_6	$2.5\delta_2^3 - 1.5\delta_2$
Φ_7	$\delta_1\delta_2$
Φ_8	$1.5\delta_1\delta_2^2 - 0.5\delta_1$
Φ_9	$1.5\delta_1^2\delta_2 - 0.5\delta_2$

coefficients (a_q) when multiplied with respective multivariate orthogonal basis (Φ_q) provide us the surrogate polynomial model (Eqn. 3.6), which is supposed to be an equivalent representation for $|H(j\omega)|$ in Eqn. 3.13.

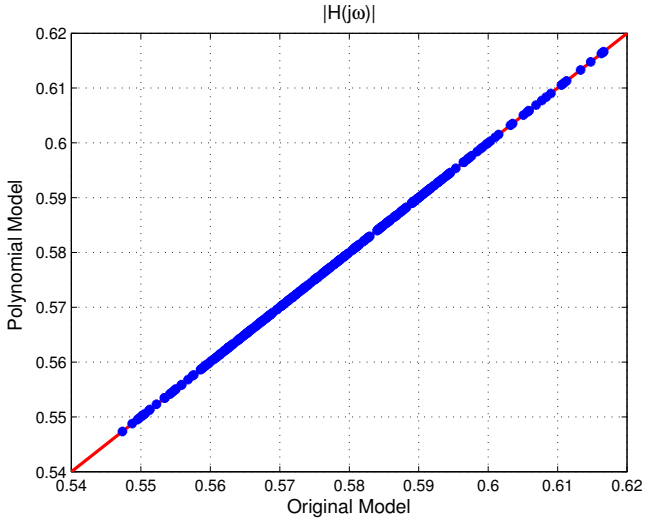

Figure 3.3: Comparison of accuracy of the surrogate model

3.4 Surrogate modelling of TVC benchmark

The dynamics of the closed loop flexible launcher model, discussed in Section 2.4.5 is considered. An H_∞ controller is provided with the model. The uncertain parameters present in the model are listed in Table 2.7. These variations results in changes in the outputs of the model. Ideally the H_{infty} controller shall provide robust performance in the presence of all these uncertainties listed in Table 2.7. We will consider the closed loop benchmark representation as 'black-box'. As briefed in Section 2.4.5, the flexible launcher model incorporates the effect of noise acting on its outputs by adding a gaussian signal with $0.02°$ and $0.15°/sec$ standard deviation for attitude and attitude rate respectively. The gaussian noise signal is realised in MATLAB simulink by utilising the "Random Number" simulink block. This simulink block contains an entry called the "Seed", which ensures that the noise signal is not repeated for each evaluation of the flexible launcher model. In order to capture the effect of the noise on the outputs in the surrogate model, the seed value of the "Random Number" simulink block is treated as an uncertainty in addition to the uncertainties considered in the Table 2.7. Hence, the total number of uncertainties q_v is fixed at 29. The cost function is the performance specification against which the controller is validated. The entire list of cost functions are given in the Table 2.8. The polynomial surrogate models are generated for each of the cost functions listed in Table 2.8.

In order to perform the worst case analysis, all the uncertainties given in Table 2.7 are normalized between $[-1, 1]$. As the uncertainties are uniformly distributed, Legendre polynomials are utilised for generating the orthogonal polynomial basis as per the Wiener-Askey scheme, given in Table 3.1. First order (q_o) surrogate models

Table 3.7: Coefficients of 1^{st} order surrogate model for each cost function

Coefficients	$\max_{t\in[t_0 t_f]} \lvert Q_\alpha(t)\rvert$	$\max_{t\in[t_0 t_f]} \lvert\theta(t)\rvert$	$\max \lvert\theta(t_{tf})\rvert$	$\max \lvert\dot{\theta}(t_{tf})\rvert$	$\max_{t\in[t_0 t_f]} \lvert\beta(t)\rvert$	Cumulated Deflection
a_0	-401.44	-2.62	-0.02	0.04	-3.70	-127.57
a_1	-11.78	-0.06	0.01	-0.04	0.36	-0.95
a_2	-1.24	-0.16	0.00	0.00	0.25	-2.07
a_3	51.79	-0.71	0.02	-0.01	-1.21	-0.97
a_4	20.33	-0.56	0.01	-0.02	-0.82	-1.22
a_5	-112.14	-0.81	0.00	0.00	-1.00	-0.12
a_6	6.37	-0.07	0.01	0.00	0.45	1.58
a_7	-17.53	0.03	-0.01	-0.02	-0.24	-1.06
a_8	-15.29	-0.65	-0.01	0.00	0.05	-1.52
a_9	-2.19	-0.19	-0.01	-0.01	-0.03	-0.75
a_10	-2.76	-0.06	0.01	-0.03	-0.44	1.82
a_11	-1.04	-0.09	0.01	0.01	0.23	-0.15
a_12	10.56	-0.02	-0.01	-0.02	0.00	2.21
a_13	-11.26	0.04	0.03	-0.01	0.03	1.56
a_14	-8.06	-0.22	-0.01	-0.03	-0.09	1.22
a_15	2.47	0.19	0.02	-0.01	-0.14	0.22
a_16	-3.10	0.32	0.01	0.00	-0.29	-1.25
a_17	-20.85	-0.09	-0.01	-0.01	0.09	-1.08
a_18	15.85	-0.05	-0.01	-0.02	0.71	0.08
a_19	-13.91	-0.14	0.02	0.01	-0.38	-1.06
a_20	-7.07	0.07	-0.01	0.02	-0.09	0.25
a_21	14.51	0.10	0.00	-0.01	-0.01	-0.12
a_22	10.80	-0.18	-0.02	-0.02	-0.46	-1.09
a_23	-29.54	-0.14	-0.02	0.01	-0.18	-0.58
a_24	2.26	-0.09	0.00	0.00	-0.60	-2.11
a_25	-9.20	0.07	0.01	0.02	0.01	2.02
a_26	6.06	0.23	0.00	-0.03	0.19	-2.54
a_27	-12.92	0.04	0.00	0.00	-0.05	-0.80
a_28	0.67	0.29	-0.02	-0.02	-0.22	0.46
a_29	-0.04	-0.22	-0.02	-0.09	0.02	1.39

are derived using the probabilistic collocation method for wind perturbation occurring at 50 seconds (refer Table 3.7). The number of collocation points required for evaluating the coefficients of the polynomial are given by $q_c = \frac{(q_v+q_o)!}{(q_v!q_o!)} = 30$, where the number of uncertainties q_v and the order q_o are fixed at 29 and 1 respectively. An identical procedure as discussed in previous section was followed. For e.g., the basic idea here is, to obtain an approximate surrogate polynomial for the cost function for e.g. $\max_{t\in[t_0\ t_f]} \left|Q_\alpha(t)\right|$ in terms of the 29 uncertain parameters.

$$\max_{t\in[t_0\ t_f]} \left|Q_\alpha(t)\right| \approx \sum_{q=0}^{M} a_q \Phi_q(\delta) \tag{3.15}$$

where $\Phi_q(\delta)$= $[1,\ \delta_1,\ \delta_2, \cdots,\ \delta_{29}]$ and $a_q = [a\_0, a\_1, \cdots, a\_29]$. Similarly, approx-

imate models are generated for the other cost functions as well in an identical manner. The coefficients of the 1^{st} order surrogate polynomial models are listed in Table 3.7.

A HDE optimisation algorithm is employed to perform the worst case analysis on the first order surrogate models. The results are tabulated as shown in Table 4.2, which contains five columns, the first column corresponds to the cost function for which the surrogate models are derived, second column is for the worst case values (Wc) obtained by performing HDE optimisation on the surrogate models. The third column represents the actual value (Lm) of the cost function when the flexible launcher model is evaluated by using the worst case parameter combination found by surrogate models. The fourth column provides the % Error which is evaluated as

$$\%Error = \frac{|Wc - Lm|}{Lm} \times 100 \tag{3.16}$$

The worst case analysis is performed by using a fixed termination criteria with maximum number of function evaluations set to 1000. It is seen that the polynomial models are very fast (in seconds) as compared to the actual model which takes approximately 15 min. The percentage error is found to be large in the case of the first order polynomial model. In order to reduce the error, second or higher order surrogate models can be derived.

Second order polynomial models are generated for each of the cost functions listed in Table 2.8. A second order polynomial chaos expansion, with 29 uncertain parameters requires 465 coefficients in Eqn. 3.6. For obtaining second order surrogate models for the cost functions listed in Table 2.8, 465 collocation points are generated and the flexible launcher model is simulated and each cost in Table 2.8 is

Table 3.8: Worst case results of 1^{st} order surrogate model for wind @ 50 sec

Cost Function	Max	Actual Value	% Error	Time (sec)
$\max_{t\in[t_0 t_f]} \lvert Q_\alpha(t)\rvert$	647.88	524.35	23.55	6.09
$\max_{t\in[t_0 t_f]} \lvert\theta(t)\rvert$	5.96	4.85	22.88	6.03
$\max \lvert\theta(t_{tf})\rvert$	0.2	0.09	122.2	5.94
$\max \lvert\dot{\theta}(t_{tf})\rvert$	1.68	0.17	500	6.24
$\max_{t\in[t_0 t_f]} \lvert\beta(t)\rvert$	8.84	6.5	36	6.13
Cumulated Deflection	190	129.8	46.37	6.18

evaluated. A set of linear equations can be formed by substituting these collocation points and their corresponding output responses in Eqn 3.6. Coefficients of the polynomial are obtained by solving these set of equations. Both polynomial and original model are evaluated at various uncertainty configurations for comparison, as shown in Figure 3.5. Ideally, all the blue points should lie on the red line indicating a highly accurate polynomial model. From the Figure 3.5, all the points are cluttered around the red line indicating a fairly accurate polynomial model. The comparison is shown for two performance criteria (given in two columns) at three different wind perturbations (along each row). In order to generate a polynomial model with further higher degree of accuracy one will have to go for higher order polynomials. The higher the order of the polynomial, the larger are the number of coefficients to be evaluated, and hence an increase in the modelling time.

The Polynomial modelling complexity is depicted in Figure 3.4. It shows that as the order of the polynomial increases so does the number of coefficients to be

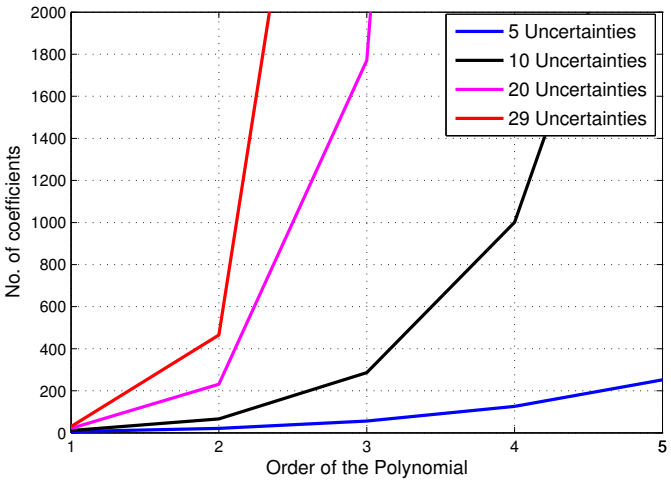

Figure 3.4: Polynomial modelling complexity.

evaluated. Also, as the number of uncertain parameters increases the total number of coefficients increases exponentially. A large number of simulations of launcher vehicle are required for development of surrogate models whose order is more than 2.

3.5 Worst case analysis

Table 3.9 contains the results of worst case analysis performed using a second order polynomial. The error between the surrogate model and the actual model is found to be small. As the time taken for performing the worst case analysis on polynomial models is considerably small, one can perform even more number of function evaluations in less amount of time. In this study, the termination criteria for hybrid differential evolution was set to a maximum function evaluations of 10000 while performing the worst case analysis on the second order polynomial models. The

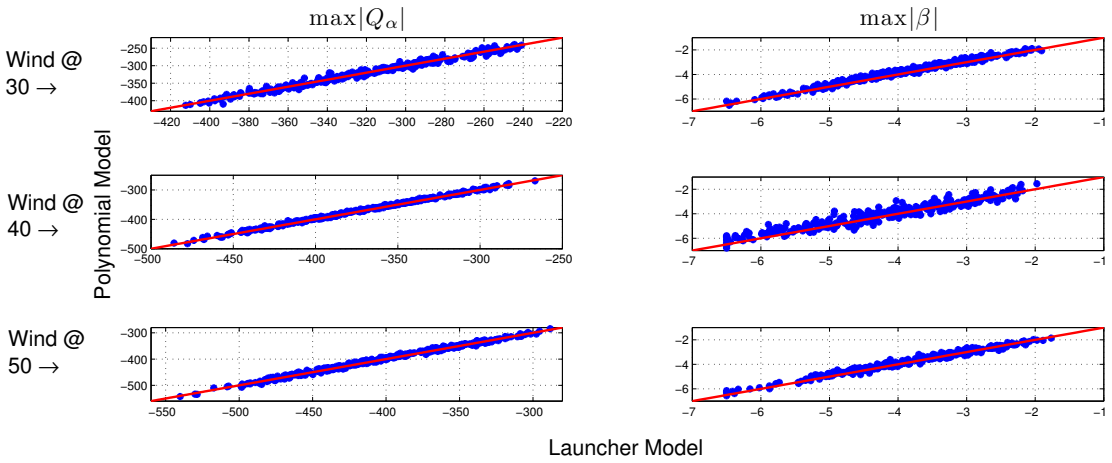

Figure 3.5: Comparison between launcher and polynomial models.

performance criterion for aerodynamic load (Q_α), is violated for wind perturbation occurring at 40 and 50 seconds. The worst case directions are shown in Figure 3.7 which suggests that the worst case direction is oriented towards dynamic pressure MQ, aerodynamic coefficient MCz and center of pressure MXf. Similar worst case directions were identified when performing worst case analysis on the original model in Section 2.4.9, Figure 2.15. The time plots are generated by using the worst case parameter combination found by using the surrogate models on the actual models and shown in Figure 3.6. For wind perturbation at 40 seconds, Table 3.9 shows for attitude cost functions that the surrogate models are unable to capture unstable cases. These unstable cases are not accurately captured by the surrogate models but they provide good estimates for stable ones. A reason is that the nonlinearity present in the original launcher model are not entirely captured

Table 3.9: Worst Case results for second order polynomial model

Cost Functions		Worst Case Values		
		30 sec	40 sec	50 sec
$\max_{t\in[t_0 t_f]} \lvert Q_\alpha(t)\rvert$	Max	448.66	510.79	557.28
	Actual Value	430.26	514.95	553.77
	%Error	4.276484	0.807845	0.6338372
	Time(sec)	200.59	199.31	200.02
$\max_{t\in[t_0 t_f]} \lvert\theta(t)\rvert$	Max	5.85	8.05	6.91
	Actual Value	6.01	Unstable	6.02
	%Error	2.66223	-	14.7840532
	Time(sec)	163.17	165.15	163.62
$\max \lvert\theta(t_{tf})\rvert$	Max	0.354	0.33	0.227
	Actual Value	0.191	Unstable	0.109
	%Error	85.340314	-	108.2568807
	Time(sec)	160.05	161.36	161.93
$\max \lvert\dot{\theta}(t_{tf})\rvert$	Max	0.211	0.212	0.195
	Actual Value	0.144	0.187	0.173
	%Error	46.527778	13.368984	12.716763
	Time(sec)	162.28	160.76	160.42
$\max_{t\in[t_0 t_f]} \lvert\beta(t)\rvert$	Max	7.5	8.48	7.75
	Actual Value	6.5	6.5	6.5
	%Error	15.384615	30.461538	19.2307692
	Time(sec)	163.33	163.06	160.09
Cumulated Deflection	Max	137.99	147.62	136.16
	Actual Value	135.48	128.57	140.78
	%Error	1.852672	14.816831	3.2817162
	Time(sec)	168.53	189.45	164.91

by the surrogate model, especially when large deviation emanating from onset of instability occurs. However, the worst case analysis performed on surrogate models was able to give the worst case parameter combinations that corresponded to instability cases in the launcher model. A possible way to overcome this is to develop a accurate local surrogate models that represent a section of the search space. But here the objective was to derive global surrogate models (i.e. one polynomial model representing the entire search space) with a fair degree of accuracy

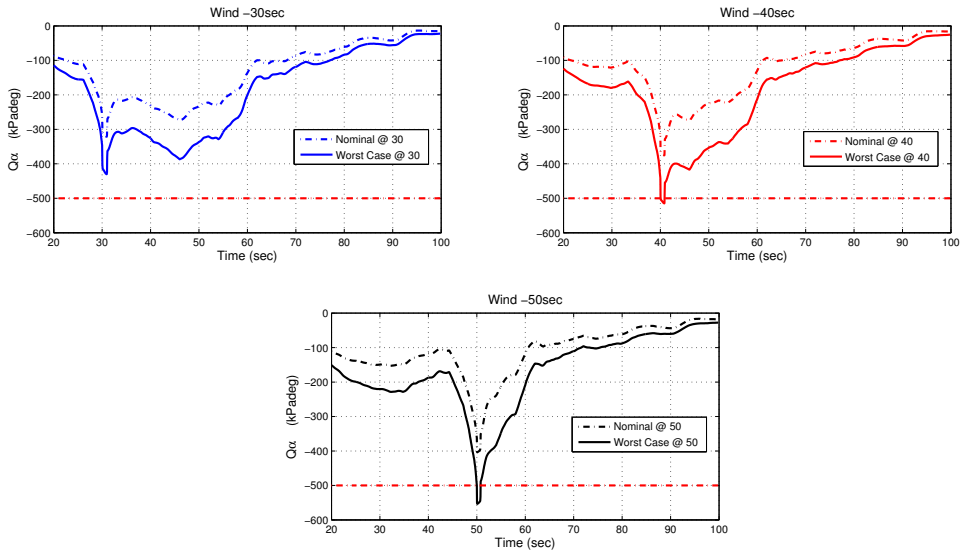

Figure 3.6: Aerodynamic AoA Q_α plots at different wind perturbation instances for $\max |Q_\alpha(t)|$

with less number of function evaluations as possible, conservatism is introduced. For example, to increase the accuracy of the surrogate model one might have to go for a third order model. But the number of coefficients for a third order surrogate model with 29 uncertainties is 4960. However, this would be computationally very expensive when compared to conventional Monte Carlo or optimisation based techniques. A work around would be to divide the parameter space into a number of strata and create local surrogate models for each one of them. With lower order local surrogate models one would be able to achieve even higher accuracy. For wind perturbation at 40 and 50 seconds, Table 3.9 shows that the accuracy of the second order surrogate model is less than 1% for Q_α cost function. For these cases, the surrogate models could be used instead of the launcher model. Time domain plots relating to attitude rate and deflection angle are shown in Figure 3.8-3.9.

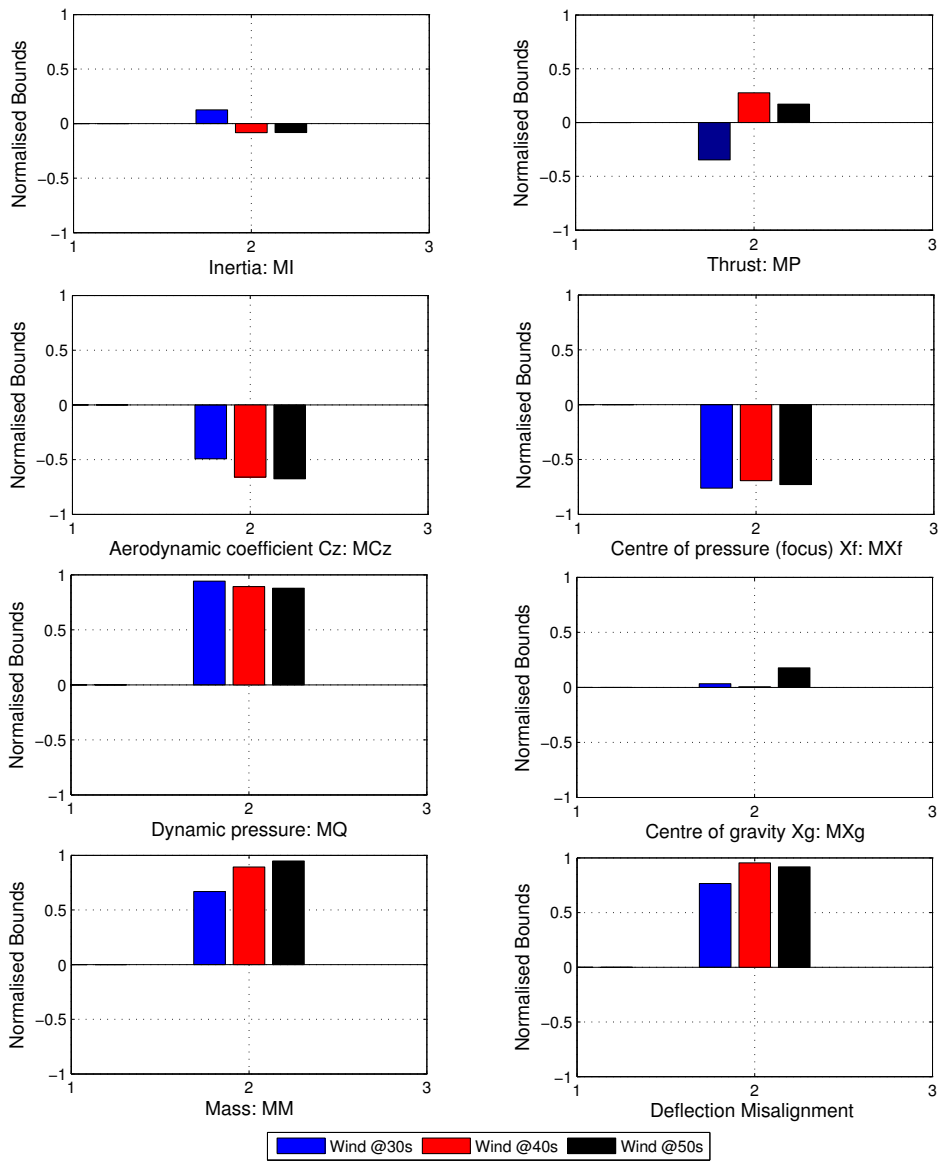

Figure 3.7: Rigid mode worst case perturbations at different wind instances for $\max |Q_\alpha(t)|$

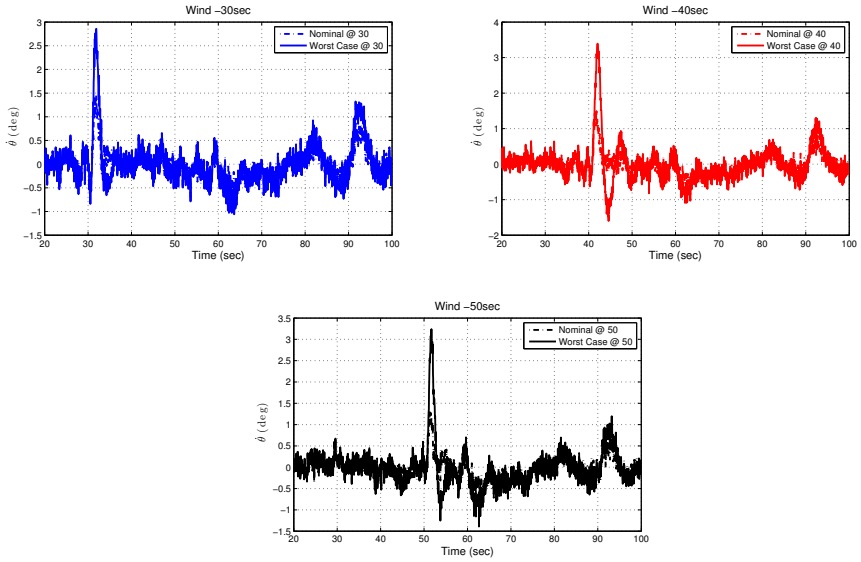

Figure 3.8: $\dot{\theta}$ plots at different wind perturbation instances for $\max|\dot{\theta}(t_f)|$

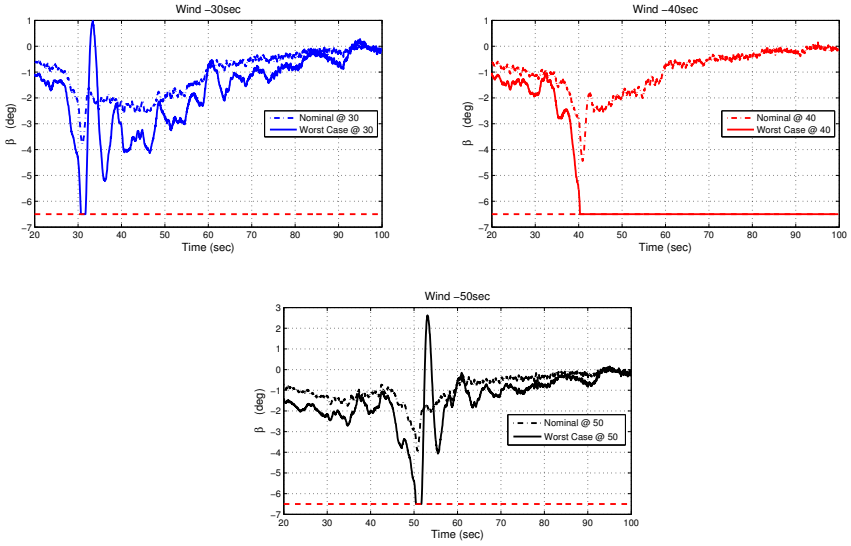

Figure 3.9: β plots at different wind perturbation instances for $\max|\beta(t)|$

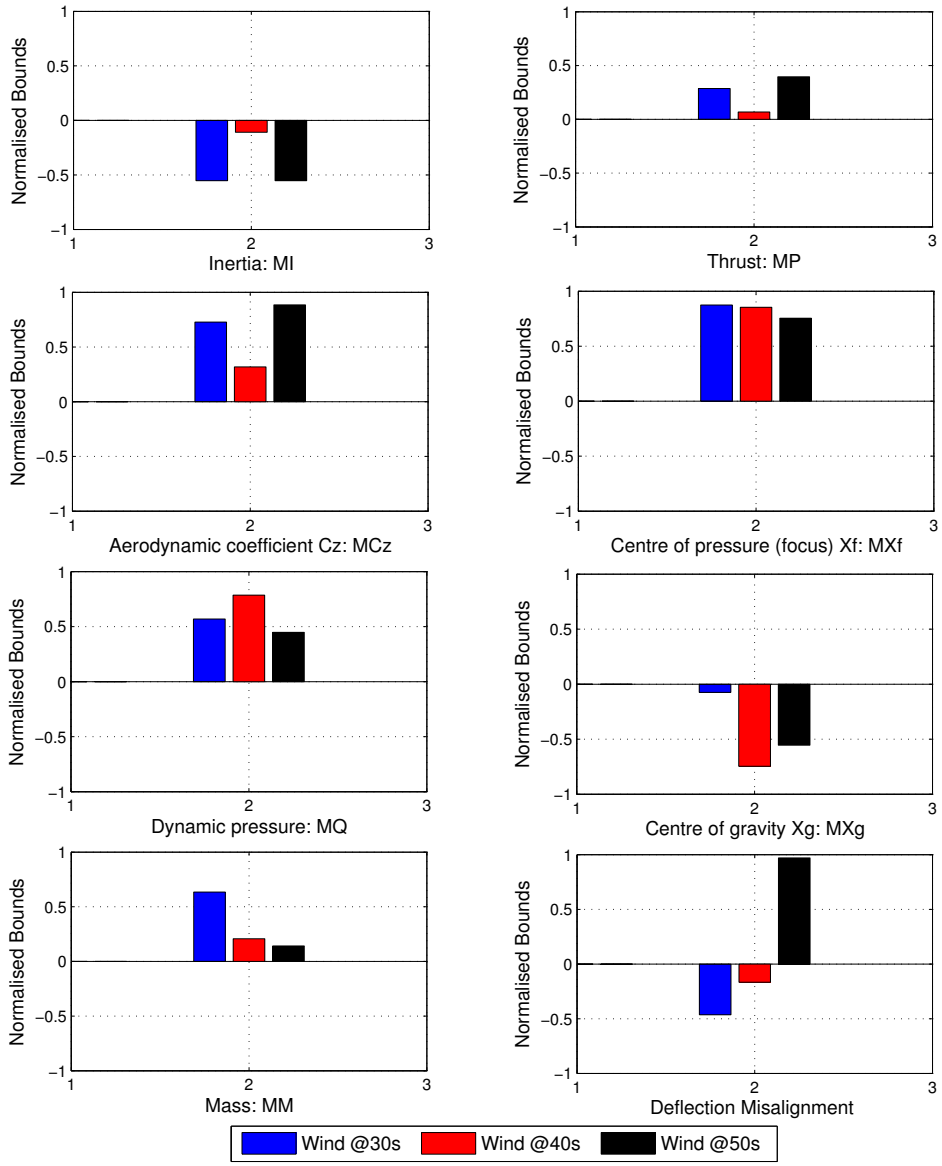

Figure 3.10: Rigid uncertain parameters maximising $|\dot{\theta}(t_f)|$

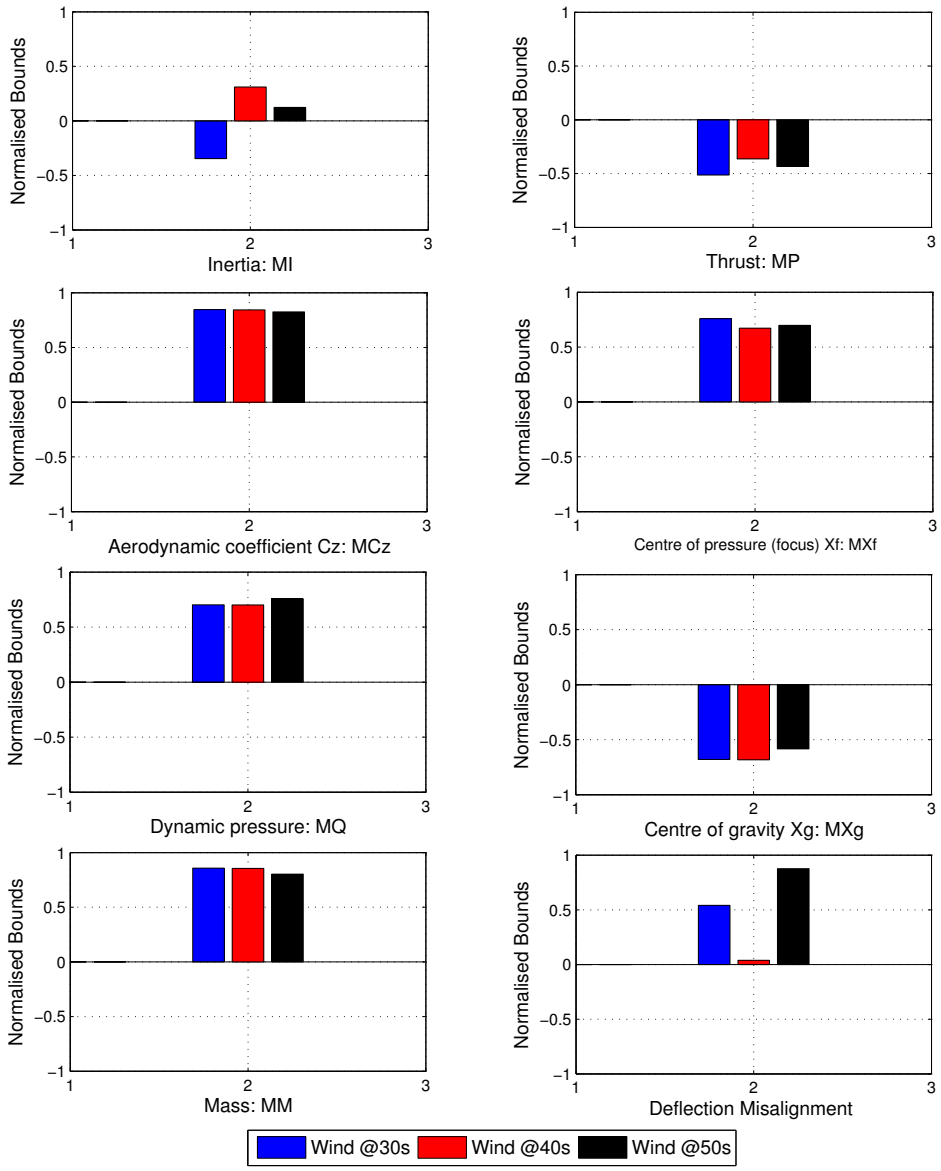

Figure 3.11: Rigid uncertain parameters maximising $|\beta(t)|$

Chapter 4

Identification of safe/failure regions in the parameter space

4.1 Introduction

It is evident that optimisation based analysis efficiently determines a worst-case solution in the multi-dimensional parameter space, which corresponds to either the controller's performance being degraded, or even the complete loss of control. Prior to identifying worst case, the optimisation based analysis evaluates other candidate potential solutions that might be violating the performance criterion and might also lie close to the nominal parameter value in the parameter space. The size of the region around nominal parameter value that satisfies all the performance criteria is a useful metric to comment on the robustness of the control law. In fact, characterising the parameter space into regions which satisfy the performance criteria and which do not would be very insightful. Techniques like operational safety margin method, [46, 120], allow the region around the nomi-

nal parameter value to be determined, whereas the Bernstein expansion method [121], conveniently characterises the entire parameter space into safe and unsafe regions. The safe region corresponds to the region in the parameter space in which all performance criteria are satisfied. The unsafe region is the complement of the safe region, i.e., where one or more of the performance criteria are violated. Both methods are investigated in this chapter.

The concept of operational safety margin quantifies the largest region around the nominal parameter value. The operational safety margin metric is a measure of the size of the safe region around a nominal parameter and thus is a practical metric to assess the robustness of a non-linear closed loop system. A comparison of different versions of controllers could be based on how big or small the region is [122, 123]. In this chapter, for the first time, the surrogate models from section Chapter 3, 3.4 are integrated to speed up the process of evaluating the operational safety margin for the launcher model.

4.2 Operational safety margin assessment

4.2.1 Basic Concept

The basic idea of operational safety margin assessment is to assess the largest region in a multi-dimensional space around the nominal parameter such that every perturbation belonging to that region/set satisfy all the performance criteria. In order to determine the exact boundaries of safe and unsafe regions, extensive search of the parameter space may have to be performed. The idea here is to find an approximate safe region in the multi-dimensional space centred around the

nominal parameter value. For this, two support sets, i.e., rectangular or spherical could be utilised. Rectangular support set is defined around the nominal parameter value by min/max bounds along each dimension of the parameter space, whereas the spherical support set is defined by utilising the nominal parameter value as the center with radius defined along each dimension. Using either one of the support sets, a safe region around the nominal parameter value is identified. It is obvious that the estimated safe region may be conservative, and depends on the support set.

The closed loop functional performance requirements are written as a set of inequality constraints $\mathbf{s}(\delta, \mathcal{C}_{\mathcal{H}_\infty}, W) < 0$, where $\mathcal{C}_{\mathcal{H}_\infty}$ is the control law used and W is the wind gust disturbance profile and $\delta \in \Delta$. The closed loop design is said to be robust and acceptable, if each i^{th} inequality constraint $\mathbf{s}_i(\delta, \mathcal{C}_{\mathcal{H}_\infty}, W) < 0$ is satisfied in the presence of various combinations of uncertain parameter perturbations. An assumption is that the nominal parameter satisfies all constraints s_i.

The uncertain parameter space (Δ - space), can be classified into safe and unsafe region, depending on the satisfaction or violation of the set of constraints $\mathbf{s}(\delta, \mathcal{C}_{\mathcal{H}_\infty}, W) < 0$, respectively. The unsafe region, denoted as $\mathcal{S}^u(\mathbf{s}) \subset \Delta$, is given by

$$\mathcal{S}^u(\mathbf{s}) := \bigcup_{i=1}^{dim(\mathbf{s})} \mathcal{S}_i^u(\mathbf{s}_i)$$

where, for S_i^u is the i^{th} unsafe region corresponding to the i^{th} inequality constraint s_i

$$\mathcal{S}_i^u(\mathbf{s}) = \{\delta \in \mathbb{R}^{dim(\delta)} | \mathbf{s}_i(\delta, \mathcal{C}_{\mathcal{H}_\infty}, W) > 0\}$$

$\mathcal{S}^u(\mathbf{s})$ is the union of all unsafe regions defined by the individual constraints. The boundary of the set is on the surface, given by the constraint $\mathbf{s}(\delta, \mathcal{C}_{\mathcal{H}_\infty}, W) = 0$.

The complementary set $\mathcal{S}'^{u}(\mathbf{s})$ becomes the safe set. At least one constraint must be violated in the unsafe region while in the safe region all the performance constraints must be satisfied.

A reference set in the parameter space needs to be defined with the nominal parameter vector δ_0 as the geometric center. This reference set is then subjected to homothetic dilations (i.e. expansion and contraction of set) until the first instance of violation of the constraints $\mathbf{s} < 0$ occur, or when $\mathbf{s} = 0$ is found. Here, $\mathbf{s} < 0$ implies violation of at least one constraint $\mathbf{s}_i < 0$. In other words, we are interested in evaluating the largest safe set, $\mathcal{S}'^{u}(\mathbf{s})$, around the nominal parameter value within which the set of constraints $\mathbf{s} < 0$ is satisfied. The size of this set is directly related to the operational safety margin. If the size is larger, it implies that the closed loop system has more robustness and can be operated over a larger uncertainty region, i.e. larger operating region.

4.2.2 Optimisation problem formulation

In this study, the chosen reference set, $\mathcal{M} \subset \Delta := \delta \in [\delta_{min},\ \delta_{max}]$, is assumed to be a hyper rectangle with each component of the uncertain parameter vector, $\delta \in \mathbb{R}^{dim(\delta)}$, defined over a bounded interval. Assume symmetry about the geometric centre which corresponds to the nominal parameter value (δ_0). Let $\mathbf{m}$ is the vector of half-lengths of the sides of the hyper-rectangle. The hyper-rectangle $\mathcal{R}(\delta_0, \mathbf{m})$ is defined as

$$\mathcal{R}(\delta_0, \mathbf{m}) := \{\delta | \delta^i \in [\delta_0^i - \mathbf{m}^i, \delta_0^i + \mathbf{m}^i], 1 \leq i \leq dim(\delta)\} \tag{4.1}$$

$\mathcal{R}(\delta_0, \mathbf{m})$ is called the reference set, which is chosen by selecting the values of

the vector of half lengths $\mathbf{m}$. This reference set, $\mathcal{R}(\delta_0, \mathbf{m})$, is depicted by dashed blue line in Figure 4.1(a) and 4.1(b). A homothetic scaling of the reference set by a scaling factor λ is $\mathcal{R}(\delta_0, \lambda\mathbf{m}) := \{\delta_0 + \lambda(\delta - \delta_0) | \delta \in \mathcal{R}(\delta_0, \mathbf{m})\}$. Suppose λ is positive, the resultant set is expanded w.r.t the reference set, in Eqn no 4.1 and if λ is negative, the resultant set is contracted w.r.t the reference set in Eqn no 4.1. The ratio of expansion, or contraction is called the similitude ratio, $\lambda \in \mathbb{R}$. The similitude ratio is a positive scaling factor. The similitude ratio condition $\lambda > 1$ corresponds to the expansion, and the similitude ratio in the range of $0 < \lambda < 1$ corresponds to the contraction of the reference set, $\mathcal{R}(\delta_0, \mathbf{m})$. By successive dilations of the reference set, i.e., expansions and contractions, the objective is to determine the largest safe set, $\mathcal{S}'^{u}(\mathbf{s})$, around the nominal parameter value. The largest set is depicted by the red line in Figure 4.1(a) and 4.1(b) and is represented as $\mathcal{R}(\delta_0, \widetilde{\lambda}\mathbf{m})$, where $\widetilde{\lambda}$ is called the critical similitude ratio. Critical similitude ratio is a non-dimensional positive scaling value denoted as $\widetilde{\lambda}$. It is the similitude ratio of the dilation, and interpreted as the operational safety margin, ρ, for satisfaction of all the functional performance requirements in the parameter space. The corresponding uncertain parameter combination is termed as critical parameter vector. Hence, although conservative this would be viewed as the onset of violation of at least one performance criterion in the certain parameter space. There could be certain directions in which an expansion might still be possible, depending on the complex topology of the safe uncertainty set.

The sets $\mathcal{R}(\delta_0, \mathbf{m})$ and the scaled set$\mathcal{R}(\delta_0, \widetilde{\lambda}\mathbf{m})$ are proportional. In Figure 4.1(a), the reference set, $\mathcal{R}(\delta_0, \mathbf{m})$, has expanded to $\mathcal{R}(\delta_0, \widetilde{\lambda}\mathbf{m})$, which implies that the unsafe region $\mathcal{S}^u$ is outside the reference set. Whereas in Figure 4.1(b), the reference set, $\mathcal{R}(\delta_0, \mathbf{m})$, has contracted to $\mathcal{R}(\delta_0, \widetilde{\lambda}\mathbf{m})$, implying that the unsafe

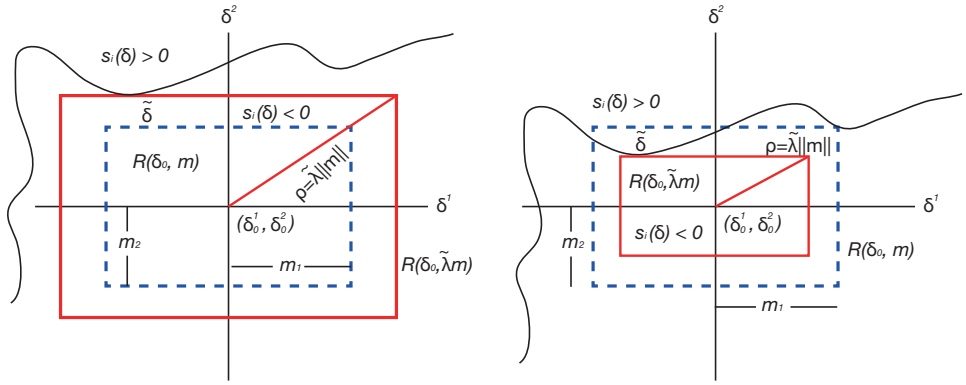

(a) Expansion (b) Contraction

Figure 4.1: Dilations of Uncertainty Set.

region to be inside the reference set. Naturally, good robustness is associated with the expansion of the reference set whereas the contraction implies poor robustness, since even a small perturbation around the nominal parameter value would result in violation of performance criteria. This is a measure of robustness of the controller, $\mathcal{C}_{\mathcal{H}_\infty}$, implying how large an uncertain parameter set be identified as safe with respect to the nominal point.

The constraint $\mathbf{s}(\delta, \mathcal{C}_{\mathcal{H}_\infty}, W)$ might have a nonlinear dependency on the parameters, and hence the computation of the critical parameter value becomes a non-convex global optimisation problem. Furthermore, for checking the satisfaction of the constraints, simulation of the closed loop model and evaluation of each performance constraint is required.

The critical parameter value corresponding to the dilation of the reference set $\mathcal{R}(\delta_0, \mathbf{m})$ in the case of the i^{th} constraint can be computed by solving

$$\widetilde{\delta} = \arg\min_{\delta} \{ ||\delta - \delta_0||_{\mathbf{m}}^{\infty} | \mathbf{s}_i(\delta, \mathcal{C}_{\mathcal{H}_\infty}, W) \geq 0 \} \tag{4.2}$$

where $||\delta - \delta_0||_{\mathbf{m}}^{\infty} := \arg\sup_i \{ \frac{|\delta - \delta_0|_i}{\mathbf{m}_i} \}$, is $\mathbf{m}$-scaled norm. Considering all the perfor-

mances, the overall critical parameter value is $\widetilde{\delta} = \widetilde{\delta_k}$, where $k = \underset{1 \leq j \leq dim\delta}{\arg\min}\{||\widetilde{\delta^j} - \delta_0||^{\infty}_{\mathbf{m}}\}$, which is associated with the critical requirement. The resultant set $\mathcal{R}(\delta_0, \widetilde{\lambda}\mathbf{m})$ is proportional to $\mathcal{R}(\delta_0, \mathbf{m})$, where $\widetilde{\lambda} = ||\widetilde{\delta} - \delta_0||^{\infty}_{\mathbf{m}}$, in a non-dimensionalised setting.

The operational safety margin is $\rho = \widetilde{\lambda} \parallel \mathbf{m} \parallel$. The robustness is ensured when $\rho \geq \|\mathbf{m}\|$ for a given controller design. In such situation, all the performance constraints $\mathbf{s}(\delta, \mathcal{C}_{\mathcal{H}_\infty}, W) \leq 0$ are satisfied in the region $\Delta = \mathcal{R}_\delta(\delta_0, \mathbf{m})$. Eqn 4.2 is reformulated as a constrained optimisation problem as follows.

$$\begin{aligned} \min \quad & ||\delta - \delta_0||^{\infty}_{\mathbf{m}} \\ \text{Subject to:} \quad & \mathbf{s}_i(\delta, \mathcal{C}_{\mathcal{H}_\infty}, W) \geq 0 \end{aligned} \tag{4.3}$$

The evaluation of operational safety margin becomes computationally very expensive when applying it to a industry standard problem. As the performance criteria are treated as constraints, the closed loop dynamical system is simulated and performance criteria is evaluated in the constraint function of the optimisation scheme. The optimisation algorithm will first search the parameter space for constraint satisfaction before evaluating the cost function. The optimisation algorithm might require to evaluate the constraints at various points in the parameter space before the constraints are satisfied. As the dynamical system is evaluated in the constraint function, the process of evaluating the operational safety margin becomes computationally expensive. Identifying the exact operational safety margin, which may be a non- convex multidimensional surface, and even disconnected regions, with an attractive and feasible computational effort is challenging. Hence, the problem is to approximate the operational safety margin that could be

conservative, yet determined with a minimal computational effort.

Computational effort can be considerably reduced, if the constraint function are provided in a polynomial form. Hence, a surrogate polynomial model is preferred instead of a closed loop dynamical model as it provides an inexpensive way to evaluate the operational safety margin. These models are developed by treating the closed loop dynamical system as a 'black-box' with uncertain parameters as the inputs and the performance constraints as the outputs. Polynomial chaos modelling approach is used to derive the surrogate models.

4.2.3 Operational safety margin of TVC benchmark model

A constrained optimisation problem to evaluate the operational safety margin for TVC benchmark model is formulated using the specifications in Table 2.8 and is as follows,

$$
\begin{aligned}
\min \quad & ||\delta - \delta_0||_{\mathbf{m}}^{\infty} \\
\textit{Subject to} \quad & \delta_{min} \leq \delta \leq \delta_{max} \\
& P_c(\delta) \geq \epsilon \\
& |Q_\alpha(t)| \geq 500kPadeg \\
& |\theta(t)| \geq 2^\circ \\
& |\dot{\theta}(t)| \geq 0.8^\circ/s \\
& |\beta(t)| \geq 6^\circ \\
& \sum_{t_0}^{t_f} |\beta_C| \geq 200^\circ
\end{aligned}
\tag{4.4}
$$

where $t \in [t_0,\ t_f]$, δ are the uncertain parameters as described in Table 2.7, $P_c(\delta)$ is the cumulative probability as described in section 2.4.9 and the constrains on the time domain specifications are as per Table 2.8. The objective is to determine the safety margins for a given control law $\mathcal{C}_{\mathcal{H}_\infty}$ at five different wind perturbations occurring at 30, 35, 40, 45 and 50 seconds. The operational safety margin is determined by solving the constrained optimisation problem in Eqn. 4.4. Since the constrained optimisation is not necessarily convex, a hybrid differential evolution method has been used to determine the critical parameter values and the safety margin over the multi-dimensional uncertain parameter space. The critical similitude ratio ($\widetilde{\lambda}$) and the operational safety margin (ρ) are evaluated for different wind perturbation cases using the flexible launcher model, and are given in Table 4.1. A high computation time i.e. more than 5 hours is required to evaluate the operational safety margin for each wind instance when the flexible launcher model is utilised.

In order to reduce the computational time, surrogate polynomial models from section 3.4, Chapter 3 are utilised as constraints. It can be seen from Table 4.1 that the computational time reduces significantly when the surrogate models are utilised. Due to the inherent error in the approximation, the critical parameter value found using polynomial model is not the same as the original launcher model.

It is found that $\widetilde{\lambda} < 1$ for the wind perturbations occurring at 35, 40, 45 and 50 seconds. This indicates a reduced level of robustness, whereas for the wind perturbation occurring at 30sec, the value of λ is slightly greater than 1 indicating good robustness. For wind perturbation occurring at 40 and 45 seconds, the critical similitude ratio ($\widetilde{\lambda}$) is 0.66 and 0.68 (for the launcher model) respectively, indicating that the reference set has contracted to a small safe region around the nominal

parameter value.

Table 4.1: Critical similitude ratio ($\widetilde{\lambda}$) and operational safety margin (ρ) results for the launcher & polynomial surrogate model

		Time instance of wind perturbations				
		30sec	35sec	40sec	45sec	50sec
Launcher Model	$\widetilde{\lambda}$	1.05	0.71	0.66	0.68	0.88
	$\rho \geq 2.65$	2.78	1.88	1.75	1.8	2.32
	CPU Time (sec)	20914.33	16524.17	16948.07	18085.58	18381.9
Polynomial Model	$\widetilde{\lambda}$	1.05	0.756	0.685	0.718	0.899
	$\rho \geq 2.65$	2.78	2	1.81	1.9	2.38
	CPU Time (sec)	181.27	442.16	211.41	366.65	204.07

4.2.4 Worst case analysis inside the safe region

To gain further insight about the levels of each performance deviations that could occur within the safe region defined by the operational safety margin, and to verify that indeed the safe region has no violation of any performance criterion, a worst case analysis is performed on the original launcher model. In each case, the perturbations are limited within the set defined by the values of operational safety margin given in Table 4.1 respectively. Optimisation based worst-case analysis

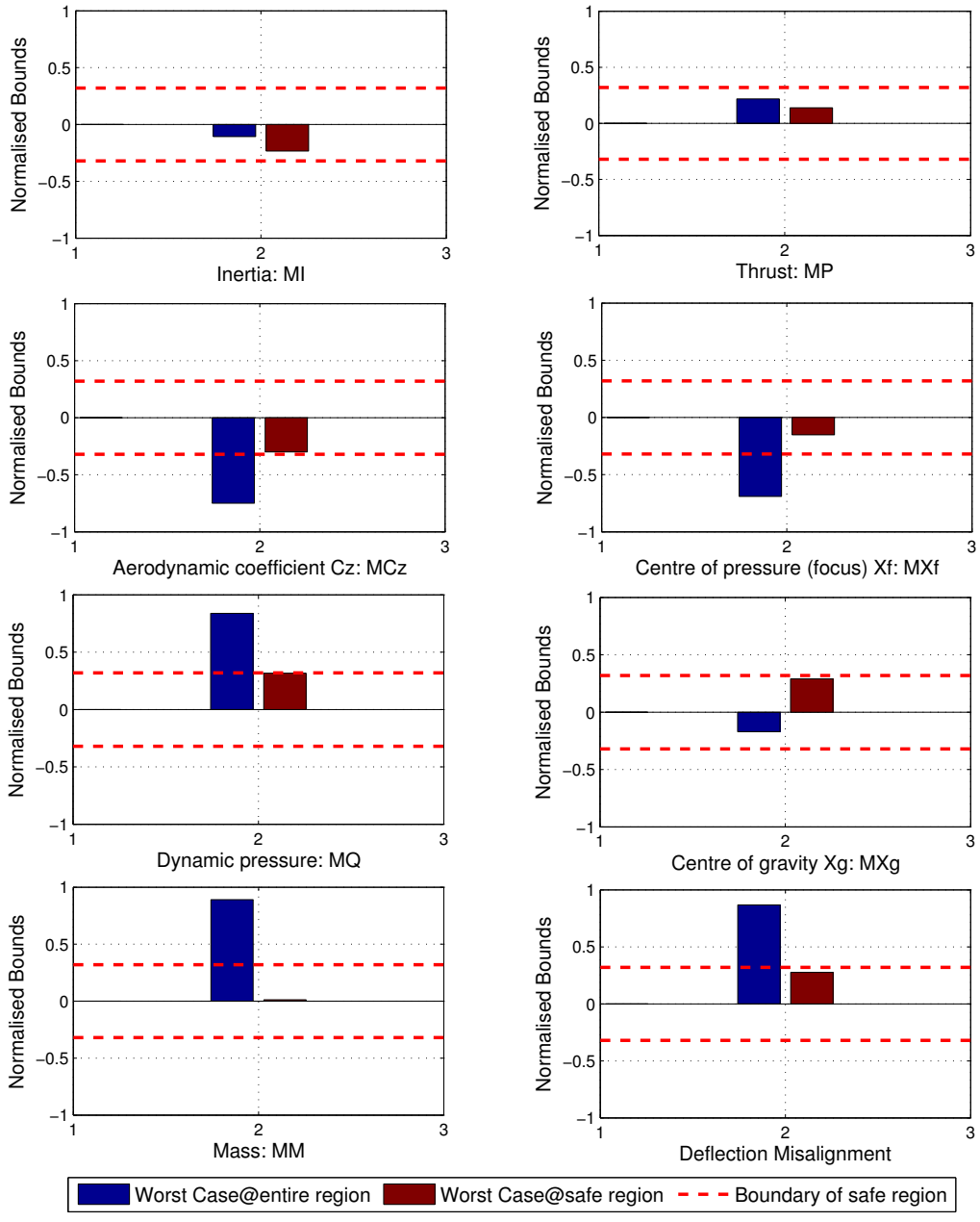

Figure 4.2: Comparison of rigid mode worst case perturbations for $\max |Q_\alpha(t)|$

Table 4.2: Worst case results inside safe region

Cost Function		Worst case values				
		30sec	35sec	40sec	45sec	50sec
$\max_{t\in[t_0 t_f]} \lvert Q_\alpha(t)\rvert$	max	388.11	393.44	423.09	467.65	476.51
	mean	340.85	355.41	385.65	425.83	423.46
	std	42.84	37.24	39.71	44.25	47.84
	failures	0	0	0	0	0
$\max_{t\in[t_0 t_f]} \lvert\beta(t)\rvert$	max	5.78	5.85	5.94	5.91	5.993
	mean	4.10	4.62	4.84	4.76	4.45
	std	0.85	0.71	0.67	0.68	0.83
	failures	0	0	0	0	0
$\max_{t\in[t_0 t_f]} \lvert\theta(t)\rvert$	max	4.51	4.24	4.21	4.53	4.13
	mean	3.51	3.46	3.56	3.51	3.04
	std	0.58	0.44	0.45	0.52	0.5
	failures	0	0	0	0	0
$\max \lvert\theta(t_{tf})\rvert$	max	0.199	0.152	0.144	0.145	0.138
	mean	0.038	0.033	0.032	0.035	0.034
	std	0.026	0.026	0.024	0.030	0.025
	failures	0	0	0	0	0
$\max \lvert\dot{\theta}(t_{tf})\rvert$	max	0.477	0.465	0.456	0.568	0.385
	mean	0.124	0.119	0.118	0.134	0.121
	std	0.095	0.095	0.090	0.101	0.101
	failures	0	0	0	0	0
Cumulated deflection	max	136.15	138.19	135.54	137.95	135.44
	mean	125.43	125.92	125.76	124.95	124.57
	std	12.1	12.31	12.00	11.81	11.42
	failures	0	0	0	0	0

is performed for the cost functions listed in Table 2.8. The parameter space is restricted to be within the reference set defined by $\mathcal{R}(\delta_0, \widetilde{\lambda}\mathbf{m})$ where $\mathbf{m}$ was kept fixed at 0.5 and $\widetilde{\lambda}$ from Table 4.1. For example, at 40 second wind perturbation, the $\widetilde{\lambda} = 0.66$ and $\mathbf{m} = 0.5$ the parameter space is restricted around the nominal parameter value $\delta_0 \pm \widetilde{\lambda} \times \mathbf{m}$ i.e. $\widetilde{\lambda} \times \mathbf{m} = 0.66 \times 0.5 = 0.33$. The red dashed line in Figure 4.2 is representative of the safe region in the multi-dimensional uncertain parameter space. The results of the worst case analysis are shown in Table 4.2.

Comparing these results with those found in Table 2.9, none of the performance criteria were exceeded and no instabilities were found. The maximum excursions for all the performance requirements are within the safe region identified by the operational safety margin. It is clear that the deflection angle performance requirement were reaching its limits and it is the first violating constraints in all the cases. Figure 4.2, provides a comparison of the worst case analysis carried out inside safe region with that carried out over the entire parameter space. The main parameters contributing to the worst case of aerodynamic load are the aerodynamic coefficient, dynamic pressure and centre of gravity. All these uncertain parameters are at their bounds when the parameter space is restricted within the safe set. This indicates that the worst case lie near the restricted boundary, and the performance criteria for the aerodynamic load will violate if these parameters exceed the restricted space.

4.3 Bernstein expansion based approach

4.3.1 Introduction

While the operational safety margin method is able to ascertain a safe region around the nominal parameter value, the Bernstein expansion method allows one to characterise the entire parameter space in safe/unsafe regions. This second method utilises the Bernstein polynomials and specifically their range enclosure property,[121, 124], to determine the safe/unsafe regions. Bernstein polynomials are named after Sergei Natanovich Bernstein, who first introduced it in a short paper, [125], which gave proof that a continuous function is approximated by a

polynomial over a defined interval. Since then Bernstein polynomials have been used for various applications: [126] deals with the computational reachability problem of a discrete time polynomial dynamical system. In [127], Lane and Riesenfeld develop methods for isolating the minima/ maxima and the roots of a polynomial with real coefficients. In computer aided geometric design, [128] discusses the use of interval polynomials and interval Bezier curves for surface approximations. In [129], utilises Bernstein polynomials to develop an algorithm for a constrained global optimisation of mixed-integer nonlinear programming problems. In the field of robust control, [121] develops two algorithms depending on Bernstein polynomials to ascertain robust stability of polynomials whose coefficients are parameter dependent polynomials. In [130], uncertain parameter space is classified into failure and safe regions using Bernstein expansion method for a polynomial inequality dependent on two uncertain parameters. A recent survey article,[131], on Bernstein polynomials and its applications over the last century was written on the 100^{th} anniversary of the Bernstein's paper [125].

4.3.2 Basic Concept

The core idea with Bernstein polynomial expansion approach is to represent a given polynomial into a Bernstein polynomial and then utilise the properties of Bernstein polynomials over a hyper-rectangular box to determine if the polynomial is satisfied or not. If the maximum value of Bernstein coefficients is negative then the hyper-rectangular box is considered as a safe region. On the other hand, if the minimum value of Bernstein coefficient is positive then the hyper-rectangular box is considered as a failure region. Whereas, if maximum value of Bernstein

coefficients is positive and minimum value is negative, then the hyper-rectangular box would contain both safe and failure regions. For more precise determination of safe/failure regions, sub-division of the hyper-rectangular box will have to be performed until a sub-divided box is considered safe or fail. This section describes the procedure for determining the Bernstein coefficients and explains the range enclosure property for determining safe and failure regions.

Define a multi-index $I = (i_1, \ldots, i_m)$ and the multi-powers $\delta^I = \delta_1^{i_1}\delta_2^{i_2} \cdot \ldots \cdot \delta_m^{i_m}$ for $\delta \in \mathbb{R}^m$. We write $I \leq N$ if $N = (n_1, \ldots, n_m)$ and if $0 \leq i_k \leq n_k$, $k = 1, \ldots, m$. Then the I^{th} Bernstein polynomial of degree N is defined as

$$B_{N,I}(\delta) = b_{n_1,i_1}(\delta_1)b_{n_2,i_2}(\delta_2) \cdot \ldots \cdot b_{n_m,i_m}(\delta_m), \tag{4.5}$$

where for $i_j = 0, \ldots, n_j$, and $j = 1, \ldots, m$

$$b_{n_j,i_j}(\delta_j) = \begin{pmatrix} n_j \\ i_j \end{pmatrix} \delta_j^{i_j}(1-\delta_j)^{n_j - i_j}. \tag{4.6}$$

The Bernstein expansion approach, [121, 132], first transforms a m-dimensional multivariate polynomial to a Bernstein polynomial in Eqn. 4.5. The polynomial representation,$F(\delta) = \sum_{q=0}^{M} a_q \Phi_q$ in Eqn. 3.6 can be transformed into a Bernstein polynomial representation in Eqn. 4.5. The polynomial $F(\delta) = \sum_{q=0}^{M} a_q \Phi_q$ in Eqn 3.6 is rewritten in terms of δ instead of the orthogonal polynomial basis as

$$F(\delta) = \sum_{I \leq N} a_I \delta^I, x \in \mathbb{R}^m, \tag{4.7}$$

where a_I are the coefficients of the polynomial $F(\delta)$, and N is its degree. Also, we

represent $\binom{N}{I}$ for $\binom{n_1}{i_1} \cdot \ldots \cdot \binom{n_m}{i_m}$.

Bernstein polynomials are defined over a unit box $U = [0,1]^m$. To transform the polynomial $F(\delta)$ in its Bernstein form, $\delta \in \mathbb{R}^m$ has to be mapped affinely onto the unit box U. For $\delta = \{\delta_1, \ldots, \delta_m\} \in \mathbb{R}^m$, the transformation of a polynomial from its power form in Eq. (4.7) into its Bernstein form results in

$$F(\delta) = \sum_{I \leq N} b_I(U) B_{N,I}(\delta), \tag{4.8}$$

where the Bernstein coefficients $b_I(U)$ of $F(\delta)$ over the unit hyper-box U are given by

$$b_I(U) = \sum_{J \leq I} \frac{\binom{I}{J}}{\binom{N}{J}} a_J, I \leq N. \tag{4.9}$$

The minimum and maximum value of the Bernstein coefficients provide bounds on the polynomial over a given interval. These bounds can be used to determine whether a polynomial inequality holds, or not, over a given interval. The idea here is to consider the surrogate polynomial models as a polynomial inequality, which would determine whether a specific performance criteria is satisfied, or not, over a given interval. Using this approach, the entire parameter space can be characterised into safe and failure regions.

The range enclosing property is used to determine the minimum and maximum value of the Bernstein coefficients $b_I(U)$ in Eq. 4.9 over a unit hyper box U.

Specifically, the range enclosing property, [121] is:

$$\forall \delta \in U : \min_{I \leq N} b_I(U) \leq F(\delta) \leq \max_{I \leq N} b_I(U) \tag{4.10}$$

The range enclosing property helps to determine whether a polynomial inequality, $F(\delta) < 0$, satisfies or not over a hyper-rectangular box. The satisfaction of the polynomial inequality $F(\delta) < 0$ corresponds to the maximum value of the Bernstein coefficients $b_I(U)$ is negative. On the other hand the inequality does not hold if the minimum value of Bernstein coefficients is non-negative.

4.3.3 An illustration of sub-division algorithm

The range enclosure property is exploited by employing a sub-division algorithm [132] to determine the regions in the parameter space where the polynomial inequality holds or not. The algorithm generates the Bernstein coefficients over a range on the m-dimensional box. The bounds of the polynomial over a given interval are found using Eq. (4.10) and the polynomial inequality is tested. When the satisfiability of a polynomial inequality is not known then the m-dimensional box is subdivided into 2^m boxes. The bounds of the Bernstein coefficients in these new boxes are computed and satisfiability of the polynomial inequality is checked. Additional subsequent subdivisions are performed for those boxes in with the polynomial inequality cannot be determined. The computational complexity increases exponentially as the dimension of the box increases. The method is illustrated with a simple numerical example taken from [55](Chapter 9, page 174). The stopping criterion of the sub-division algorithm is based on the volume of the m-dimensional boxes i.e. product of length along each dimension. The algorithm is

stopped, whenever the volume of the sub-divided boxes is less than 10^{-5}.

Example Consider the System

$$\dot{x}(t) = f(\delta)x(t), \tag{4.11}$$

with $x \in \mathbb{R}$ and

$$\begin{aligned} f(\delta) \;=\; & 672.2\delta_1^6 + 401.7\delta_1^5\delta_2 - 75\delta_1^5 - 727.9\delta_1^4\delta_2^2 + 233.6\delta_1^4\delta_2 - 30.5\delta_1^4 - 254.5\delta_1^3\delta_2^3 \\ & -71\delta_1^3\delta_2^2 - 19.6\delta_1^3\delta_2 + 26.6\delta_1^3 - 233.5\delta_1^2\delta_2^3 + 40.2\delta_1^2\delta_2^2 + 64.3\delta_1^2\delta_2^4 + 2\delta_1^2\delta_2 \\ & +6.6\delta_1^2 - 282.1\delta_1\delta_2^5 + 152\delta_1\delta_2^4 - 9.3\delta_1\delta_2^3 - 19.7\delta_1\delta_1^2 + 3.7\delta_1\delta_2 + 1.9\delta_1 \\ & +251.8\delta_2^6 + 234.6\delta_2^5 - 64.8\delta_2^4 - 19.9\delta_2^3 + 9\delta_2^2 + 1.7\delta_2 - 3.1 \end{aligned} \tag{4.12}$$

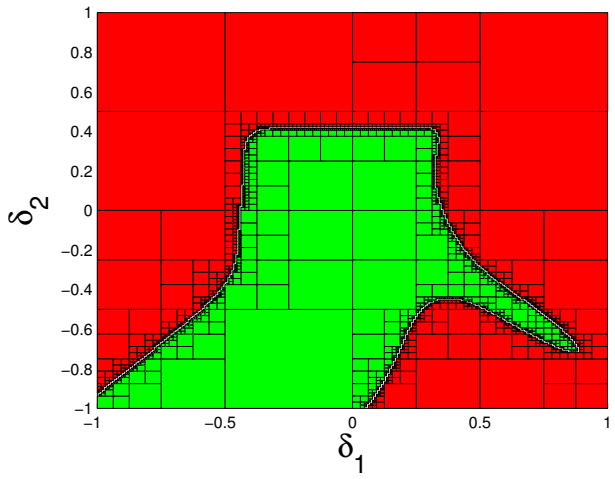

Figure 4.3: Stability regions: green region=stable red region = unstable

is a bivariate ($m = 2$) polynomial in $\delta = (\delta_1, \delta_2)$, $\delta \in [-1\ 1]$ and the degree of the polynomial is $N = 6$, such that $f(0) < 0$ and $f(\delta) < 0$ for δ belonging to the stable region. The idea is to characterise the two dimensional parameter space

into safe and unsafe regions. A sub-division based algorithm is employed and the steps involved are enumerated in Table 4.3

Table 4.3: Sub-division algorithm based characterisation of uncertain parameter space

Pseudo-Code
1) Start with either considering the entire parameter space as a hyper-rectangle or with a pre-defined set of hyper-rectangles.
2) **For** 1 to Number of hyper-rectangular boxes **do**.
a) Compute Bernstein coefficients using Eq. 4.9.
b) Find maximum and minimum value of Bernstein coefficients
c) **If** maximum value is negative **do**
i) Hyper-rectangular box is a safe region
d) **ElseIf** minimum value is positive
i) Hyper-rectangular box is a failure region
e) **Else**
i) Hyper-rectangular box contains both safe and failure regions
ii) Divide this box along each parameter and create smaller hyper-rectangular boxes
f) **End**
g) **If** termination criteria is satisfied
i) Termination criteria is related to the volume of the hyper-rectangular box.
ii) Exit For loop.
h) **Else**
i) Continue
i) **End**
3) **End**.

Bernstein coefficients for the system in Eq. 4.12 are evaluated using Eq. 4.9. Subsequently, the range enclosure property of Eq. 4.10 is utilised to classify the stable and unstable regions in the parameter space. Figure 4.3 depicts the classification of two dimensional parameter space into safe and unsafe regions. The green colour region indicates safe/stable set. The region in red colour indicates unsafe set corresponding to instability.The total time taken to evaluate the entire param-

eter space was approximately 30 seconds, and is much faster than the methods reported in [55] where Lyapunov based analytical methods were used which took more than one minute to classify safe and failure regions. Simulation based methods will require finer grids of the parameter space and evaluation of these grids will be computationally very expensive. Notice that, Bernstein expansion method only evaluates Bernstein coefficients over a hyper-rectangular box and utilises the range enclosure property to determine the safe and failure regions. Such a sub-division based algorithm is computationally inexpensive to evaluate a 2 dimensional parameter space. But the computation time increases exponentially as the number of parameters is increased as it requires division along each parameter.

4.3.4 Application: TVC benchmark model

A sensitivity analysis is performed on the worst case found for the performance criterion on $|Q_\alpha(t)|$ with the wind perturbation occuring at 50 second of the flight instant. For performing the sensitivity analysis, launcher model is evaluated by varying rigid parameters one at a time while keeping the rest of the rigid parameters fixed at worst case value. The flexible modes are set to the nominal parameter value. It can be seen from Figure 4.4, that even when the uncertain parameters corresponding to flexible modes are set to their nominal values, performance criteria is violated by rigid parameters alone. It shows that rigid parameters have major contribution in the worst case found. This allows us to develop surrogate polynomial models with rigid parameters alone and characterise the uncertain parameter space into safe and failure regions.

Employing a sub-division algorithm on the TVC benchmark model with all

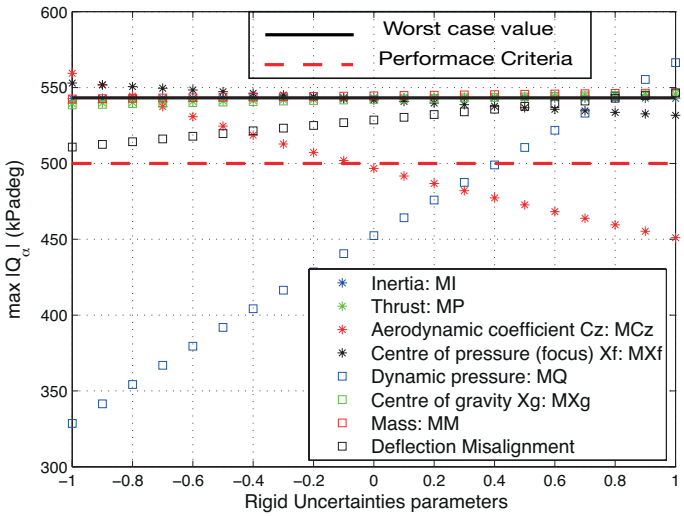

Figure 4.4: Sensitivity analysis: flexible uncertain parameters set to nominal values with rigid parameters varying

the 28 uncertain parameters is computationally expensive. If we start with the entire parameter space with all the 28 uncertainties under consideration then the number of hyper-rectangles after initial sub-division along all the 28 uncertainties will be equal to $2^{28} = 268435456$. Often, the number of safe and failure regions found during this initial iteration will be very few or none at all. Even so, one is left with large number of hyper-rectangles to investigate and if no safe or failure regions is found then further sub-division might be required. Each sub-division will result in 268435456 boxes. In order to reduce the computational effort involved, we develop a polynomial model for the TVC benchmark by considering the rigid uncertain parameters alone. Also, worst case analysis performed on the TVC benchmark showed that the rigid parameters were the key parameters contributing to worst case values. The computational burden will reduce considerably when just 8 uncertain parameters are considered.

In Section 4.2.4, it is observed that the performance criterion related to the deflection angle is the first to violate among the criteria listed in Table 4.2. Also, Table 4.2 shows that the results of the worst case analysis inside the safe region, it is observed that performance criteria related to the aerodynamic load and the deflection angle are at their bounds as compared to other performance criteria. For application of the Bernstein expansion on TVC models, only these two performance criteria are considered for the classification of uncertain parameter space into safe and failure regions. Also, surrogate polynomial models are converted into polynomial inequalities as

$$\begin{aligned} F_{Q\alpha} - 500 &< 0 \\ F_{\beta} - 6 &< 0 \end{aligned} \tag{4.13}$$

Note that negative values are indicative of safe regions while positive values correspond to failure regions. Bernstein expansion approach is applied to polynomial inequalities in Eqn. 4.13, for wind perturbation occurring at 40 and 70 seconds of the flight instant. Instead of a sub-division algorithm, a pre-defined set of hyper-rectangles were generated and then evaluated by Bernstein approach in order to reduce the computational burden. The entire uncertain parameter space, $\delta_i \in [-1\ 1]$ (for $i = 1, \ldots, 8$), was divided into 16777216 hyper-rectangles. Each individual hyper-rectangle had a length of 0.25 along each dimension and hence had a volume of $Vol_{\mathcal{R}_i} = (0.25)^8 = 1.5259 \times 10^{-05}$. Since it is difficult to visualise the higher dimensional uncertain parameter space, in general the 2-d slices of the multi-dimensional uncertain parameter space are generated for each cases of

wind perturbation (refer Figure 4.5). In Section 2.4.9, Chapter 2, four rigid uncertain parameters namely aerodynamic coefficient (MCz), centre of pressure (MXf), Dynamic pressure (MQ) and centre of gravity (MXg), were found as the main contributors to worst case. 2-D slices of these four parameters at wind instances of 40 and 70 seconds are shown in Figure 4.5.

These 2-D slices are a conservative way to visualise the higher dimension hyper-rectangles. The Figure 4.5(a), is classified into three regions, green regions corresponds to safe regions, magenta colour represents regions which may be safe or failure regions depending on the other uncertain parameter values, white regions corresponds to region which require further investigation. The entire 2-D slice, when centre of gravity and centre of pressure are considered, can correspond to safe or failure regions. It is observed that even when these two parameters have nominal parameter value, failure regions can be found depending on certain combinations of other uncertain parameters. This indicates that a failure region lies close to the nominal parameter value in the higher dimension. Operational safety margin analysis (refer Section 4.2.3) had showed that the reference set had contracted which indicated a small safe region around the nominal parameter value. This explains the high number of failures found by the Monte Carlo analysis and the unstable cases found by the optimisation based worst case analysis (refer Table No 2.9). Entire rigid parameter space is found to be safe for the case when wind perturbation is occurring at 70 seconds of the flight instant (refer Figure 4.5(b)). This result validates the result found by worst case analysis i.e. no worst cases for wind at 70 seconds are found (refer Table No 2.9 - 2.10).

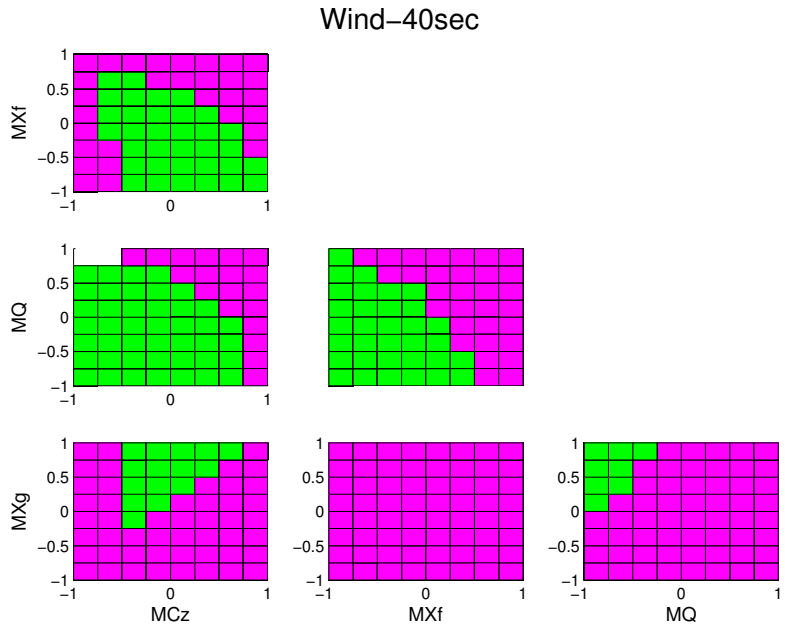

(a) Green regions=safe, magenta regions=safe/unsafe regions, white regions=further investigation is needed

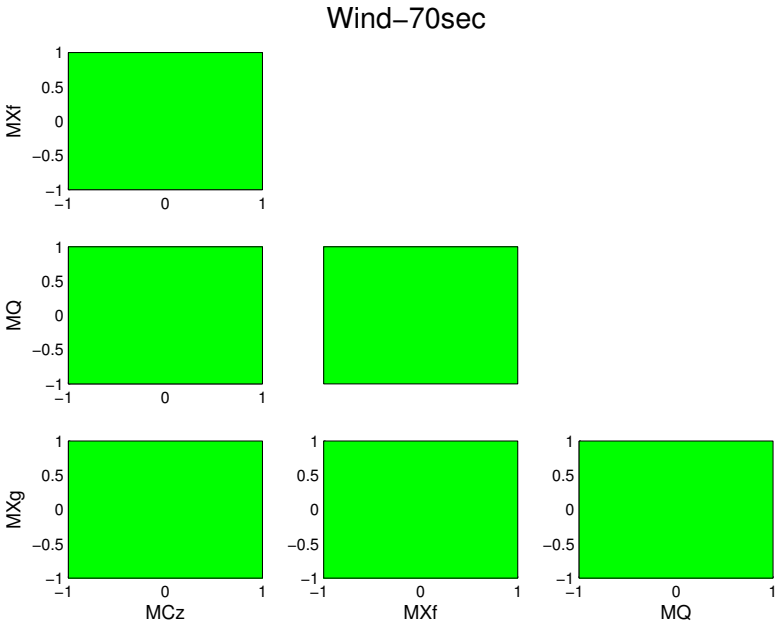

(b) Entire parameter is safe: Wind-70sec

Figure 4.5: 2-D slice of parameter space.

4.4 Risk assessment

Assessment of robustness of a controller in the presence of the uncertain parameter variations is necessary to determine if a redesign of the controller is needed or not. Optimisation based worst case analysis provides a single worst case point in the uncertain parameter space which corresponds to the poor robustness, or complete failure of controllers ability to stabilise the spacecraft. Often times this worst case point lies on the boundary of the uncertain parameter space. The probability of a uncertain parameter to occur on the bounds is assumed to be low, and not sufficiently high enough to perform a redesign of the controller. The population based optimisation algorithm could generate other sub-optimal solutions which have violated the performance criteria and could lie in a region where the uncertain parameters might have a better probability to occur. It would be advantageous to investigate these sub-optimal solutions. Unfortunately, optimisation analysis doesn't provide any statistical information that could provide the probability of performance criteria violation. Monte Carlo analysis provides statistical information to assess the probability of performance criteria violation. If the performance criteria violation is considered as failure then failure probability gives an idea as to how many failures can be expected in a given Monte Carlo campaign of sample size N. Number of failures will vary with each Monte Carlo campaign, and so does the failure probability. So, for example, 10 Monte Carlo campaigns can give 10 different failures, and thus 10 different failure probabilities. Hence, the failure probability from one Monte Carlo campaign might not be sufficient to conclude whether a redesign is necessary.

Due to the time complexity involved with the simulator, it may not be possible

to perform more than one Monte Carlo campaign. In such cases, Binomial failure analysis, [133], provides an upper and lower bound on the failure probabilities of observing k or fewer failures among a sample size of N ($k \leq N$). The upper bound on the failure probability corresponds to 10% of the Monte Carlo campaigns i.e. out of 100 Monte Carlo campaigns, 10 will exhibit a maximum of k failures. Similarly, a lower bound on the failure probability corresponds to 90% of Monte Carlo campaigns that exhibit at the most k failures. Using the Binomial failure analysis, estimates on upper and lower bound on failure probabilities can be found without actually performing Monte Carlo campaigns. These bounds are directly related to the risk of accepting a bad design and to the risk of rejecting a good design. Based on the risk, the control design engineer could determine if a redesign of controller is necessary or not.

4.4.1 Binomial failure analysis

Consider a Monte Carlo campaign with sample size, N=1000, of which 10 samples exhibit failure ([133]). One might incorrectly assume that the failure probability is 10/1000, or 1% and that this sample is typical. In fact, if a second Monte Carlo campaign is performed then one might find a different number of failures with a new failure probability. As discussed in the previous section, bounds on the failure probability provides to the controller designer the risk of accepting a bad design and the risk of rejecting a good design. How binomial failure analysis can be used to estimate an upper and lower bounds on the failure probability is shown in [133].

According to binomial failure analysis, the cumulative probability $F_{bin}(k|p, N)$ of observing k or fewer failures among a sample size of N with failure probability

p is given by:

$$F_{bin}(k|p,N) = \sum_{j=0}^{k} \binom{N}{j} p^j (1-p)^{N-j} \tag{4.14}$$

Using Eq. 4.14, for the given k and N, the cumulated probability $F_{bin}(k|p,N)$ is plotted in Figure 4.6 by varying p between 0 and 1. This figure is called the operating characteristic (OC) for a sampling plan (k,N). From Figure 4.6, it can be observed that about 58.3% of 100 Monte Carlo campaigns will exhibit 10 or fewer failures at a failure probability of $p = 1\%$. This means that there is 58.3% chance of accepting a controller design which would exhibit 10 or fewer failures if the failure probability is 1%. As exact failure probability is not known, it is desirable to know the upper and lower bounds on the failure probability. The upper bound is evaluated from the Figure at $F_{bin} = 10\%$ which corresponds to $p = 1.53\%$. This implies that there is 10% chance of accepting a controller design for failure probability $p = 1.53\%$. This risk of accepting a bad controller design is called consumer risk (CR). On the other hand, the lower bound is evaluated at $F_{bin} = 90\%$ which corresponds to $p = 0.7\%$. It corresponds to the risk of rejecting a good controller design and is called producer risk (PR). Hence the failure probability corresponding to consumer and producer risk is $p_c = 1.53\%$ and $p_p = 0.7\%$, respectively.

4.4.2 Application: TVC benchmark model

In this section, the Binomial failure analysis is applied to the TVC benchmark model. Since, the performance criterion s_4 of Table 2.8 is the first to violate

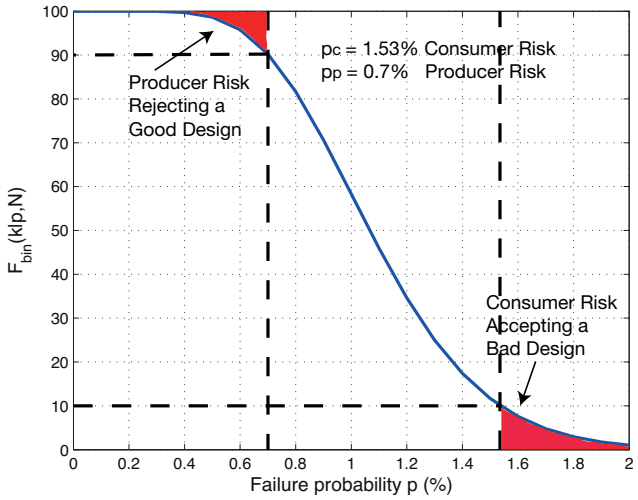

Figure 4.6: Risk assessment for a sample plan of (10,1000).

among the listed criteria given in Section 4.2.4, consumer risk and producer risk were evaluated for deflection angle criteria. The bounds on the failure probability was evaluated at five different wind perturbations occurring at 30, 35, 40, 45 and 50 seconds. Worst case analysis performed on the TVC benchmark model in Section 2.4.9, showed no performance criteria violations for wind perturbations occurring at 60 and 70 seconds. Hence, these instances were not considered. Consumer risk and producer risk were evaluated based on the number of failures obtained from a Monte Carlo campaign (refer Table 2.10) performed with a sample size of $N = 1000$.

The bounds on the failure probability have been tabulated in Table 4.4. A high number of failures were recored by Monte Carlo for wind perturbation occurring at 45 seconds, 111 failure were found in Table 2.10 of Section 2.4.9. The consumer risk, i.e. 10 out of 100 Monte Carlo campaigns will exhibit a failure probability of $p_c = 12.5\%$, where as the producer risk i.e. 90 out of 100 Monte Carlo campaigns

will exhibit a failure probability of $p_p = 9.93\%$. A redesign of the controller would be necessary since high failure probabilities were found for the wind perturbation occurring at 35, 40 and 45 seconds. This is consistent with the results found by the worst case analysis and operational uncertainty margin estimation. During the worst case analysis, unstable cases were found at these wind instances along with sustained actuator saturation. Also, the operational uncertainty margin is particularly low for these wind instances indicating that the safe region around the nominal parameter value is small, indicating poor robustness. Redesign of the controller to take into account the effect of wind perturbation occurring at 35, 40 and 45 seconds is necessary.

Table 4.4: CR and PR for various wind instances corresponding to the deflection angle requirement

	30sec	35sec	40sec	45 sec	50sec
No. of Faliures	13	67	93	111	29
Consumer Risk, (p_c)	1.89%	7.82%	10.58%	12.5%	3.7 %
Producer Risk, (p_p)	0.95%	5.78%	8.24%	9.93%	2.33 %

4.4.3 Assigning risk to region around worst case

Control design engineers from the aerospace industry often ask for the probability of failure for a worst case computed using optimisation based worst case analysis. It usually assumed that the risk of the solution computed using optimisation based worst case analysis is very low and hence no redesign of the controller is required. In fact, the exact value of failure probability cannot be assigned to a optimisation based result. A way to apply the Binomial failure analysis to worst case result would be to find out the failure region around the worst case using the Bernstein

expansion method. Once a failure region is identified, Monte Carlo samples can be generated and observed whether if any of these samples lie inside the failure region around worst case.

Table 4.5: Bounds of failure region around worst case

Bounds of failure region		
Parameters	Lower bound	Upper Bound
MI	-0.25	0.57
MP	-0.15	0.66
MCz	0.5	1
MXf	0.38	1
MQ	0.41	1
MXg	0.04	0.86
MM	-0.1	0.72
$\Delta\beta$	-0.04	0.78

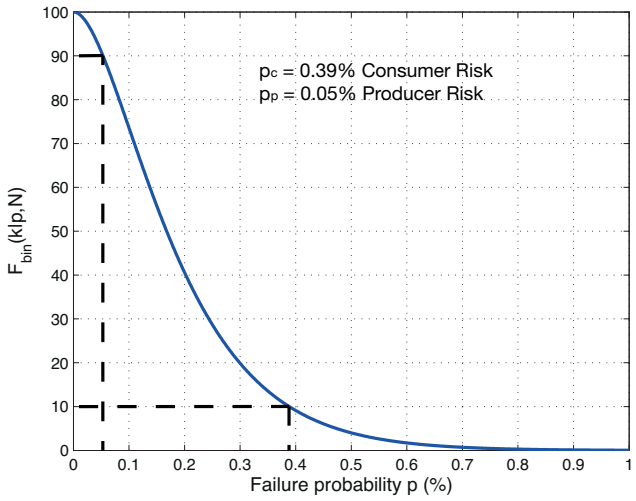

Figure 4.7: Risk assessment for a sample plan of (1,1000).

In Section 4.3.4, the Bernstein expansion method was applied to TVC benchmark model for wind occurring at 40 seconds. The worst case result for the perfor-

mance criteria corresponding to the deflection angle requirement was considered for risk assessment. A failure region was identified around the worst case point, whose bounds along each dimension is provided in Table No 4.5. Uncertain parameter combinations generated from a Monte Carlo campaign were tested for this failure region. The results from the Monte Carlo campaign performed in Section 2.4.9 of Chapter 2 were used. It was observed that no uncertain parameter combination lie inside the failure region apart from the worst case obtained from the optimisation based worst case analysis. So the risk of observing $k = 1$ or fewer failures is evaluated using Binomial failure analysis and is shown in Figure 4.7. Consumer and producer risk are found to be 0.39% and 0.05% respectively. These values were very small and hence no re-design of the controller is necessary based on result generated by the worst case alone.

Chapter 5

Conclusions and future work

5.1 Conclusions

Simulation based V&V methods have been a popular tool for European aerospace related industries. They are comparatively easy to implement, and adaptable to complex and non linear dynamic models. The thesis presents the successful application of simulation and optimisation based methods on the V&V analysis of a flexible satellite model for the Earth observing BIOMASS mission and the flexible launch vehicle models. The robustness of the attitude control system of the flexible satellite model in the presence of significantly large number of uncertainties (132 uncertain parameters including that of several flexible modes) has been verified. Frequency domain metrics, such as sensitivity and complementary sensitivity function, are formulated as worst-case optimisation problems and analysed using local, global and hybrid (a mix of global and local) optimisation algorithms that include SQP, GA, DE, HGA and HDE algorithms. Wang et. al. [52], performed a similar analysis on a flexible satellite model, this was with far lesser number of uncertainties. This thesis also presents the assessment of the performance of the optimisation based analysis framework to determine the worst case perturba-

tion efficiently in the presence of larger number of variables - assessing a realistic industrial benchmark model with maximum number of uncertainties considered. The conclusion from the research study is consistent with the previous studies , [43, 44, 51, 52, 54, 134], and the comparatively superior performance of the HDE algorithm was comprehensively demonstrated even in the presence of larger number of uncertainties.

Subsequent part of the research reported in this thesis focuses on the flexible launch vehicle model with medium level of uncertainties. The roll coupling effect in the flexible launch vehicle model was studied using the optimisation based analysis framework. MIMO margins were computed by perturbing all input channels simultaneously in order to destabilise the closed loop system. The amount of perturbation applied to destabilise the system gives the MIMO margins. Worst case MIMO margins were then determined in order to study the effects of roll coupling. During the atmospheric flight phase of the launch vehicle, certain perturbations can introduce an unwanted roll torque which can further induce oscillations in the yaw and pitch axis due to roll coupling. Optimisation based V&V, were able to determine the worst case MIMO margins for different roll rates. It was observed that as the roll rate increased, the MIMO margins degraded significantly.

Additionally, optimisation based V&V analysis have been carried out to assess the worst-case limits of the performance objectives of aerodynamic load, pitch angle and cumulative deflection of the flexible launch vehicle model during its thrust vector control phase. The impact on these performance objectives under the presence of external wind perturbation and several rigid and flexible mode uncertain parameters of the model were investigated. The search for sets of uncertain parameters that simultaneously optimise the performance objectives on the maximum

deviations of the aerodynamic load and the deflection angle was formulated as a multi-objective optimisation problem and solved using the non-dominated sorting differential evolution (NSDE) algorithm. The non-trivial solutions obtained using the NSDE algorithm have been compared with that obtained using a popularly employed non-dominated sorting genetic algorithm. The results showed comparable performance.

The thesis presents the benefits of developing surrogate models for performing computationally faster simulation and optimisation based V&V analysis. A non intrusive polynomial chaos method which utilised the probabilistic collocation sampling scheme was employed for obtaining the surrogate polynomial models. First and second order polynomial models were generated for different performance objectives of the TVC benchmark model. Second order surrogate models developed for performance criteria relating to the aerodynamic load and deflection angle requirement, have showed good approximation to the original launcher model. For other criteria, a higher order polynomial model might provide better approximation at a cost of increasing the number of coefficients required for the higher order polynomial model. Since probabilistic collocation method was employed here, the number of simulations of the original model were equal to the number of coefficients of the polynomial. Third order polynomial representation for the performance objective of the flexible launcher would require more than 2000 coefficients. Hence developing a third order polynomial model becomes computationally challenging. Thus, the trade-off for obtaining reliable and accurate polynomial surrogate models at the reasonable computational overhead was studied.

The surrogate models developed were utilised for performing optimisation based V&V analysis. These surrogate models were computationally very fast and re-

quired approximately 200 seconds to perform 10,000 function evaluations, the actual model would have taken several hours of computation time. The worst case performance metrics were evaluated very rapidly with the use of better surrogate models. Worst case directions for the uncertain parameters were also accurately identified, which matched perfectly with those generated by the original model. A surrogate modelling tool was developed in MATLAB and added as a new feature to the WCAT -II toolbox [135].

The thesis also presents methods for characterising a safe region around the nominal parameter value as well as establishing other disjoint safe regions in the uncertain parameter space. To this end, operational uncertainty margin estimation method was applied to identify a safe region around the nominal parameter value. This method determines the distance between the nominal parameter value and the boundary of safe/fail region and also quantifies this distance into a safety margin metric in the uncertain parameter space. This metric was evaluated by defining an optimisation problem to identify the boundary of safe and fail region closest to the nominal parameter value. This optimisation problem is then solved for both original TVC benchmark and its corresponding surrogate model. AS expected, surrogate model generates the results very rapidly and is favourable to be used instead of the original model as computational time is reduced from hours to just couple of minutes. Operational safety margin estimation was also coded in MATLAB and made available as another feature of the WCAT-II toolbox [135].

In order to classify the entire parameter space into safe and fail regions, Bernstein expansion method was applied to the TVC surrogate models. This method classified a given range of uncertain parameters into safe or fail or into a region which requires further division of the provided range. This problem is NP-hard

when entire parameter space is required to be classified and the computational complexity depends on the number of uncertain parameters at hand. The method becomes infeasible for the TVC benchmark problem, which has 28 uncertain parameters. A sensitivity analysis of the given worst case, determined that the rigid parameters alone were mainly responsible for the worst case values, whereas flexible parameters have comparatively lesser contribution towards the worst case. Hence, Bernstein expansion method was employed on a surrogate model based on rigid uncertain parameters alone. For wind perturbation occurring at 70 sec (Figure 4.5(b)), this method accurately identified the entire parameter space as being a safe region, whereas for wind perturbation occurring at 40 seconds, both safe and fail regions were identified. Bernstein expansion method has been also kept as an advanced feature in the WCAT-II toolbox [135].

Finally, Binomial failure analysis was applied to the failure regions to assign upper and lower bounds of failure probability. This method was again applied to the TVC benchmark problem and estimated high failure probabilities for wind perturbation occurring at 40 and 45 seconds. This validated the worst case results generated during optimisation based V&V analysis where many cases of instabilities were found. The result suggested that re-design of the controller was required in order to guarantee safety of the mission.

5.2 Future work

Combing techniques like operational safety margin estimation, surrogate modelling and optimisation methods for controller tuning, can be taken up as a possible future work. The problem can be formulated as a multi-objective optimisation

problem with operational safety margin as one of its objectives. If safety margin estimation is utilised as one of the objective in multi objective controller tuning then it would give us an idea about the safe region around nominal parameter value for each controller configuration evaluated by the optimisation algorithm. This would be advantageous as robustness of the controller w.r.t the uncertainty perturbations could be determined for each potential solution in the Pareto front. The controller configuration in the Pareto front with maximum safety margin value could be chosen as the solution. However combining safety margin estimation with multi objective optimisation would lead to a nested optimisation problem as safety margin estimation is an optimisation problem in itself. The computational overhead of such a problem can be very expensive. In order to overcome this issue, surrogate models could be developed and utilised for estimation of the safety margin, thus reducing the over all time involved for computing.

To elaborate, a proposed mutliobjective controller tuning for a launcher model during it's orbital phase with longitudinal spin can be formulated as follows:

$$\begin{aligned} u^* \quad := \quad & \min_{u \in \mathcal{C}} J_i(u) \\ & \texttt{sub to } g_j(u) \geq 0 \end{aligned} \tag{5.1}$$

where u is the controller tuning parameters, the objectives are defined as $J_i = [J_1 \ J_2 \ J_3]$; and constraints as $g_j = [g_1 \ g_2 \ g_3 \ g_4]$. The three objectives J_i are defined for minimising the number of of activation, minimising the de-pointing angle and maximising the operational safety margin metric respectively. The four constraints are related to the total fuel consumption, angular rate in x & y axis and roll speed accuracy. The controller configuration (u) consists of 26 parameters re-

lated to the roll speed command profile, controller PD gains, deadzone thresholds and estimator gains. The developed surrogate modelling, safety margin estimation and optimisation algorithms in MATLAB, available as different features of the WCAT-II toolbox, could be directly utilised to solve the non-traditional optimisation problem.

The proposed methodologies in this thesis can also be implemented for tuning model parameters for a Rover Dynamic Model (RDM). ESA is investigating opportunities for the next exploration mission and technological developments leading to a future Mars sample return missions. As a part of such a mission, a sample fetch rover would retrieve samples for an ascent vehicle. To achieve this objective, improvements are required with respect to the current state-of-the-art rover exploration. In this framework, the RDM parameters have to be tuned such that the rover is able to perform various manoeuvres like traversing up/down on a slope, making a point turn on a slope, climbing over a rocky surface on Mars terrain with ease. To this end, Astrium Ltd. have incorporated the wheel-soil interaction into the RDM based on the Mars yard developed at Astirum Stevenage. The developed RDM is of high fidelity and requires approximately a minute for completing a single simulation run. A multi-objective problem could be formulated for tuning parameters like longitudinal and latitudinal slip ratio's while performance metrics are related to the rover ability of going up/down, point turn on a slope with minimum slippage as possible and also the rovers ability to climb rocks. The multi-objective analysis of RDM model will be computationally very expensive. To overcome this, surrogate models with good polynomial approximation to the original RDM model could be used to reduce the computational effort. Another aspect of this project is that the performance metrics are defined at different slope

angles which increases the number of objectives to be more than 3. Accurate visualisation of Pareto front for higher dimensional design data presents a challenge and requires further investigation. Visualisation of such a higher dimensional data set should be accurate and should help the designer in selecting a potential solution from the Pareto set of optimal solutions.

Another potential future research area is the application of surrogate modelling tools for industrial application where higher dimensional data are present. The curse of higher dimension makes surrogate modelling infeasible for such kind of models. A method to overcome this issue would be to reduce the number of parameters involved hence reducing the dimension. When dealing with models with large number of uncertain parameters, there is a possibility that not all parameters will contribute towards the worst case for a given performance metric. In fact some of them might have very little or negligible contribution towards worst case. Another way around, would be to use the same number of parameters as in the original model but removing the coefficients from the polynomial expression which have negligible contribution. The method of sparse polynomials chaos can be utilised for developing the surrogate models which provides a method for automatically detecting significant coefficients of the polynomial model.

Surrogate polynomial modelling method is not restricted to aerospace industry and has many applications across various fields, some of which are mentioned here. One potential application area is in the field of climatic sciences, where researchers are conducting investigations on the impact of location, altitude, magnitude and timing of volcanic eruptions on global climate. The goal of these studies is to define a new index called volcanic climate index which considers all the above stated factors and its impact on global climate. To this end, models have to be developed

based on the data available on the factors mentioned above. The surrogate modelling techniques could be applied in such a scenario to develop models describing the volcanic climatic index. Another surrogate modelling application would be the use of polynomial chaos modelling method in developing observers/controllers schemes in distributed parameter systems such as flow control. For example, the Navier-Stokes problem, in which the low dimensional quadratically nonlinear models can be generated using polynomial chaos method and works are in progress in this direction.

Risk assessment discussed in this thesis is based on Monte Carlo analysis and the statistics involved there in. There are techniques available in literature which are based on optimisation methods for evaluating risk for redesigning a controller. These methods are called the cross entropy method and buffered failure probability method. Application of such methods in evaluating worst cases or while optimising controller tuning parameters would elevate the importance of these applications significantly, as the industry still relies on Monte Carlo analysis and its statistical guarantees for redesigning a controller.

Bibliography

[1] M. Ganet-Schoeller, "SAFE-V TN2.3 traditional DV&V benchmarks definition ESA TRP ao/1-6322/09/nl/jk," Astrium Space Transportation, Tech. Rep., 2011.

[2] C. Belcastro and C. Belcastro, "On the validation of safety critical aircraft systems, part I: An overview of analytical & simulation methods," in *Proceedings of AIAA Guidance, Navigation, and Control Conference and Exhibit.* AIAA 2003-5559, August 2003.

[3] B. H. Thacker, S. W. Doebling, F. M. Hemez, M. C. Anderson, J. E. Pepin, and E. A. Rodriguez, "Concepts of model verification and validation," Los Alamos National Laboratory, Tech. Rep., 2004.

[4] R. W. Pratt, Ed., *Flight Control Systems*, ser. Progress in Astronautics and Aeronautics. American Institute of Aeronautics and Astronautics, 2000.

[5] J. M. Maciejowski, *Multivariable feedback design.* Addison-Wesley, 1989.

[6] M. H. Lowenberg, "Stability and controllability evaluation of sustained flight manoeuvres," in *Proceedings of 21st Atmospheric Flight Mechanics Conference.* AIAA 1996-3422, July 1996.

[7] C. Fielding, A. Varga, S. Bennani, and M. Selier, *Advanced techniques for clearance of flight control laws*, ser. Lecture Notes in Control and Information Sciences. Springer, 2002.

[8] K. Zhou, J. C. Doyle, and K. Glover, *Robust and optimal control*. New Jersey: Prentice Hall, 1996.

[9] J. F. Magni, "Linear fractional representation toolbox: Modelling, order reduction, gain scheduling," System Control and Flight Dynamics Department, Onera, Toulouse, France, Tech. Rep., 2004.

[10] R. P. Braatz, P. M. Young, J. C. Doyle, and M. Morari, "Compulational complexity of μ calculation," *IEEE Transactions on Automatic Control*, vol. 39, no. 5, pp. 1000–1001, 1994.

[11] A. Megretski and A. Rantzer, "System analysis via integral quadratic constraints," *IEEE Transactions on Automatic Control*, vol. 42, no. 6, pp. 819–830, 1997.

[12] J. M. Biannic, C. Roos, and A. Knauf, "Design and robustness analysis of fighter aircraft flight control laws," *European Journal of Control*, vol. 12, no. 1, pp. 71–85, 2006.

[13] K. Krishnaswamy, G. Papageorgiou, S. Glavaski, and A. Papachristodoulou, "Analysis of aircraft pitch axis stability augmentation system using sum of squares optimization," in *Proceedings of American Control Conference*, vol. 3, 2005, pp. 1497–1502.

[14] R. Katayanagi, "Exact evaluation of stability margin of multiloop flight control systems," *Journal of Guidance, Control, and Dynamics*, vol. 24, no. 1, pp. 137–140, 2001.

[15] V. Patel, G. Deodhare, and S. Chetty, "Near real time stability margin estimation from piloted 3-2-1-1 inputs," in *Proceedings of AIAA's Aircraft Technology, Integration, and Operations (ATIO) 2002 Technical Forum.* AIAA 2002-5820, October 2002.

[16] M. Lichter, A. Bateman, and G. Balas, "Flight test evaluation of a runtime stability margin estimation tool," in *Proceedings of AIAA Guidance, Navigation, and Control Conference.* AIAA 2009-6257, August 2009.

[17] S. Boyd, L. E. Ghaoui, E. Feron, and V. Balakrishnan, "Linear matrix inequalities in system and control theory," *Society for Industrial and Applied Mathematics (SIAM)*, vol. 15, 1994.

[18] J. Tierno and P. Young, "An improved μ lower bound via adaptive power iteration," in *Proceedings of the 31st IEEE Conference on Decision and Control,*, vol. 4, 1992, pp. 3181–3186.

[19] A. Packard and J. Doyle, "The complex structured singular value," *Automatica*, vol. 29, no. 1, pp. 71–109, 1 1993.

[20] R. Jones, "Structured singular value analysis for real parameter variations," in *Proceedings of AIAA Guidance, Navigation and Control Conference.* AIAA 1987-2589, August 1987.

[21] D. R. Lane, "A new algorithm for the real structured singular value," in *Proceedings of American Control Conference*, vol. 3, 1990, pp. 3036–3040.

[22] P. Seiler, A. Packard, and G. Balas, "A gain based lower bound algorithm for real and mixed mu problem," *Automatica*, vol. 46, pp. 493–500, 2010.

[23] G. Ferreres, *A practical approach to robustness analysis with aeronautical applications*. New York: Kluwer Academic, 1999.

[24] T. Mannchen, D. G. Bates, and I. Postlethwaite, "Worst case uncertain parameter combinations for flight control system analysis," in *Proceedings of IFAC World Congress*, Barcelona, Spain, 2002.

[25] G. Vinnicombe, *Uncertainty and feedback: H_∞ loop shaping and v-gap metric*. World scientific publishing company, 2000.

[26] S. L. Gatley, D. G. Bates, and I. Postlethwaite, "A partitioned integrated flight and propulsion control system with engine safety limiting," *Control Engineering Practice*, vol. 8, no. 8, pp. 845–859, 2000.

[27] H. K. Khalil, "Nonlinear systems," *Prentice Hall*, 2002.

[28] C. Y. Kao, A. Megretski, and U. Jönsson, "Specialized fast algorithms for IQC feasibility and optimization problems," *Automatica*, vol. 40, no. 2, pp. 239–252, 2004.

[29] J. Veenman, H. Koroglu, and C. Scherer, "Analysis of the controlled NASA HL20 atmospheric re-entry vehicle based on dynamic IQCs," in *Proceedings of AIAA Guidance, Navigation, and Control Conference*. AIAA 2009-5637, 2009.

[30] A. Marcos, J. Veenman, C. Scherer, G. D. Zaiacomo, D. Mostaza, M. Kerr, H. Köroglu, and S. Bennani, *Application of LPV Modeling, Design and Analysis Methods to a Re-entry Vehicle.* American Institute of Aeronautics and Astronautics, 2010.

[31] E. Prempain, "An application of the sum of squares decomposition to the L2gain computation for a class of non linear systems," in *Proceedings of the 44th IEEE Conference on Decision and Control, and European Control Conference. CDC-ECC '05.*, Dec 2005, pp. 6865–6868.

[32] C. Maier and A. Papachristodulu, "Enhanced frameworks for safety verification of autonomous rendezvous systems," in *Proceedings of 18th IFAC Symposium on Automatic Control in Aerospace*, Nara, Japan, 2010.

[33] E. Doedel and J. P. Kernevez, "AUTO, software for continuation and bifurcation problems in ordinary differential equations," Tech. Rep., 1986.

[34] M. H. Lowenberg and P. P. Menon, "An analysable nonlinear criterion for clearance of flight control laws," in *Proceedings of AIAA Guidance, Navigation and Control Conference and Exhibit.* AIAA 2007-6507, 2007.

[35] S. Juliana, Q. P. Chu, J. A. Mulder, and T. J. Van Baten, "Flight envelope clearance of atmospheric re-entry module with flight control," in *Proceedings of AIAA Guidance, Navigation, and Control Conference and Exhibit.* AIAA 2004-5170, August 2004.

[36] H. Chernoff, "A measure of asymptotic efficiency for tests of a hypothesis based on the sum of observations," *The Annals of Mathematical Statistics*, vol. 23, no. 4, pp. 493–507, 1952.

[37] M. Vidyasagar, "Statistical learning theory and randomized algorithms for control," *IEEE Control Systems Technology*, vol. 18, no. 6, pp. 69–85, 1998.

[38] D. G. Bates and M. Hagström, *Nonlinear analysis and synthesis techniques for aircraft control.* Berlin, Heidelberg: Springer-Verlag, 2007.

[39] U. Korte, "Tasks and needs of the industrial clearance process," in *In Advanced Techniques for Clearance of Flight Control Laws.* Springer-Verlag, Germany, 2002, pp. 13–33.

[40] P. N. Desai and F. M. Cheatwood, "Entry dispersion analysis for the genesis sample return capsule," *Journal of Spacecraft and Rockets*, vol. 38, no. 3, pp. 345–350, 2001.

[41] P. N. Desai and P. Knocke, "Mars exploration rovers entry, descent, and landing trajectory analysis," *The Journal of the Astronautical Sciences*, vol. 55, no. 3, pp. 311–323, 2007.

[42] L. Forssell, "Flight clearance analysis using global nonlinear optimisation-based search algorithms," in *Proceedings of AIAA Guidance, Navigation, and Control Conference and Exhibit.* AIAA 2003-5481, August 2003.

[43] P. P. Menon, K. Jongrae, D. G. Bates, and I. Postlethwaite, "Clearance of nonlinear flight control laws using hybrid evolutionary optimization," *IEEE Transactions on Evolutionary Computation*, vol. 10, no. 6, pp. 689–699, Dec. 2006.

[44] P. P. Menon, D. G. Bates, and I. Postlethwaite, "Nonlinear robustness analy-

sis of flight control laws for highly augmented aircraft," *Control Engineering Practice*, vol. 15, no. 6, pp. 655 – 662, 2007.

[45] N. Paulino, E. D. Sotto, S. Salehi, A. Kron, J. F. Hamel, W. Wang, P. Menon, D. G. Bates, A. Papachristodoulou, and C. Maier, "Vvaf - worst case & safety analysis tools for autonomous rendezvous system," in *Proceedings of AIAA Guidance, Navigation, and Control Conference*. American Institute of Aeronautics and Astronautics, 2010.

[46] A. K. Kamath, P. P. Menon, M. Ganet-Schoeller, G. Maurice, S. Bennani, and D. G. Bates, "Robust safety margin assessment and constrained worst-case analysis of a launcher vehicle," in *Proceedings of 7th IFAC Symposium on Robust Control Design*, vol. 7, no. 1, 2012, pp. 254–259.

[47] ——, "Worst case analysis of a launcher vehicle using surrogate models," in *Proceedings of 7th IFAC Symposium on Robust Control Design*, vol. 7, no. 1, 2012, pp. 260–265.

[48] ——, "Efficient computation of the operational safety margin for a flexible launcher during the thrust vector control phase," *Submitted to Aerospace Science and Technology*, 2014.

[49] ——, "Classifying uncertain parameter space into safe and unsafe regions for a flexible launcher vehicle in its thrust vector control phase," *Submitted to Aerospace Science and Technology*, 2014.

[50] P. S. Goel and P. K. Maharana, "An active damping technique for satellites with flexible appendages," *Acta Astronautica*, vol. 36, no. 5, pp. 239 – 250, 1995.

[51] P. P. Menon, D. G. Bates, and I. Postlethwaite, "Hybrid evolutionary optimisation methods for the clearance of nonlinear flight control laws," in *44th IEEE Conference on Decision and Control, European Control Conference. CDC-ECC '05.*, December 2005, pp. 4053–4058.

[52] W. Wang, P. P. Menon, D. G. Bates, and S. Bennani, "Robustness analysis of attitude and orbit control systems for flexible satellites," *Control Theory Applications, IET*, vol. 4, no. 12, pp. 2958–2970, December.

[53] M. Ganet-Schoeller and G. Maurice, "Hybrid optimisation tools for worst case analysis of flexible launcher," in *Proceedings of International ESA Conference on Guidance, Navigation and Control Systems*, Czech Republic, June 2011.

[54] P. P. Menon, I. Postlethwaite, S. Bennani, A. Marcos, and D. G. Bates, "Robustness analysis of a reusable launch vehicle flight control law," *Control Engineering Practice*, vol. 17, no. 7, pp. 751 – 765, 2009.

[55] A. Varga, A. Hansson, and G. Puyou, *Optimization based clearance of flight control laws: a civil aircraft application*, ser. Lecture Notes in Control and Information Sciences. Springer, 2011.

[56] P. P. Menon, I. Postlethwaite, S. Bennani, A. Marcos, and D. G. Bates, "Multiobjective worst-case analysis of a re-entry vehicle control law," in *Proceedings of the 17th IFAC World Congress*, vol. 17, Seoul, Korea, July 2008, pp. 2532–2537.

[57] D. G. Bates, W. Wang, P. P. Menon, and S. Bennani, "Verification and validation of controllers using the worst-case analysis tool," in *Proceedings of*

the 8th International ESA Conference on Guidance, Navigation and Control, 2011.

[58] J. F. Magni, S. Bennani, J. Terlouw, G. Grübel, and H. D. Joos, *Multi-objective parameter synthesis (MOPS)*, ser. Lecture Notes in Control and Information Sciences. Springer Berlin Heidelberg, 1997, vol. 224, pp. 13–21.

[59] H. D. Joos, "A multiobjective optimisation-based software environment for control systems design," in *Proceedings of IEEE International Symposium on Computer Aided Control System Design*, 2002, pp. 7–14.

[60] ——, "Flight control law clearance using optimisation-based worst-case search," in *Proceedings of 6th IFAC Symposium on Robust Control Design*, vol. 6, no. 1, 2009, pp. 331–336.

[61] J. Nocedal and S. J. Wright, *Numerical optimization*, 2nd ed. Springer, 1999.

[62] "Optimization toolbox user's guide," The Mathworks, Tech. Rep., 2000.

[63] D. Goldberg and J. Holland, "Genetic algorithms and machine learning," in *Machine Learning*. Kluwer Academic Publishers, 1988, vol. 3, no. 2, pp. 95–99.

[64] R. L. Haupt and D. H. Werner, *Genetic algorithms in electromagnetics*. John Wiely & Sons, 2007.

[65] P. Rocca, M. Benedetti, M. Donelli, D. Franceschini, and A. Massa, "Evo-

lutionary optimization as applied to inverse scattering problems," *Inverse Problems*, vol. 25, no. 12, pp. 1–41, December 2009.

[66] N. Mansour, F. Kanj, and H. Khachfe, "Evolutionary algorithm for protein structure prediction," in *Proceedings of Sixth International Conference on Natural Computation*, vol. 8, 2010, pp. 3974–3977.

[67] V. J. Gillet, "Applications of evolutionary computation in drug design," in *Applications of Evolutionary Computation in Chemistry.* Springer, 2004, vol. 110, pp. 133–152.

[68] D. S. Weile and E. Michielssen, "Genetic algorithm optimization applied to electromagnetics: a review," *IEEE Transactions on Antennas and Propagation*, vol. 45, no. 3, pp. 343–353, 1997.

[69] R. Storn and K. Price, "Differential evolution –a simple and efficient heuristic for global optimization over continuous spaces," *Journal of Global Optimization*, vol. 11, no. 4, pp. 341–359, 1997.

[70] P. Rocca, G. Oliveri, and A. Massa, "Differential evolution as applied to electromagnetics," *IEEE Magazine Antennas and Propagation*, vol. 53, no. 1, pp. 38–49, 2011.

[71] J. Kim, D. G. Bates, and I. Postlethwaite, "Nonlinear robust performance analysis of an aeroelastic system," in *Proceedings of the 16th IFAC World Congress*, 2005, pp. 4–8.

[72] L. Davis, *Handbook of Genetic Algorithms.* New York: Van Nostrand Reinhold, 1991.

[73] J. Yen, J. C. Liao, B. Lee, and D. Randolph, "A hybrid approach to modeling metabolic systems using a genetic algorithm and simplex method," *IEEE Transactions on Systems, Man, and Cybernetics, Part B: Cybernetics*, vol. 28, no. 2, pp. 173–191, 1998.

[74] B. Mansoornejad, N. Mostoufi, and J. F. Farhang, "A hybrid GA-SQP optimization technique for determination of kinetic parameters of hydrogenation reactions," *Computers and Chemical Engineering*, vol. 32, no. 7, pp. 1447–1455, 2008.

[75] T. Rogalsky and R. W. Derksen, "Hybridization of differential evolution for aerodynamic design," in *Proceedings of the 8th annual conference of the computational fluid dynamics society of Canada*, 2000, pp. 729–736.

[76] M. Watt, M. Yu, A. Falcoz, A. Kron, P. P. Menon, F. Ankersen, and L. Massotti, "Integrated structure/control optimisation applied to the biomass earth observation mission," in *Proceedings of AIAA Guidance, Navigation, and Control (GNC) Conference*. AIAA 2013-4714, 2013.

[77] M. Watt, M. Yu, A. Falcoz, P. Singh, and C. Warren, "BIOMASS normal mode aocs : classical versus robust design," in *Proceedings of International ESA Conference on Guidance, Navigation and Control Systems*, Czech Republic, June 2011.

[78] S. Skogestad and I. Postlethwaite, *Multivariable feedback control: Analysis and Design*, 2nd ed. New York: John Wiely & Sons, 2005.

[79] A. Marcos, H. G. D. Marina, V. Mantini, C. Roux, and S. Bennani, "Optimization-based worst-case analysis of a launcher during the atmo-

spheric ascent phase," in *Proceedings of AIAA Guidance, Navigation, and Control (GNC) Conference*. AIAA 2013-4645, 2013.

[80] C. Roux and I. Cruciani, "Roll coupling effects on the stability margins for vega launcher," in *Proceedings of AIAA Atmospheric Flight Mechanics Conference and Exhibit*. AIAA 2007-6630, 2007.

[81] M. Ganet-Schoeller and M. Ducamp, "LPV control for flexible launcher," in *Proceedings of AIAA Guidance, Navigation, and Control Conference*. AIAA 2010-8193, 2010.

[82] M. Ganet-Schoeller, J. Bourdon, and G. Gelly, "Non-linear and robust stability analysis for atv rendezvous control," in *Proceedings of AIAA Guidance, Navigation, and Control Conference*. AIAA 2009-5951, 2009.

[83] D. L. Johnson, "Terrestrial environment (climatic) - criteria guidelines for use in aerospace vehicle development," NASA Technical Memorandum 4511, Revision, 1993.

[84] I. Rongier and J. Droz, "Robustness of Ariane 5 GNC algorithms," in *Proceedings of the 4th ESA International Conference on Spacecraft Guidance, Navigation and Control Systems,*. ESTEC, Noordwijk, The Netherlands, October, 1999.

[85] C. A. Coello Coello, "An updated survey of evolutionary multiobjective optimization techniques: state of the art and future trends," in *Proceedings of Congress on Evolutionary Computation*, vol. 1, 1999.

[86] J. D. Schaffer, "Multiple objective optimization with vector evaluated genetic

algorithms," in *Proceedings of the 1st International Conference on Genetic Algorithms*. Hillsdale, NJ, USA: L. Erlbaum Associates Inc., 1985, pp. 93–100.

[87] C. M. Fonseca and P. J. Fleming, "Genetic algorithms for multiobjective optimization: Formulation, discussion and generalization." in *Proceedings of the Fifth International Conference on Genetic Algorithms*, vol. 93, 1993, pp. 416–423.

[88] N. Srinivas and K. Deb, "Muiltiobjective optimization using nondominated sorting in genetic algorithms," *Evolutionary Computation*, vol. 2, no. 3, pp. 221–248, 1994.

[89] J. Horn, N. Nafpliotis, and D. E. Goldberg, "A niched pareto genetic algorithm for multiobjective optimization," in *Proceedings of the First IEEE Conference on Evolutionary Computation, IEEE World Congress on Computational Intelligence*, vol. 1, 1994, pp. 82–87.

[90] F. Xue, A. C. Sanderson, and R. J. Graves, "Pareto-based multi-objective differential evolution," in *Proceedingds of the 2003 Congress on Evolutionary Computation*, vol. 2, 2003, pp. 862–869.

[91] K. Deb, S. Agrawal, A. Pratap, and T. Meyarivan, *A Fast Elitist Non-dominated Sorting Genetic Algorithm for Multi-objective Optimization: NSGA-II*, ser. Lecture Notes in Computer Science. Springer Berlin Heidelberg, 2000, vol. 1917, pp. 849–858.

[92] A. Seshadri, "A fast elitist multiobjective genetic algorithm: NSGA-II," *MATLAB Central*, 2006.

[93] W. Wang, P. Menon, D. G. Bates, S. Ciabuschi, N. Paulino, E. Sotto, A. Bidaux, A. Garus, A. Kron, S. Salehi, and S. Bennani, "Verification and validation of autonomous rendezvous systems in the terminal phase," in *Proceedings of AIAA Guidance, Navigation, and Control Conference*. American Institute of Aeronautics and Astronautics, August 2012.

[94] R. Jin, W. Chen, and T. W. Simpson, "Comparative studies of metamodelling techniques under multiple modelling criteria," in *Structural and Multidisciplinary Optimization*. Springer-Verlag, 2001, vol. 23, no. 1, pp. 1–13.

[95] J. H. Friedman, "Multivariate adaptive regression splines," *The Annals of Statistics*, vol. 19, no. 1, pp. 1–67, 1991.

[96] A. Khuri and S. Mukhopadhyay, "Response surface methodology," *Wiley Interdisciplinary Reviews: Computational Statistics*, vol. 2, no. 2, pp. 128–149, 2010.

[97] J. P. C. Kleijnen, "Kriging metamodeling in simulation: A review," *European Journal of Operational Research*, vol. 192, no. 3, pp. 707–716, 2009.

[98] H. S. Chung and J. J. Alonso, "Comparison of approximation models with merit functions for design optimization," in *Proceedings of 8th Symposium on Multidisciplinary Analysis and Optimization*, vol. 200. AIAA 2000-4754, September 2000.

[99] B. Cheng and D. M. Titterington, "Neural networks: A review from a statistical perspective," *Statistical Science*, vol. 9, no. 1, pp. 2–30, 1994.

[100] R. Ghanem and P. D. Spanos, *Stochastic finite elements: a spectral approach*. Dover Publications, 2003.

[101] K. Karhunen, "Zur spektraltheorie stochastischer prozesse,," in *Annales Academiae Scientiarum Fennicae,*, 1946.

[102] D. Xiu and G. E. Karniadakis, "Modeling uncertainty in steady state diffusion problems via generalized polynomial chaos," *Computer Methods in Applied Mechanics and Engineering*, vol. 191, no. 43, pp. 4927 – 4948, 2002.

[103] N. Wiener, "The homogeneous chaos," *American Journal of Mathematics*, vol. 60, no. 4, pp. 897–936, 1938.

[104] R. H. Cameron and W. T. Martin, "Transformations of Weiner integrals under translations," *Annals of Mathematics*, vol. 45, no. 2, pp. 386–396, 1944.

[105] D. Xiu and G. Karniadakis, "The wiener–askey polynomial chaos for stochastic differential equations," *SIAM Journal on Scientific Computing*, vol. 24, no. 2, pp. 619–644, 2002.

[106] R. Ghanem and J. Red-Horse, "Propagation of probabilistic uncertainty in complex physical systems using a stochastic finite element approach," *Physica D: Nonlinear Phenomena*, vol. 133, pp. 137 – 144, 1999.

[107] R. Ghanem, "Ingredients for a general purpose stochastic finite elements implementation," *Computer Methods in Applied Mechanics and Engineering*, vol. 168, no. 1, pp. 19–34, 1999.

[108] T. Y. Hou, W. Luo, B. Rozovskii, and H. M. Zhou, "Wiener chaos expansions and numerical solutions of randomly forced equations of fluid mechanics," *Journal of Computational Physics*, vol. 216, no. 2, pp. 687 – 706, 2006.

[109] D. Xiu and G. E. Karniadakis, "Modeling uncertainty in flow simulations via generalized polynomial chaos," *Journal of Computational Physics*, vol. 187, no. 1, pp. 137 – 167, 2003.

[110] Z. K. Nagy and R. D. Braatz, "Distributional uncertainty analysis using polynomial chaos expansions," in *Proceedings of IEEE International Symposium on Computer-Aided Control System Design*, 2010, pp. 1103–1108.

[111] F. S. Hover and M. S. Triantafyllou, "Application of polynomial chaos in stability and control," *Automatica*, vol. 42, no. 5, pp. 789 – 795, 2006.

[112] T. Singh, P. Singla, and U. Konda, "Polynomial chaos based design of robust input shapers," *Journal of dynamic systems, measurement, and control*, vol. 132, no. 5, 2010.

[113] J. Fisher and R. Bhattacharya, "Linear quadratic regulation of systems with stochastic parameter uncertainties," *Automatica*, vol. 45, no. 12, pp. 2831 – 2841, 2009.

[114] S. Hosder, R. Walters, and M. Balch, "Efficient sampling for non-intrusive polynomial chaos applications with multiple uncertain input variables," in *Proceedings of 48th AIAA/ASME/ASCE/AHS/ASC Structures, Structural Dynamics, and Materials Conference*. AIAA 2007-1939, 2007.

[115] G. J. A. Loeven, J. A. S. Witteveen, and H. Bijl, "Probabilistic collocation:

An efficient non-intrusive approach for arbitrarily distributed parametric uncertainties," in *Proceedings of 45th AIAA Aerospace Sciences Meeting and Exhibit*. AIAA 2007-317, January 2007.

[116] G. H. Golub and J. H. Welsch, "Calculation of gauss quadrature rules," *Mathematics of Computation*, vol. 23, no. 106, pp. 221–230, 1969.

[117] M. D. Webster, M. A. Tatanf, and G. J. McRae, "Application of the probabilistic collocation method for an uncertainty analysis of a simple ocean model," Tech. Rep. 4, 1996.

[118] E. E. Tyrtyshnikov, "A matrix view on the root distribution for orthogonal polynomials," *Structured Matrices: Recent Developments in Theory and Computation, Nova Science, New York*, pp. 149–156, 2001.

[119] A. H. C. Smith, A. Monti, and F. Ponci, "Uncertainty and worst-case analysis in electrical measurements using polynomial chaos theory," *IEEE Transactions on Instrumentation and Measurement*, vol. 58, no. 1, pp. 58–67, 2009.

[120] L. G. Crespo, D. P. Giesy, and S. P. Kenny, "Robustness analysis and robust design of uncertain systems," *AIAA Journal*, vol. 46, pp. 388–396, 2008.

[121] M. Zettler and J. Garloff, "Robustness analysis of polynomials with polynomial parameter dependency using Bernstein expansion," *IEEE Transactions on Automatic Control*, vol. 43, no. 3, pp. 425–431, 1998.

[122] M. Matsutani, T. Gibson, J. Jang, L. G. Crespo, and A. Annaswamy, "An adaptive control technology for safety of a GTM-like aircraft," in *Proceedings of American Control Conference*, 2009, pp. 3238–3243.

[123] L. G. Crespo, M. Matsutani, J. Jang, T. Gibson, and A. Annaswamy, "Design and verification of an adaptive controller for the generic transport model," in *Proceedings of AIAA Guidance, Navigation, and Control Conference*. AIAA 2009-5618, 2009.

[124] G. T. Cargo and O. Shisha, "The Bernstein form of a polynomial," *Journal of Research of the National Bureau of Standards*, vol. 70B, no. 1, pp. 79–81, 1966.

[125] S. N. Bernstein, "Démonstration du théorème de weierstrass fondée sur le calcul des probabilités," *Communications de la Société Mathématique de Kharkov 2*, vol. Series XIII, no. 1, pp. 1–2, 192.

[126] T. Dang and R. Testylier, "Reachability analysis for polynomial dynamical systems using the bernstein expansion," *Reliable Computing*, vol. 17, no. 2, pp. 128–152, 2012.

[127] J. M. Lane and R. F. Riesenfeld, "Bounds on a polynomial," in *BIT Numerical Mathematics*. Kluwer Academic Publishers, 1981, vol. 21, no. 1, pp. 112–117.

[128] T. W. Sederberg and R. T. Farouki, "Approximation by interval bézier curves," *IEEE Computer Graphics and Applications*, vol. 12, no. 5, pp. 87–95, 1992.

[129] B. V. Patil, P. S. V. Nataraj, and S. Bhartiya, "Global optimization of mixed-integer nonlinear (polynomial) programming problems: the Bernstein polynomial approach," *Computing*, vol. 94, no. 2-4, pp. 325–343, 2012.

[130] L. G. Crespo, C. A. Munoz, A. J. Narkawicz, S. P. Kenny, and D. P. Giesy, "Uncertainty analysis via failure domain characterization: polynomial requirement functions," in *Proceedings of European Safety and Reliability Conference. Troyes, France*, September 2011.

[131] R. T. Farouki, "The Bernstein polynomial basis: A centennial retrospective," *Computer Aided Geometric Design*, vol. 29, no. 6, pp. 379 – 419, 2012.

[132] J. Garloff, "The Bernstein expansion and its applications," *Journal of the American Romanian Academy*, vol. 25, no. 27, pp. 80–85, 2003.

[133] J. M. Hanson and B. B. Beard, "Applying monte carlo simulation to launch vehicle design and requirements verification," *Journal of Spacecraft and Rockets*, vol. 49, no. 1, pp. 136–144, 2012.

[134] W. Wang, "Worst case analysis of space systems," Ph.D. dissertation, College of Engineering, Mathematics and Physical Sciences, 2011.

[135] A. K. Kamath, "Worst Case Analysis Tools -II," University of Exeter, Tech. Rep., 2013.

[136] W. H. Press, S. A. Taukolsky, W. T. Vetterling, and B. P. Flannery, *Numerical Recipes in C: The Art of Scientific Computing*. Cambridge University Press, 1992.

Appendix A: Recurrence relations for orthogonal polynomials

The weight functions ($w(\delta)$) and the recurrence relations that generate the basis of orthogonal polynomials in Table 3.1 are given as follows, [136]:

Gauss-Hermite:

$$\begin{aligned} w(\delta) &= e^{-\delta^2} \qquad\qquad -\infty < \delta < \infty \\ \Phi_{q+1}(\delta) &= \delta\Phi_q - q\Phi_{q-1}(\delta) \end{aligned} \tag{2}$$

Gauss-Laguerre:

$$\begin{aligned} w(\delta) &= \delta^{\alpha}e^{-\delta} \qquad\qquad \alpha > -1, 0 < \delta < \infty \\ (q+1)\Phi^{\alpha}_{q+1}(\delta) &= (-\delta + 2q + \alpha + 1)\Phi^{\alpha}_{q} - (q+\alpha)\Phi^{\alpha}_{q-1}(\delta) \end{aligned} \tag{3}$$

Gauss-Legendre:

$$\begin{aligned} w(\delta) &= 1 \qquad\qquad -1 < \delta < 1 \\ (q+1)\Phi_{q+1}(\delta) &= (2q+1)\delta\Phi_q - q\Phi_{q-1}(\delta) \end{aligned} \tag{4}$$

Gauss-Jacobi:

$$\begin{aligned} w(\delta) &= (1-\delta)^{\alpha}(1+\delta)^{\beta} \qquad \alpha,\beta > -1, -1 < \delta < 1 \\ c_q \Phi_{q+1}^{(\alpha,\beta)}(\delta) &= (d_q + e_q\delta)\Phi_q^{(\alpha,\beta)} - f_q \Phi_{q-1}^{(\alpha,\beta)} \end{aligned} \tag{5}$$

where the coefficients c_q, d_q, e_q and f_j are given by:

$$\begin{aligned} c_q &= 2(q+1)(q+\alpha+\beta+1)(2q+\alpha+\beta) \\ d_q &= (2q+\alpha+\beta+1)(\alpha^2-\beta^2) \\ e_q &= (2q+\alpha+\beta)(2q+\alpha+\beta+1)(2q+\alpha+\beta+2) \\ f_q &= 2(q+\alpha)(q+\beta)(2q+\alpha+\beta+2) \end{aligned}$$